

4. SITE 982¹

Shipboard Scientific Party²

HOLE 982A

Position: 57°30.992'N, 15°52.001'W
Start hole: 1815 hr, 15 July 1995
End hole: 1200 hr, 16 July 1995
Time on hole: 17.75 hr (0.74 days)
Seafloor (drill pipe measurement from rig floor, mbrf): 1146.3
Total depth (drill pipe measurement from rig floor, mbrf): 1395.0
Distance between rig floor and sea level (m): 11.0
Water depth (drill pipe measurement from sea level, m): 1135.3
Penetration (mbsf): 248.7
Coring totals:
Type: APC
Number: 27
Cored: 248.7 m
Recovered: 253.23 m, 101.7%

Formation:

Unit I: 0–57.4 mbsf; Holocene to late Pliocene; nannofossil ooze alternating with nannofossil clays, silty clays
Unit II: 57.4–248.7 mbsf; late Pliocene to late Miocene; nannofossil ooze, partly with clay, chalk in the lower part

HOLE 982B

Position: 57°31.002'N, 15°51.993'W
Start hole: 1200 hr, 16 July 1995
End hole: 0230 hr, 19 July 1995
Time on hole: 62.5 hr (2.60 days)
Seafloor (drill pipe measurement from rig floor, mbrf): 1145.0
Total depth (drill pipe measurement from rig floor, mbrf): 1759.9
Distance between rig floor and sea level (m): 11.0
Water depth (drill pipe measurement from sea level, m): 1134.0
Penetration (mbsf): 614.9
Coring totals:
Type: APC
Number: 26
Cored: 243.0 m
Recovered: 246.51 m, 101.4%
Type: XCB
Number: 39
Cored: 371.9 m
Recovered: 241.96 m, 65.1%

Total:

Number: 65
Cores: 614.9 m
Recovered: 488.47 m, 79.4%

Formation:

Unit I: 0–57.4 mbsf; Holocene to late Pliocene; nannofossil ooze alternating with nannofossil clays, silty clays
Unit II: 57.4–614.9 mbsf; late Pliocene to early Miocene; nannofossil ooze, partly with clay, chalk in the lower part

HOLE 982C

Position: 57°31.009'N, 15°51.992'W
Start hole: 0230 hr, 19 July 1995
End hole: 1615 hr, 19 July 1995
Time on hole: 13.75 hr (0.57 days)
Seafloor (drill pipe measurement from rig floor, mbrf): 1144.7
Total depth (drill pipe measurement from rig floor, mbrf): 1395.5
Distance between rig floor and sea level (m): 11.0
Water depth (drill pipe measurement from sea level, m): 1133.7
Penetration (meters below seafloor, mbsf): 250.8
Coring totals:
Type: APC
Number: 27
Cored: 250.8 m
Recovered: 256.49 m, 102.3%

Formation:

Unit I: 0–57.4 mbsf; Holocene to late Pliocene; nannofossil ooze alternating with nannofossil clays, silty clays
Unit II: 57.4–250.8 mbsf; late Pliocene to late Miocene; nannofossil ooze, partly with clay, chalk in the lower part

HOLE 982D

Position: 57°31.009'N, 15°51.992'W
Start hole: 1615 hr, 19 July 1995
End hole: 2115 hr, 19 July 1995
Time on hole: 5.0 hr (0.21 days)
Seafloor (drill pipe measurement from rig floor, mbrf): 1144.7
Total depth (drill pipe measurement from rig floor, mbrf): 1174.2
Distance between rig floor and sea level (m): 11.0
Water depth (drill pipe measurement from sea level, m): 1133.7
Penetration (meters below seafloor, mbsf): 29.5
Drilled (m): 20.0 (0–20 mbsf)
Coring totals:
Type: APC
Number: 1

¹Jansen, E., Raymo, M.E., Blum, P., et al., 1996. *Proc. ODP, Init. Repts.*, 162: College Station, TX (Ocean Drilling Program).

²Shipboard Scientific Party is given in the list preceding the Table of Contents.

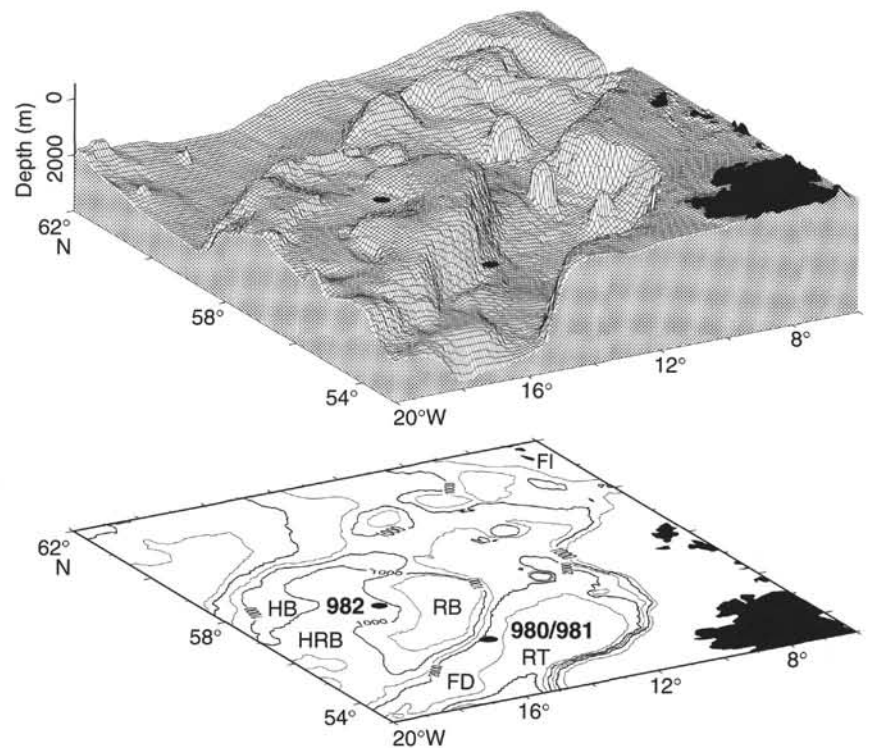


Figure 1. Bathymetric map showing location of Site 982, as well as Sites 980/981. Physiographic features: RB = Rockall Bank, FD = Feni Drift, RT = Rockall Trough, FI = Faeroe Islands, HRB = Hattan-Rockall Basin, HB = Hattan Bank.

Cored: 9.5 m

Recovered: 9.78 m, 101.8%

Formation:

Unit I: 0–29.5 mbsf; Pleistocene; nanofossil ooze alternating with nanofossil clays, silty clays

Principal results: Site 982 (NAMD-1), at 1134 m water depth on the Rockall Plateau (Fig. 1), will allow documentation of the evolution of intermediate-water circulation in the North Atlantic as well as the evolution of North Atlantic floral and faunal assemblages over the Neogene. This site, located very close to Deep Sea Drilling Project (DSDP) Site 116, was drilled 25 years later, to the day. The original hole was rotary drilled and discontinuously cored (in high seas), and our objective in redrilling the site with the APC/XCB system was to recover a continuous, carbonate-rich sequence of sediments extending to the early Miocene. This was successfully achieved and the triple APC coring down to 235 mbsf appears to have provided a complete sequence of the last approximately 7 Ma. XCB coring from 235 to 615 mbsf in Hole 982B provided good documentation of the 19–7-Ma interval. Recovery dropped below 480 mbsf where silicified layers began to appear.

The sediments have an average calcium carbonate content of around 86% and are predominantly composed of nanofossil ooze with variable amounts of clay, clayey nanofossil mixed sediments, and clays with variable amounts of nanofossils and silt. A distinct boundary dividing the sequence into two units (“glacial” and “preglacial”) occurs at approximately 57.4 mbsf (~2.7 Ma). The boundary is marked by sharp downcore decreases in siliclastic sediments and magnetic susceptibility and sharp downcore increases in calcium carbonate content and spectral reflectance. Unit I sediments are dominated by variable amounts of calcareous nanofossils, clay, and, to a lesser extent, silt and foraminifers. These variations are indicative of the considerable color contrast observed between the oozes and clays within the unit, particularly when compared with Unit II. The compositional changes form distinct high-amplitude cyclic variations which occur on a 0.5- to 3-m scale and which are mainly related to relative changes in the proportions of biogenic carbonate, detrital clay minerals, and to a lesser extent, detrital silt. All dropstones observed in Site 982 sediments occur in Unit I.

Unit II sediments are dominated by biogenic carbonate, primarily nanofossil ooze, with only minor amounts of clay, and, to an even lesser extent, biogenic silica. The mean carbonate content of Unit II, 90.8%, is considerably higher than that of Unit I. The unit is characterized by very light gray, light gray, and very light greenish gray nanofossil ooze. The 195.5- to 480.0-mbsf interval is very homogenous, and within this 284.5-m-thick Miocene interval the sediments become harder, approaching chalk. The lower part of the unit contains chert-like silicified layers. Several distinct ash layers were identified in the unit.

The multisensor track (MST) data were used to evaluate continuity of recovery, and a firm composite section was developed down to about 200 mbsf (approximately the last 6.5 Ma). Below this depth we appear to have recovered a complete sedimentary sequence down to about 260 m, but exact correlations between holes were not so obvious. The MST records also were used to provide detailed correlations to Sites 981 and 982 over the last 2.5 Ma, and a corresponding cyclicity is documented in high detail between all three sites.

Age control for the sequence is primarily based on paleomagnetic data and calcareous nanofossils and foraminifers. The magnetic signal is too weak to provide reliable polarity sequences below the Matuyama/Gauss boundary (2.6 Ma), below which calcareous fossils provide the primary age control. The bottom of the drilled sequence is at about 19 Ma, and no major breaks in sedimentation are indicated by shipboard analyses. Possible short gaps may be present at about 2 Ma and 7 Ma. This needs to be resolved by shore-based work. Sedimentation rates average about 21 m/m.y. for the middle Pliocene through Pleistocene. Below this level sedimentation rates increase to about 37 m/m.y.

At 268 mbsf a sharp horizon was identified, where only a silicified foraminifer sand cobble was recovered. This horizon, in sediments 7–8 Ma old, marks the upper regional seismic reflector of the Rockall Basin (Reflector R1). Downhole logs indicate that the silicified material is a 4-m-thick sequence, which we interpret as a turbidite. The silicified layer apparently has formed a diffusion barrier, dampening or disabling pore-water diffusion, as shown by marked differences in pore-water profiles above and below the layer. The apparent lack of diffusion may open possibilities for studying differences in ocean chemistry (especially salinity) before and after the Messinian salinity events.

There is generally good agreement between the physical properties of the cores, the downhole logs, and the seismic stratigraphy of the site. Downhole logs identified a series of ash layers, as well as indurated/silicified layers at the bottom of the hole where recovery was poor. Seismic stratigraphy in the area of Site 982 identified seven seismic units bounded by eight prominent reflectors. Five of these were identified during DSDP Leg 12 and three new ones are defined here. The deepest core recovered fell between Reflectors R2 and R3.

BACKGROUND AND OBJECTIVES

The Rockall Plateau (Fig. 1) is a shallow platform at about 1000 m water depth which lies roughly between Iceland and Ireland. To the north lies the Faeroe-Iceland Ridge and associated intermediate water overflows from the Nordic Seas. To the south, the topography drops off sharply into the Rockall Trough, which has a depth of about 2500 m. Site 982 was drilled in a central bathymetric depression on the plateau, the Hatton-Rockall Basin; the shallower Hatton Bank rises to the northwest and the shallower Rockall Bank is found about 30 km to the southeast. Much of the Rockall Bank is at less than 200 m water depth (including tiny Rockall Island) and the area of subaerial exposure would thus increase greatly during sea-level falls. Considering the probable subsidence history of the bank, this area could have been the source of the foraminiferal turbidites and minor terrigenous components found in Miocene sediments at this site (see "Lithostratigraphy" section, this chapter). The Rockall Plateau is believed to be underlain by continental crust, which separated from Greenland sometime during the Paleocene (e.g., Laughton, Berggren, et al., 1972). Seafloor spreading between the Rockall Plateau and Iceland started just prior to Anomaly 24 time (Avery et al., 1969), or 54 Ma on the magnetic polarity time scale of Cande and Kent (1995).

The major scientific objective in drilling Site 982 is to study the Neogene evolution of thermohaline circulation in the North Atlantic. At 1133 m water depth, this site is ideally located for the study of North Atlantic Intermediate Water (NAIW) mass behavior (1) on glacial-interglacial time scales of the Pliocene–Pleistocene, (2) over the late Miocene to late Pliocene interval encompassing the uplift of the Isthmus of Panama and the Messinian Salinity Crisis, and, finally, (3) over the middle to late Miocene interval when the Iceland–Faeroe Ridge subsided to depths that allowed deep-water exchange between the Nordic Seas and the North Atlantic. Further, the recovery of a pre-middle Miocene section should allow documentation of NAIW mass circulation at times when no northern-source deep water is thought to have formed (Wright and Miller, 1993). Two other questions of interest are how the high-latitude North Atlantic responded to early intervals of Antarctic glaciation (as implied by the existence of glacially derived sediments in the Southern Ocean area), and how the onset of small- to medium-scale glaciation in the Northern Hemisphere in the late Miocene–Pliocene (Jansen and Sjøholm, 1991; Wolf and Thiede, 1991; Fronval and Jansen, in press) affected North Atlantic water-mass structure.

In addition to studying problems related to water-mass evolution, the Site 982 sequence will be used to study the evolution of floral and faunal groups during the Neogene. The middle to late Miocene record of planktonic foraminifers encompasses the diversification of the globorotalid clade, whose evolutionary record is poorly known from the temperate to subpolar North Atlantic. Sites previously drilled near the Rockall Plateau (DSDP Sites 116, 406, 552, and 610) yielded diverse globorotalid assemblages; however, these sites are bedeviled by incomplete recovery and poor to moderate preservation.

OPERATIONS

The operational plan for Site 982 (NAMD-1) called for three APC holes drilled to approximately 200 mbsf, and one XCB hole drilled to 500 mbsf. Standard Quad combination and FMS logging was to be conducted in the deep hole, with the added possibility of running the magnetic susceptibility tool.

At 1506 hr on 15 July 1995 the ship slowed down to 6.0 kt and the seismic gear was deployed for a 9-nmi (about 1.5-hr) predrilling survey of Site 982 (NAMD-1). Based on the survey, we chose Site 982 about 300 m to the northeast of the proposed site NAMD-1 in order to avoid small-scale faulting observed in the seismic records (see "Seismic Stratigraphy" section, this chapter). By 1815 hr on 15 July, the seismic profiling gear had been recovered, the vessel had returned to the drilling location based on GPS coordinates, and the positioning beacon had been deployed, initiating Site 982 and Hole 982A.

A standard APC/XCB bottom-hole assembly was used for all holes at Site 982, including a nonmagnetic drill collar. Subsequent (B and C) holes were offset 15 m to the north, while Hole 982D was offset 5 m to the north. The mudline was established for each hole except Hole 982D. The APC firing depth was offset by a few meters for subsequent holes to establish continuous sediment sections except for Hole 982D. Position, depths, and coring totals for each hole are summarized at the top of this chapter. All cores are listed in Table 1.

Coring at Hole 982A proceeded without incident until Core 982A-27H would not come free with 100,000 lb of overpull. The previous Core 982A-26H required 40,000 lb of overpull. Both cores had full stroke indications. The washover technique was used but was limited to 4.0 m due to drilling kelly limitations. After several heave cycles and limited jarring attempts, the driller continued to apply increasing tension to the coring assembly. During an up heave the overpull reached 150,000 lb and the barrel apparently came free. Upon recovery it was found that the pin thread on the upper inner core barrel had parted, leaving the lower 15-ft inner barrel, liner seal sub, and core shoe in the hole. Advance by recovery was used to determine final hole depth, and the hole was terminated at that point. Hole 982A had reached the scientific target for triple coring and Hole 982B was to be deepened instead of this hole.

Coring at Hole 982B was without incident until Core 982B-26H. This core penetrated to a depth of 243.0 mbsf, just one core above the point where the high overpull and subsequent inner barrel connection failure occurred. Although Core 26H required only 25,000 lb of overpull to extract from the formation it was considered prudent to switch to XCB coring at that point. Coring was suspended at a depth of 614.9 mbsf when the scientific target was reached. The last four XCB cores, from 576.4 to 614.9 mbsf, were characterized by low recovery, averaging between 2% and 8%.

Upon completion of coring operations at Hole 982B, two annular-hole volumes of sea water were circulated. A wiper trip identified no overpull or drag. Only 1.5 m of fill was found at total depth, which was readily circulated out. The pipe was pulled to a logging depth of 82.6 mbsf. No drilling mud was required during the drilling operation, and the hole was considered to be in excellent condition. Two successful logging runs were made on this hole. The first run, with the Quad combo suite of tools, was deployed to within 1.9 m of bottom. The second run, with the FMS, reached to within 4.9 m of bottom. After completing the logging operations the upgraded LDEO/BRG wireline heave compensator control system was tested. After the final suite of tools was recovered and the logging sheaves were rigged down, the drill pipe was tripped above mudline, clearing the seafloor and ending Hole 982B.

Table 1. Coring summary for Site 982.

Core	Date (July 1995)	Time (UTC)	Depth (mbsf)	Length cored (m)	Length recovered (m)	Recovery (%)	Core	Date (July 1995)	Time (UTC)	Depth (mbsf)	Length cored (m)	Length recovered (m)	Recovery (%)
162-982A-							37X	17	0355	336.0-345.6	9.6	7.94	82.7
1H	15	2210	0.0-8.2	8.2	8.23	100.0	38X	17	0425	345.6-355.2	9.6	8.22	85.6
2H	15	2240	8.2-17.7	9.5	9.75	102.0	39X	17	0500	355.2-364.9	9.7	7.43	76.6
3H	15	2300	17.7-27.2	9.5	8.84	93.0	40X	17	0540	364.9-374.5	9.6	7.41	77.2
4H	15	2315	27.2-36.7	9.5	9.81	103.0	41X	17	0620	374.5-384.1	9.6	7.07	73.6
5H	15	2330	36.7-46.2	9.5	9.86	104.0	42X	17	0705	384.1-393.8	9.7	6.55	67.5
6H	16	0005	46.2-55.7	9.5	9.82	103.0	43X	17	0745	393.8-403.4	9.6	6.11	63.6
7H	16	0045	55.7-65.2	9.5	9.62	101.0	44X	17	0830	403.4-413.0	9.6	6.8	70.8
8H	16	0115	65.2-74.7	9.5	9.78	103.0	45X	17	0915	413.0-422.6	9.6	9.75	101.0
9H	16	0150	74.7-84.2	9.5	8.92	93.9	46X	17	0955	422.6-432.2	9.6	7.43	77.4
10H	16	0220	84.2-93.7	9.5	9.82	103.0	47X	17	1040	432.2-441.8	9.6	6.47	67.4
11H	16	0245	93.7-103.2	9.5	9.63	101.0	48X	17	1130	441.8-451.4	9.6	8.35	87.0
12H	16	0315	103.2-112.7	9.5	9.72	102.0	49X	17	1200	451.4-461.0	9.6	7.00	72.9
13H	16	0335	112.7-122.2	9.5	9.68	102.0	50X	17	1235	461.0-470.6	9.6	6.70	69.8
14H	16	0405	122.2-131.7	9.5	9.76	103.0	51X	17	1310	470.6-480.2	9.6	8.39	87.4
15H	16	0425	131.7-141.2	9.5	9.65	101.0	52X	17	1350	480.2-489.7	9.5	8.50	89.5
16H	16	0450	141.2-150.7	9.5	9.83	103.0	53X	17	1425	489.7-499.3	9.6	8.94	93.1
17H	16	0515	150.7-160.2	9.5	9.64	101.0	54X	17	1505	499.3-508.9	9.6	6.93	72.2
18H	16	0540	160.2-169.7	9.5	9.84	103.0	55X	17	1545	508.9-518.5	9.6	9.67	101.0
19H	16	0605	169.7-179.2	9.5	9.84	103.0	56X	17	1630	518.5-528.1	9.6	9.85	102.0
20H	16	0630	179.2-188.7	9.5	9.69	102.0	57X	17	1735	528.1-537.7	9.6	7.64	79.6
21H	16	0700	188.7-198.2	9.5	9.87	104.0	58X	17	1840	537.7-547.4	9.7	3.91	40.3
22H	16	0730	198.2-207.7	9.5	9.54	100.0	59X	17	1930	547.4-557.0	9.6	0.70	7.3
23H	16	0800	207.7-217.2	9.5	9.88	104.0	60X	17	2055	557.0-566.7	9.7	4.20	43.3
24H	16	0820	217.2-226.7	9.5	9.74	102.0	61X	17	2215	566.7-576.4	9.7	3.55	36.6
25H	16	0845	226.7-236.2	9.5	9.71	102.0	62X	17	2315	576.4-586.0	9.6	0.78	8.1
26H	16	0910	236.2-245.7	9.5	9.76	103.0	63X	18	0020	586.0-595.6	9.6	0.38	4.0
27H	16	1015	245.7-248.7	3.0	3.00	100.0	64X	18	0150	595.6-605.3	9.7	0.47	4.8
							65X	18	0315	605.3-614.9	9.6	0.21	2.2
			Coring totals:	248.7	253.20	101.8				Coring totals:	614.9	488.50	79.4
162-982B-							162-982C-						
1H	16	1255	0.0-5.5	5.5	5.56	101.0	1H	19	0400	0.0-3.8	3.8	3.78	99.5
2H	16	1315	5.5-15.0	9.5	9.83	103.0	2H	19	0430	3.8-13.3	9.5	9.69	102.0
3H	16	1335	15.0-24.5	9.5	9.76	103.0	3H	19	0500	13.3-22.8	9.5	10.02	105.5
4H	16	1355	24.5-34.0	9.5	9.23	97.1	4H	19	0530	22.8-32.3	9.5	10.06	105.9
5H	16	1410	34.0-43.5	9.5	9.80	103.0	5H	19	0600	32.3-41.8	9.5	9.87	104.0
6H	16	1435	43.5-53.0	9.5	9.65	101.0	6H	19	0630	41.8-51.3	9.5	9.72	102.0
7H	16	1450	53.0-62.5	9.5	9.66	101.0	7H	19	0700	51.3-60.8	9.5	9.79	103.0
8H	16	1510	62.5-72.0	9.5	9.56	100.0	8H	19	0725	60.8-70.3	9.5	9.76	103.0
9H	16	1530	72.0-81.5	9.5	9.80	103.0	9H	19	0745	70.3-79.8	9.5	9.76	103.0
10H	16	1550	81.5-91.0	9.5	9.72	102.0	10H	19	0815	79.8-89.3	9.5	9.84	103.0
11H	16	1610	91.0-100.5	9.5	9.79	103.0	11H	19	0840	89.3-98.8	9.5	10.02	105.5
12H	16	1630	100.5-110.0	9.5	9.71	102.0	12H	19	0905	98.8-108.3	9.5	9.80	103.0
13H	16	1645	110.0-119.5	9.5	9.81	103.0	13H	19	0930	108.3-117.8	9.5	9.69	102.0
14H	16	1710	119.5-129.0	9.5	9.76	103.0	14H	19	0955	117.8-127.3	9.5	9.86	104.0
15H	16	1735	129.0-138.5	9.5	9.78	103.0	15H	19	1015	127.3-136.8	9.5	9.63	101.0
16H	16	1750	138.5-148.0	9.5	9.73	102.0	16H	19	1035	136.8-146.3	9.5	9.71	102.0
17H	16	1810	148.0-157.5	9.5	9.43	99.2	17H	19	1100	146.3-155.8	9.5	9.98	105.0
18H	16	1830	157.5-167.0	9.5	9.64	101.0	18H	19	1120	155.8-165.3	9.5	9.66	101.0
19H	16	1850	167.0-176.5	9.5	9.80	103.0	19H	19	1145	165.3-174.8	9.5	9.88	104.0
20H	16	1910	176.5-186.0	9.5	9.71	102.0	20H	19	1210	174.8-184.3	9.5	8.16	85.9
21H	16	1930	186.0-195.5	9.5	9.74	102.0	21H	19	1225	184.3-193.8	9.5	9.57	101.0
22H	16	1950	195.5-205.0	9.5	9.37	98.6	22H	19	1250	193.8-203.3	9.5	9.87	104.0
23H	16	2010	205.0-214.5	9.5	9.18	96.6	23H	19	1310	203.3-212.8	9.5	9.19	96.7
24H	16	2030	214.5-224.0	9.5	9.55	100.0	24H	19	1350	212.8-222.3	9.5	9.79	103.0
25H	16	2055	224.0-233.5	9.5	9.47	99.7	25H	19	1420	222.3-231.8	9.5	9.76	103.0
26H	16	2115	233.5-243.0	9.5	9.48	99.8	26H	19	1440	231.8-241.3	9.5	9.85	103.0
27X	16	2140	243.0-249.3	6.3	6.51	103.0	27H	19	1505	241.3-250.8	9.5	9.78	103.0
28X	16	2210	249.3-258.9	9.6	7.20	75.0							
29X	16	2235	258.9-268.5	9.6	5.77	60.1							
30X	16	2305	268.5-278.2	9.7	0.08	0.8							
31X	16	2335	278.2-287.8	9.6	9.58	99.8							
32X	17	0030	287.8-297.4	9.6	5.84	60.8							
33X	17	0110	297.4-307.1	9.7	8.16	84.1							
34X	17	0150	307.1-316.7	9.6	8.08	84.1							
35X	17	0235	316.7-326.3	9.6	6.36	66.2							
36X	17	0320	326.3-336.0	9.7	7.05	72.7							
										Coring totals:	250.8	256.50	102.3
							162-982D-						
							1H	19	1725	20.0-29.5	9.5	9.78	103.0
										Coring totals:	9.5	9.78	103.0

Coring at Hole 982C proceeded without incident until the scientific target for the hole had been reached. Core orientation on this hole using the Tensor tool was conducted on Cores 982C-3H through 7H.

The vessel was offset 5 m north in preparation for spudding Hole 982D. This hole was to be a single APC core across an area not recovered completely in the previous three holes. The same water depth as Hole 982C was used as a reference point for drilling down 20 mbsf. APC Core 1H was then taken, recovering 9.76 m.

The positioning beacon was recovered and the vessel was secured for transit and got underway at 2112 hr on 19 July 1995.

COMPOSITE DEPTHS

Continuity of the sedimentary sequence at Site 982 was documented for the upper 255 mbsf, extending from the late Miocene to the Holocene. A composite section was developed as described in the "Composite Depths" section, "Explanatory Notes" chapter, this volume. Core 982D-1H was drilled to bridge a potential coring gap in the sequence resulting from the near alignment of core breaks at 982A-3H, 982B-3H, and 982C-3H. The offsets that comprise the composite depth section at Site 982 are given in Table 2.

Table 2. Site 982 composite depths.

Core, section	Length (cm)	Depth (mbsf)	Depth (mcd)	Offset (mcd - mbsf)	Core, section	Length (cm)	Depth (mbsf)	Depth (mcd)	Offset (mcd - mbsf)
162-982A-					12H-3	150	106.20	119.69	13.49
1H-1	150	0.00	0.00	0.00	12H-4	150	107.70	121.19	13.49
1H-2	150	1.50	1.50	0.00	12H-5	150	109.20	122.69	13.49
1H-3	150	3.00	3.00	0.00	12H-6	150	110.70	124.19	13.49
1H-4	150	4.50	4.50	0.00	12H-7	52	112.20	125.69	13.49
1H-5	150	6.00	6.00	0.00	12H-CC	20	112.72	126.21	13.49
1H-6	64	7.50	7.50	0.00	13H-1	150	112.70	127.62	14.92
1H-CC	9	8.14	8.14	0.00	13H-2	150	114.20	129.12	14.92
2H-1	150	8.20	9.50	1.30	13H-3	150	115.70	130.62	14.92
2H-2	150	9.70	11.00	1.30	13H-4	150	117.20	132.12	14.92
2H-3	150	11.20	12.50	1.30	13H-5	150	118.70	133.62	14.92
2H-4	150	12.70	14.00	1.30	13H-6	150	120.20	135.12	14.92
2H-5	150	14.20	15.50	1.30	13H-7	53	121.70	136.62	14.92
2H-6	150	15.70	17.00	1.30	13H-CC	15	122.23	137.15	14.92
2H-7	63	17.20	18.50	1.30	14H-1	150	122.20	138.02	15.82
2H-CC	12	17.83	19.13	1.30	14H-2	150	123.70	139.52	15.82
3H-1	150	17.70	19.78	2.08	14H-3	150	125.20	141.02	15.82
3H-2	150	19.20	21.28	2.08	14H-4	150	126.70	142.52	15.82
3H-3	150	20.70	22.78	2.08	14H-5	150	128.20	144.02	15.82
3H-4	150	22.20	24.28	2.08	14H-6	150	129.70	145.52	15.82
3H-5	150	23.70	25.78	2.08	14H-7	56	131.20	147.02	15.82
3H-6	121	25.20	27.28	2.08	14H-CC	20	131.76	147.58	15.82
3H-CC	13	26.41	28.49	2.08	15H-1	150	131.70	148.98	17.28
4H-1	150	27.20	29.70	2.50	15H-2	150	133.20	150.48	17.28
4H-2	150	28.70	31.20	2.50	15H-3	150	134.70	151.98	17.28
4H-3	150	30.20	32.70	2.50	15H-4	150	136.20	153.48	17.28
4H-4	150	31.70	34.20	2.50	15H-5	150	137.70	154.98	17.28
4H-5	150	33.20	35.70	2.50	15H-6	150	139.20	156.48	17.28
4H-6	150	34.70	37.20	2.50	15H-7	38	140.70	157.98	17.28
4H-7	68	36.20	38.70	2.50	15H-CC	27	141.08	158.36	17.28
4H-CC	13	36.88	39.38	2.50	16H-1	150	141.20	159.32	18.12
5H-1	150	36.70	40.63	3.93	16H-2	150	142.70	160.82	18.12
5H-2	150	38.20	42.13	3.93	16H-3	150	144.20	162.32	18.12
5H-3	150	39.70	43.63	3.93	16H-4	150	145.70	163.82	18.12
5H-4	150	41.20	45.13	3.93	16H-5	150	147.20	165.32	18.12
5H-5	150	42.70	46.63	3.93	16H-6	150	148.70	166.82	18.12
5H-6	150	44.20	48.13	3.93	16H-7	56	150.20	168.32	18.12
5H-7	66	45.70	49.63	3.93	16H-CC	27	150.76	168.88	18.12
5H-CC	20	46.36	50.29	3.93	17H-1	150	150.70	169.70	19.00
6H-1	150	46.20	52.73	6.53	17H-2	150	152.20	171.20	19.00
6H-2	150	47.70	54.23	6.53	17H-3	150	153.70	172.70	19.00
6H-3	150	49.20	55.73	6.53	17H-4	150	155.20	174.20	19.00
6H-4	150	50.70	57.23	6.53	17H-5	150	156.70	175.70	19.00
6H-5	150	52.20	58.73	6.53	17H-6	150	158.20	177.20	19.00
6H-6	150	53.70	60.23	6.53	17H-7	46	159.70	178.70	19.00
6H-7	56	55.20	61.73	6.53	17H-CC	18	160.16	179.16	19.00
6H-CC	26	55.76	62.29	6.53	18H-1	150	160.20	179.70	19.50
7H-1	150	55.70	63.67	7.97	18H-2	150	161.70	181.20	19.50
7H-2	150	57.20	65.17	7.97	18H-3	150	163.20	182.70	19.50
7H-3	150	58.70	66.67	7.97	18H-4	150	164.70	184.20	19.50
7H-4	150	60.20	68.17	7.97	18H-5	150	166.20	185.70	19.50
7H-5	150	61.70	69.67	7.97	18H-6	150	167.70	187.20	19.50
7H-6	150	63.20	71.17	7.97	18H-7	64	169.20	188.70	19.50
7H-7	45	64.70	72.67	7.97	18H-CC	20	169.84	189.34	19.50
7H-CC	17	65.15	73.12	7.97	19H-1	150	169.70	190.48	20.78
8H-1	150	65.20	73.98	8.78	19H-2	150	171.20	191.98	20.78
8H-2	150	66.70	75.48	8.78	19H-3	150	172.70	193.48	20.78
8H-3	150	68.20	76.98	8.78	19H-4	150	174.20	194.98	20.78
8H-4	150	69.70	78.48	8.78	19H-5	150	175.70	196.48	20.78
8H-5	150	71.20	79.98	8.78	19H-6	150	177.20	197.98	20.78
8H-6	150	72.70	81.48	8.78	19H-7	64	178.70	199.48	20.78
8H-7	65	74.20	82.98	8.78	19H-CC	20	179.34	200.12	20.78
8H-CC	13	74.85	83.63	8.78	20H-1	150	179.20	199.54	20.34
9H-1	150	74.70	84.53	9.83	20H-2	150	180.70	201.04	20.34
9H-2	150	76.20	86.03	9.83	20H-3	150	182.20	202.54	20.34
9H-3	150	77.70	87.53	9.83	20H-4	150	183.70	204.04	20.34
9H-4	150	79.20	89.03	9.83	20H-5	150	185.20	205.54	20.34
9H-5	150	80.70	90.53	9.83	20H-6	150	186.70	207.04	20.34
9H-6	118	82.20	92.03	9.83	20H-7	51	188.20	208.54	20.34
9H-CC	24	83.38	93.21	9.83	20H-CC	18	188.71	209.05	20.34
10H-1	150	84.20	95.63	11.43	21H-1	150	188.70	209.75	21.05
10H-2	150	85.70	97.13	11.43	21H-2	150	190.20	211.25	21.05
10H-3	150	87.20	98.63	11.43	21H-3	150	191.70	212.75	21.05
10H-4	150	88.70	100.13	11.43	21H-4	150	193.20	214.25	21.05
10H-5	150	90.20	101.63	11.43	21H-5	150	194.70	215.75	21.05
10H-6	150	91.70	103.13	11.43	21H-6	150	196.20	217.25	21.05
10H-7	68	93.20	104.63	11.43	21H-7	60	197.70	218.75	21.05
10H-CC	14	93.88	105.31	11.43	21H-CC	27	198.30	219.35	21.05
11H-1	150	93.70	106.05	12.35	22H-1	150	198.20	220.13	21.93
11H-2	150	95.20	107.55	12.35	22H-2	150	199.70	221.63	21.93
11H-3	150	96.70	109.05	12.35	22H-3	150	201.20	223.13	21.93
11H-4	150	98.20	110.55	12.35	22H-4	150	202.70	224.63	21.93
11H-5	150	99.70	112.05	12.35	22H-5	150	204.20	226.13	21.93
11H-6	150	101.20	113.55	12.35	22H-6	150	205.70	227.63	21.93
11H-7	46	102.70	115.05	12.35	22H-7	26	207.20	229.13	21.93
11H-CC	17	103.16	115.51	12.35	22H-CC	28	207.46	229.39	21.93
12H-1	150	103.20	116.69	13.49	23H-1	150	207.70	230.90	23.20
12H-2	150	104.70	118.19	13.49	23H-2	150	209.20	232.40	23.20

Table 2 (continued).

Core, section	Length (cm)	Depth (mbsf)	Depth (mcd)	Offset (mcd - mbsf)	Core, section	Length (cm)	Depth (mbsf)	Depth (mcd)	Offset (mcd - mbsf)
23H-3	150	210.70	233.90	23.20	8H-6	150	70.00	76.83	6.83
23H-4	150	212.20	235.40	23.20	8H-7	36	71.50	78.33	6.83
23H-5	150	213.70	236.90	23.20	8H-CC	20	71.86	78.69	6.83
23H-6	150	215.20	237.39	23.20	9H-1	150	72.00	79.94	7.94
23H-7	65	216.70	239.90	23.20	9H-2	150	73.50	81.44	7.94
23H-CC	23	217.35	240.55	23.20	9H-3	150	75.00	82.94	7.94
24H-1	150	217.20	241.39	24.19	9H-4	150	76.50	84.44	7.94
24H-2	150	218.70	242.89	24.19	9H-5	150	78.00	85.94	7.94
24H-3	150	220.20	244.39	24.19	9H-6	150	79.50	87.44	7.94
24H-4	150	221.70	245.89	24.19	9H-7	65	81.00	88.94	7.94
24H-5	150	223.20	245.39	24.19	9H-CC	15	81.65	89.59	7.94
24H-6	150	224.70	248.89	24.19	10H-1	150	81.50	90.71	9.21
24H-7	53	226.20	250.39	24.19	10H-2	150	83.00	92.21	9.21
24H-CC	21	226.73	250.92	24.19	10H-3	150	84.50	93.71	9.21
25H-1	150	226.70	252.08	25.38	10H-4	150	86.00	95.21	9.21
25H-2	150	228.20	253.58	25.38	10H-5	150	87.50	96.71	9.21
25H-3	150	229.70	255.08	25.38	10H-6	150	89.00	98.21	9.21
25H-4	150	231.20	256.58	25.38	10H-7	55	90.50	99.71	9.21
25H-5	150	232.70	258.08	25.38	10H-CC	17	91.05	100.26	9.21
25H-6	150	234.20	259.58	25.38	11H-1	150	91.00	101.07	10.07
25H-7	50	235.70	261.08	25.38	11H-2	150	92.50	102.57	10.07
25H-CC	21	236.20	261.58	25.38	11H-3	150	94.00	104.07	10.07
26H-1	150	236.20	261.58	25.38	11H-4	150	95.50	105.57	10.07
26H-2	150	237.70	263.08	25.38	11H-5	150	97.00	107.07	10.07
26H-3	150	239.20	264.58	25.38	11H-6	150	98.50	108.57	10.07
26H-4	150	240.70	266.08	25.38	11H-7	60	100.00	110.07	10.07
26H-5	150	242.20	267.58	25.38	11H-CC	19	100.60	110.67	10.07
26H-6	150	243.70	269.08	25.38	12H-1	150	100.50	110.99	10.49
26H-7	57	245.20	270.58	25.38	12H-2	150	102.00	112.49	10.49
26H-CC	19	245.77	271.15	25.38	12H-3	150	103.50	113.99	10.49
27H-1	150	245.70	271.08	25.38	12H-4	150	105.00	115.49	10.49
27H-2	150	247.20	272.58	25.38	12H-5	150	106.50	116.99	10.49
162-982B-					12H-6	150	108.00	118.49	10.49
1H-1	150	0.00	0.00	0.00	12H-7	52	109.50	119.99	10.49
1H-2	150	1.50	1.50	0.00	12H-CC	19	110.02	120.51	10.49
1H-3	150	3.00	3.00	0.00	13H-1	150	110.00	121.54	11.54
1H-4	88	4.50	4.50	0.00	13H-2	150	111.50	123.04	11.54
1H-CC	18	5.38	5.38	0.00	13H-3	150	113.00	124.54	11.54
2H-1	150	5.50	6.82	1.32	13H-4	150	114.50	126.04	11.54
2H-2	150	7.00	8.32	1.32	13H-5	150	116.00	127.54	11.54
2H-3	150	8.50	9.82	1.32	13H-6	150	117.50	129.04	11.54
2H-4	150	10.00	11.32	1.32	13H-7	62	119.00	130.54	11.54
2H-5	150	11.50	12.82	1.32	13H-CC	19	119.62	131.16	11.54
2H-6	150	13.00	14.32	1.32	14H-1	150	119.50	132.10	12.60
2H-7	62	14.50	15.82	1.32	14H-2	150	121.00	133.60	12.60
2H-CC	21	15.12	16.44	1.32	14H-3	150	122.50	135.10	12.60
3H-1	150	15.00	17.16	2.16	14H-4	150	124.00	136.60	12.60
3H-2	150	16.50	18.66	2.16	14H-5	150	125.50	138.10	12.60
3H-3	150	18.00	20.16	2.16	14H-6	110	127.00	139.60	12.60
3H-4	150	19.50	21.66	2.16	14H-7	90	128.10	140.70	12.60
3H-5	150	21.00	23.16	2.16	14H-CC	26	129.00	141.60	12.60
3H-6	150	22.50	24.66	2.16	15H-1	150	129.00	143.06	14.06
3H-7	58	24.00	26.16	2.16	15H-2	150	130.50	144.56	14.06
3H-CC	18	24.58	26.74	2.16	15H-3	150	132.00	146.06	14.06
4H-1	150	24.50	27.58	3.08	15H-4	150	133.50	147.56	14.06
4H-2	150	26.00	29.08	3.08	15H-5	150	135.00	149.06	14.06
4H-3	150	27.50	30.58	3.08	15H-6	150	136.50	150.56	14.06
4H-4	150	29.00	32.08	3.08	15H-7	62	138.00	152.06	14.06
4H-5	150	30.50	33.58	3.08	15H-CC	16	138.62	152.68	14.06
4H-6	150	32.00	35.08	3.08	16H-1	150	138.50	153.24	14.74
4H-CC	23	33.50	36.58	3.08	16H-2	150	140.00	154.74	14.74
5H-1	150	34.00	38.08	4.08	16H-3	150	141.50	156.24	14.74
5H-2	150	35.50	39.58	4.08	16H-4	150	143.00	157.74	14.74
5H-3	150	37.00	41.08	4.08	16H-5	150	144.50	159.24	14.74
5H-4	150	38.50	42.58	4.08	16H-6	150	146.00	160.74	14.74
5H-5	150	40.00	44.08	4.08	16H-7	52	147.50	162.24	14.74
5H-6	150	41.50	45.58	4.08	16H-CC	21	148.02	162.76	14.74
5H-7	62	43.00	47.08	4.08	17H-1	150	148.00	163.59	15.59
5H-CC	18	43.62	47.70	4.08	17H-2	150	149.50	165.09	15.59
6H-1	150	43.50	49.01	5.51	17H-3	150	151.00	166.59	15.59
6H-2	150	45.00	50.51	5.51	17H-4	150	152.50	168.09	15.59
6H-3	150	46.50	52.01	5.51	17H-5	150	154.00	169.59	15.59
6H-4	150	48.00	53.51	5.51	17H-6	150	155.50	171.09	15.59
6H-5	150	49.50	55.01	5.51	17H-7	18	157.00	172.59	15.59
6H-6	150	51.00	56.51	5.51	17H-CC	25	157.18	172.77	15.59
6H-7	50	52.50	58.01	5.51	18H-1	150	157.50	174.08	16.58
6H-CC	15	53.00	58.51	5.51	18H-2	150	159.00	175.58	16.58
7H-1	150	53.00	58.77	5.77	18H-3	150	160.50	177.08	16.58
7H-2	150	54.50	60.27	5.77	18H-4	150	162.00	178.58	16.58
7H-3	150	56.00	61.77	5.77	18H-5	150	163.50	180.08	16.58
7H-4	150	57.50	63.27	5.77	18H-6	150	165.00	181.58	16.58
7H-5	150	59.00	64.77	5.77	18H-7	50	166.50	183.08	16.58
7H-6	150	60.50	66.27	5.77	18H-CC	14	167.00	183.58	16.58
7H-7	49	62.00	67.77	5.77	19H-1	150	167.00	184.79	17.79
7H-CC	17	62.49	68.26	5.77	19H-2	150	168.50	186.29	17.79
8H-1	150	62.50	69.33	6.83	19H-3	150	170.00	187.79	17.79
8H-2	150	64.00	70.83	6.83	19H-4	150	171.50	189.29	17.79
8H-3	150	65.50	72.33	6.83	19H-5	150	173.00	190.79	17.79
8H-4	150	67.00	73.83	6.83	19H-6	150	174.50	192.29	17.79
8H-5	150	68.50	75.33	6.83	19H-7	49	176.00	193.79	17.79
					19H-CC	30	176.49	194.28	17.79

Table 2 (continued).

Core, section	Length (cm)	Depth (mbsf)	Depth (mcd)	Offset (mcd - mbsf)	Core, section	Length (cm)	Depth (mbsf)	Depth (mcd)	Offset (mcd - mbsf)
20H-1	150	176.50	195.16	18.66	33X-CC	37	305.19	325.78	20.59
20H-2	150	178.00	196.66	18.66	34X-1	150	307.10	327.69	20.59
20H-3	150	179.50	198.16	18.66	34X-2	150	308.60	329.19	20.59
20H-4	150	181.00	199.66	18.66	34X-3	150	310.10	330.69	20.59
20H-5	150	182.50	201.16	18.66	34X-4	150	311.60	332.19	20.59
20H-6	150	184.00	202.66	18.66	34X-5	150	313.10	333.69	20.59
20H-7	57	185.50	204.16	18.66	34X-6	23	314.60	335.19	20.59
20H-CC	14	186.07	204.73	18.66	34X-CC	35	314.83	335.42	20.59
21H-1	150	186.00	205.60	19.60	35X-1	150	316.70	337.29	20.59
21H-2	150	187.50	207.11	19.60	35X-2	150	318.20	338.79	20.59
21H-3	150	189.00	208.60	19.60	35X-3	150	319.70	340.29	20.59
21H-4	150	190.50	210.10	19.60	35X-4	150	321.20	341.79	20.59
21H-5	150	192.00	211.60	19.60	35X-CC	36	322.70	343.29	20.59
21H-6	150	193.50	213.10	19.60	36X-1	150	326.30	346.89	20.59
21H-7	60	195.00	214.60	19.60	36X-2	150	327.80	348.39	20.59
21H-CC	14	195.60	215.20	19.60	36X-3	150	329.30	349.89	20.59
22H-1	150	195.50	214.51	19.01	36X-4	150	330.80	352.89	20.59
22H-2	150	197.00	216.01	19.01	36X-5	69	332.30	352.89	20.59
22H-3	150	198.50	217.51	19.01	36X-CC	36	332.99	353.58	20.59
22H-4	150	200.00	219.01	19.01	37X-1	150	336.00	356.59	20.59
22H-5	150	201.50	220.51	19.01	37X-2	150	337.50	358.09	20.59
22H-6	150	203.00	222.01	19.01	37X-3	150	339.00	359.59	20.59
22H-CC	37	204.50	223.51	19.01	37X-4	150	340.50	361.09	20.59
23H-1	150	205.00	225.42	20.42	37X-5	150	342.00	362.59	20.59
23H-2	150	206.50	226.92	20.42	37X-6	24	343.50	364.09	20.59
23H-3	150	208.00	228.42	20.42	37X-CC	20	343.74	364.33	20.59
23H-4	150	209.50	229.92	20.42	38X-1	150	345.60	366.19	20.59
23H-5	150	211.00	231.42	20.42	38X-2	150	347.10	367.69	20.59
23H-6	130	212.50	232.92	20.42	38X-3	150	348.60	369.19	20.59
23H-CC	38	213.80	234.22	20.42	38X-4	150	350.10	370.69	20.59
24H-1	150	214.50	233.95	19.45	38X-5	150	351.60	372.19	20.59
24H-2	150	216.00	235.45	19.45	38X-6	37	353.10	373.69	20.59
24H-3	150	217.50	236.95	19.45	38X-CC	35	353.47	374.06	20.59
24H-4	150	219.00	238.45	19.45	39X-1	150	355.20	375.79	20.59
24H-5	150	220.50	239.95	19.45	39X-2	150	356.70	377.29	20.59
24H-6	150	222.00	241.45	19.45	39X-3	150	358.20	378.79	20.59
24H-7	46	223.50	242.95	19.45	39X-4	150	359.70	380.29	20.59
24H-CC	9	223.96	243.41	19.45	39X-5	108	361.20	381.79	20.59
25H-1	150	224.00	244.59	20.59	39X-CC	35	362.28	382.87	20.59
25H-2	150	225.50	246.09	20.59	40X-1	150	364.90	385.49	20.59
25H-3	150	227.00	247.59	20.59	40X-2	150	366.40	386.99	20.59
25H-4	150	228.50	249.09	20.59	40X-3	150	367.90	388.49	20.59
25H-5	150	230.00	250.59	20.59	40X-4	150	369.40	389.99	20.59
25H-6	150	231.50	252.09	20.59	40X-5	105	370.90	391.49	20.59
25H-7	24	233.00	253.59	20.59	40X-CC	36	371.95	392.54	20.59
25H-CC	12	233.24	253.83	20.59	41X-1	150	374.50	395.09	20.59
26H-1	150	233.50	254.09	20.59	41X-2	150	376.00	398.09	20.59
26H-2	150	235.00	255.59	20.59	41X-3	150	377.50	398.09	20.59
26H-3	150	236.50	257.09	20.59	41X-4	150	379.00	399.56	20.59
26H-4	150	238.00	258.59	20.59	41X-5	69	380.50	401.09	20.59
26H-5	150	239.50	260.09	20.59	41X-CC	38	381.19	401.78	20.59
26H-6	150	241.00	261.59	20.59	42X-1	150	384.10	404.69	20.59
26H-7	26	242.50	263.09	20.59	42X-2	150	385.60	406.19	20.59
26H-CC	22	242.76	263.35	20.59	42X-3	150	387.10	407.69	20.59
27X-1	150	243.00	263.59	20.59	42X-4	150	388.60	409.19	20.59
27X-2	150	244.50	265.09	20.59	42X-5	21	390.10	410.69	20.59
27X-3	150	246.00	266.59	20.59	42X-CC	34	390.31	410.90	20.59
27X-4	150	247.50	268.09	20.59	43X-1	150	393.80	414.39	20.59
27X-5	30	249.00	269.59	20.59	43X-2	150	395.30	415.89	20.59
27X-CC	21	249.30	269.89	20.59	43X-3	150	396.80	417.39	20.59
28X-1	150	249.30	269.89	20.59	43X-4	134	398.30	418.89	20.59
28X-2	150	250.80	271.39	20.59	43X-CC	27	399.64	420.23	20.59
28X-3	150	252.30	272.89	20.59	44X-1	150	403.40	423.99	20.59
28X-4	150	253.80	274.39	20.59	44X-2	150	404.90	425.49	20.59
28X-5	98	255.30	275.89	20.59	44X-3	150	406.40	426.99	20.59
28X-CC	22	256.28	276.87	20.59	44X-4	150	407.90	428.49	20.59
29X-1	150	258.90	279.49	20.59	44X-5	40	409.40	429.99	20.59
29X-2	150	260.40	280.99	20.59	44X-CC	40	409.80	430.39	20.59
29X-3	150	261.90	282.49	20.59	45X-1	150	413.00	433.59	20.59
29X-4	108	263.40	283.99	20.59	45X-2	150	414.50	435.09	20.59
29X-CC	19	264.48	285.07	20.59	45X-3	150	416.00	436.59	20.59
30X-CC	8	268.50	289.03	20.59	45X-4	150	417.50	438.09	20.59
31X-1	150	278.20	298.79	20.59	45X-5	150	419.00	439.59	20.59
31X-2	150	279.70	300.29	20.59	45X-6	150	420.50	441.09	20.59
31X-3	150	281.20	301.79	20.59	45X-7	40	422.00	442.59	20.59
31X-4	150	282.70	303.29	20.59	45X-CC	35	422.40	442.99	20.59
31X-5	150	284.20	304.79	20.59	46X-1	150	422.60	443.19	20.59
31X-6	150	285.70	306.29	20.59	46X-2	150	424.10	444.69	20.59
31X-7	37	287.20	307.79	20.59	46X-3	150	425.60	446.19	20.59
31X-CC	21	287.57	308.16	20.59	46X-4	150	427.10	447.69	20.59
32X-1	150	287.80	308.39	20.59	46X-5	106	428.60	449.19	20.59
32X-2	150	289.30	309.89	20.59	46X-CC	37	429.66	450.25	20.59
32X-3	150	290.80	311.39	20.59	47X-1	150	432.20	452.79	20.59
32X-4	98	292.30	312.89	20.59	47X-2	150	433.70	454.29	20.59
32X-CC	36	293.28	313.87	20.59	47X-3	150	435.20	455.79	20.59
33X-1	150	297.40	317.99	20.59	47X-4	150	436.70	457.29	20.59
33X-2	150	298.90	319.49	20.59	47X-CC	47	438.20	458.79	20.59
33X-3	150	300.40	320.99	20.59	48X-1	150	441.80	462.39	20.59
33X-4	150	301.90	322.49	20.59	48X-2	150	443.30	463.89	20.59
33X-5	150	303.40	323.99	20.59	48X-3	150	444.80	465.39	20.59
33X-6	29	304.90	325.49	20.59	48X-4	150	446.30	466.89	20.59

Table 2 (continued).

Core, section	Length (cm)	Depth (mbsf)	Depth (mcd)	Offset (mcd - mbsf)	Core, section	Length (cm)	Depth (mbsf)	Depth (mcd)	Offset (mcd - mbsf)
48X-5	150	447.80	468.39	20.59	2H-5	150	9.80	9.00	-0.80
48X-6	45	449.30	469.89	20.59	2H-6	150	11.30	10.50	-0.80
48X-CC	40	449.75	470.57	20.59	2H-7	54	12.80	12.00	-0.80
49X-1	150	451.40	471.99	20.59	2H-CC	15	13.34	12.54	-0.80
49X-2	150	452.90	473.49	20.59	3H-1	150	13.30	13.28	-0.02
49X-3	150	454.40	474.99	20.59	3H-2	150	14.80	14.78	-0.02
49X-4	150	455.90	476.49	20.59	3H-3	150	16.30	16.28	-0.02
49X-5	70	457.40	477.99	20.59	3H-4	150	17.80	17.78	-0.02
49X-CC	30	458.10	478.69	20.59	3H-5	150	19.30	19.28	-0.02
50X-1	150	461.00	481.59	20.59	3H-6	150	20.80	20.78	-0.02
50X-2	150	462.50	483.09	20.59	3H-7	86	22.30	22.28	-0.02
50X-3	150	464.00	484.59	20.59	3H-CC	16	23.16	23.14	-0.02
50X-4	150	465.50	486.09	20.59	4H-1	150	22.80	26.32	3.52
50X-5	41	467.00	487.59	20.59	4H-2	150	24.30	27.82	3.52
50X-CC	29	467.41	488.00	20.59	4H-3	150	25.80	29.32	3.52
51X-1	150	470.60	491.19	20.59	4H-4	150	27.30	30.82	3.52
51X-2	150	472.10	492.69	20.59	4H-5	150	28.80	32.32	3.52
51X-3	150	473.60	494.19	20.59	4H-6	150	30.30	33.82	3.52
51X-4	150	475.10	495.69	20.59	4H-7	85	31.80	35.32	3.52
51X-5	150	476.60	497.19	20.59	4H-CC	21	32.65	36.17	3.52
51X-6	55	478.10	498.69	20.59	5H-1	150	32.30	35.56	3.26
51X-CC	34	478.65	499.24	20.59	5H-2	150	33.80	37.06	3.26
52X-1	150	480.20	500.79	20.59	5H-3	150	35.30	38.56	3.26
52X-2	150	481.70	502.29	20.59	5H-4	150	36.80	40.06	3.26
52X-3	150	483.20	503.79	20.59	5H-5	150	38.30	41.56	3.26
52X-4	150	484.70	505.29	20.59	5H-6	150	39.80	43.06	3.26
52X-5	150	486.20	506.79	20.59	5H-7	63	41.30	44.56	3.26
52X-6	60	487.70	508.29	20.59	5H-CC	24	41.93	45.19	3.26
52X-CC	40	488.30	508.89	20.59	6H-1	150	41.80	46.38	4.58
53X-1	150	489.70	510.29	20.59	6H-2	150	43.30	47.88	4.58
53X-2	150	491.20	511.79	20.59	6H-3	150	44.80	49.38	4.58
53X-3	150	492.70	513.29	20.59	6H-4	150	46.30	50.88	4.58
53X-4	150	494.20	514.79	20.59	6H-5	150	47.80	52.38	4.58
53X-5	150	495.70	516.29	20.59	6H-6	150	49.30	53.88	4.58
53X-6	107	497.20	517.79	20.59	6H-7	55	50.80	55.38	4.58
53X-CC	37	498.27	518.86	20.59	6H-CC	17	51.35	55.93	4.58
54X-1	150	499.30	519.89	20.59	7H-1	150	51.30	56.95	5.65
54X-2	150	500.80	521.39	20.59	7H-2	150	52.80	58.45	5.65
54X-3	150	502.30	522.89	20.59	7H-3	150	54.30	59.95	5.65
54X-4	150	503.80	524.39	20.59	7H-4	150	55.80	61.45	5.65
54X-5	56	505.30	525.89	20.59	7H-5	150	57.30	62.95	5.65
54X-CC	37	505.86	526.45	20.59	7H-6	150	58.80	64.45	5.65
55X-1	150	508.90	529.49	20.59	7H-7	56	60.30	65.95	5.65
55X-2	150	510.40	530.99	20.59	7H-CC	23	60.86	66.51	5.65
55X-3	150	511.90	532.49	20.59	8H-1	150	60.80	66.59	5.79
55X-4	150	513.40	533.99	20.59	8H-2	150	62.30	68.09	5.79
55X-5	150	514.90	535.49	20.59	8H-3	150	63.80	69.59	5.79
55X-6	150	516.40	536.99	20.59	8H-4	150	65.30	71.09	5.79
55X-7	42	517.90	538.49	20.59	8H-5	150	66.80	72.59	5.79
55X-CC	25	518.32	538.91	20.59	8H-6	150	68.30	74.09	5.79
56X-1	150	518.50	539.09	20.59	8H-7	54	69.80	75.59	5.79
56X-2	150	520.00	540.59	20.59	8H-CC	22	70.34	76.13	5.79
56X-3	150	521.50	542.09	20.59	9H-1	150	70.30	76.12	5.82
56X-4	150	523.00	543.59	20.59	9H-2	150	71.80	77.62	5.82
56X-5	150	524.50	545.09	20.59	9H-3	150	73.30	79.12	5.82
56X-6	150	526.00	546.59	20.59	9H-4	150	74.80	80.62	5.82
56X-7	40	527.50	548.09	20.59	9H-5	150	76.30	82.12	5.82
56X-CC	45	527.90	548.49	20.59	9H-6	150	77.80	83.62	5.82
57X-1	150	528.10	548.69	20.59	9H-7	51	79.30	85.12	5.82
57X-2	150	529.60	550.19	20.59	9H-CC	25	79.81	85.63	5.82
57X-3	150	531.10	551.69	20.59	10H-1	150	79.80	86.99	7.19
57X-4	150	532.60	553.19	20.59	10H-2	150	81.30	88.49	7.19
57X-5	128	534.10	554.69	20.59	10H-3	150	82.80	89.99	7.19
57X-CC	36	535.38	555.97	20.59	10H-4	150	84.30	91.49	7.19
58X-1	150	537.70	558.29	20.59	10H-5	150	85.80	92.99	7.19
58X-2	150	539.20	559.79	20.59	10H-6	150	87.30	94.49	7.19
58X-3	58	540.70	561.29	20.59	10H-7	56	88.80	95.99	7.19
58X-CC	33	541.28	561.87	20.59	10H-CC	19	89.36	96.55	7.19
59X-CC	70	547.40	567.99	20.59	11H-1	150	89.30	97.47	8.17
60X-1	150	557.00	577.59	20.59	11H-2	150	90.80	98.97	8.17
60X-2	150	558.50	579.09	20.59	11H-3	150	92.30	100.47	8.17
60X-3	84	560.00	580.59	20.59	11H-4	150	93.80	101.97	8.17
60X-CC	36	560.84	581.43	20.59	11H-5	150	95.30	103.47	8.17
61X-1	150	566.70	587.29	20.59	11H-6	150	96.80	104.97	8.17
61X-2	150	568.20	588.79	20.59	11H-7	80	98.30	106.47	8.17
61X-3	23	569.70	590.29	20.59	11H-CC	22	99.10	107.27	8.17
61X-CC	32	569.93	590.52	20.59	12H-1	150	98.80	107.85	9.05
62X-1	47	576.40	596.99	20.59	12H-2	150	100.30	109.35	9.05
62X-CC	31	576.87	597.46	20.59	12H-3	150	101.80	110.85	9.05
63X-CC	38	586.00	606.59	20.59	12H-4	150	103.30	112.35	9.05
64X-CC	47	595.60	616.19	20.59	12H-5	150	104.80	113.85	9.05
65X-CC	21	605.30	626.89	20.59	12H-6	150	106.30	115.35	9.05
162-982C-					12H-7	53	107.80	116.85	9.05
1H-1	150	0.00	0.15	0.15	12H-CC	27	108.33	117.38	9.05
1H-2	150	1.50	1.65	0.15	13H-1	150	108.30	118.75	10.45
1H-3	60	3.00	3.15	0.15	13H-2	150	109.80	120.25	10.45
1H-CC	18	3.60	3.75	0.15	13H-3	150	111.30	121.75	10.45
2H-1	150	3.80	3.00	-0.80	13H-4	150	112.80	123.25	10.45
2H-2	150	5.30	4.50	-0.80	13H-5	150	114.30	124.75	10.45
2H-3	150	6.80	6.00	-0.80	13H-6	150	115.80	126.25	10.45
2H-4	150	8.30	7.50	-0.80	13H-7	47	117.30	127.75	10.45

Table 2 (continued).

Core, section	Length (cm)	Depth (mbsf)	Depth (mcd)	Offset (mcd – mbsf)	Core, section	Length (cm)	Depth (mbsf)	Depth (mcd)	Offset (mcd – mbsf)
13H-CC	22	117.77	128.22	10.45	21H-6	100	191.80	211.70	19.90
14H-1	150	117.80	128.93	11.13	21H-7	90	192.80	212.70	19.90
14H-2	150	119.30	130.43	11.13	21H-CC	17	193.70	213.60	19.90
14H-3	150	120.80	131.93	11.13	22H-1	150	193.80	212.68	18.88
14H-4	150	122.30	133.43	11.13	22H-2	150	195.30	214.18	18.88
14H-5	150	123.80	134.93	11.13	22H-3	150	196.80	215.68	18.88
14H-6	150	125.30	136.43	11.13	22H-4	150	198.30	217.18	18.88
14H-7	60	126.80	137.93	11.13	22H-5	150	199.80	218.68	18.88
14H-CC	26	127.40	138.53	11.13	22H-6	150	201.30	220.18	18.88
15H-1	150	127.30	140.38	13.08	22H-7	67	202.80	221.68	18.88
15H-2	150	128.80	141.88	13.08	22H-CC	20	203.47	222.35	18.88
15H-3	150	130.30	143.38	13.08	23H-1	150	203.30	223.09	19.79
15H-4	150	131.80	144.88	13.08	23H-2	125	204.80	224.59	19.79
15H-5	150	133.30	146.38	13.08	23H-3	57	206.05	225.84	19.79
15H-6	150	134.80	147.88	13.08	23H-4	150	206.62	226.41	19.79
15H-7	45	136.30	149.38	13.08	23H-5	150	208.12	227.91	19.79
15H-CC	18	136.75	149.83	13.08	23H-6	150	209.62	229.41	19.79
16H-1	150	136.80	150.68	13.88	23H-7	52	211.12	230.91	19.79
16H-2	150	138.30	152.18	13.88	23H-CC	85	211.64	231.43	19.79
16H-3	150	139.80	153.68	13.88	24H-1	150	212.80	232.40	19.60
16H-4	150	141.30	155.18	13.88	24H-2	150	214.30	233.90	19.60
16H-5	150	142.80	156.68	13.88	24H-3	150	215.80	235.40	19.60
16H-6	150	144.30	158.18	13.88	24H-4	150	217.30	236.90	19.60
16H-7	55	145.80	159.68	13.88	24H-5	150	218.80	238.40	19.60
16H-CC	16	146.35	160.23	13.88	24H-6	150	220.30	239.90	19.60
17H-1	150	146.30	161.75	14.45	24H-7	59	221.80	241.40	19.60
17H-2	150	147.80	162.25	14.45	24H-CC	20	222.39	241.99	19.60
17H-3	150	149.30	164.75	14.45	25H-1	150	222.30	242.96	20.66
17H-4	150	150.80	165.25	14.45	25H-2	150	223.80	244.46	20.66
17H-5	150	152.30	166.75	14.45	25H-3	150	225.30	245.96	20.66
17H-6	150	153.80	168.25	14.45	25H-4	150	226.80	247.46	20.66
17H-7	75	155.30	169.75	14.45	25H-5	150	228.30	248.96	20.66
17H-CC	23	156.05	170.50	14.45	25H-6	150	229.80	250.46	20.66
18H-1	150	155.80	171.69	15.89	25H-7	55	231.30	251.96	20.66
18H-2	150	157.30	173.19	15.89	25H-CC	21	231.85	252.51	20.66
18H-3	150	158.80	174.69	15.89	26H-1	150	231.80	252.46	20.66
18H-4	150	160.30	176.19	15.89	26H-2	150	233.30	253.96	20.66
18H-5	150	161.80	177.69	15.89	26H-3	150	234.80	255.46	20.66
18H-6	150	163.30	179.19	15.89	26H-4	150	236.30	256.96	20.66
18H-7	48	164.80	180.69	15.89	26H-5	150	237.80	258.46	20.66
18H-CC	18	165.28	181.17	15.89	26H-6	150	239.30	259.96	20.66
19H-1	150	165.30	181.73	16.43	26H-7	63	240.80	261.46	20.66
19H-2	150	166.80	183.23	16.43	26H-CC	22	241.43	262.09	20.66
19H-3	150	168.30	184.73	16.43	27H-1	150	241.30	261.96	20.66
19H-4	150	169.80	186.23	16.43	27H-2	150	242.80	263.46	20.66
19H-5	150	171.30	187.73	16.43	27H-3	150	244.30	264.96	20.66
19H-6	150	172.80	189.23	16.43	27H-4	150	245.80	266.46	20.66
19H-7	70	174.30	190.73	16.43	27H-5	150	247.30	267.96	20.66
19H-CC	18	175.00	191.43	16.43	27H-6	150	248.80	269.46	20.66
20H-1	150	174.80	193.21	18.41	27H-7	62	250.30	270.96	20.66
20H-2	150	176.30	194.71	18.41	27H-CC	16	250.92	271.58	20.66
20H-3	150	177.80	196.21	18.41	162-982D-				
20H-4	150	179.30	197.71	18.41	1H-1	150	20.00	21.93	1.93
20H-5	94	180.80	199.21	18.41	1H-2	150	21.50	23.43	1.93
20H-6	90	181.74	200.15	18.41	1H-3	150	23.00	24.93	1.93
20H-CC	32	182.64	201.05	18.41	1H-4	150	24.50	26.43	1.93
21H-1	150	184.30	204.20	19.90	1H-5	150	26.00	27.93	1.93
21H-2	150	185.80	205.70	19.90	1H-6	150	27.50	29.43	1.93
21H-3	150	187.30	207.20	19.90	1H-7	57	29.00	30.93	1.93
21H-4	150	188.80	208.70	19.90	1H-CC	21	29.57	31.50	1.93
21H-5	150	190.30	210.20	19.90					

Note: Depths are from the top of each section.

Spectral reflectance in the 650–700-nm band (see “Lithostratigraphy” section, this chapter) and gamma-ray attenuation porosity (GRAPE) were the primary parameters used to develop the composite section. Magnetic susceptibility measurements collected at 3-cm intervals were useful for correlations between the upper six cores in each hole, but dropped to background levels by 60 mcd. Natural gamma radiation and *P*-wave velocity measurements from the multisensor track (MST) were also used to confirm the hole-to-hole correlations. Magnetic susceptibility, GRAPE, and natural gamma radiation tended to be positively correlated. GRAPE and spectral reflectance data showed a weak negative correlation in the upper 40 mcd and a positive correlation below that. The relative independence of GRAPE and reflectance commonly made it possible to resolve and correlate sedimentary features in one record that were not apparent in the other. MST and spectral reflectance records that were used for correlation are displayed on the mcd scale in Figure 2 (see also back pocket).

The base of the composite depth section is at 255 mcd. The remainder of the Hole 982B cores have been appended to the composite below this depth. No adjustments of relative depths of the Hole 982B cores were made below 245 mcd. Due to the relatively poor recovery in the XCB cores (Cores 982B-27X and deeper), there are significant gaps in the sedimentary sequence in this interval, as demonstrated by comparison to the wireline log of Hole 982B (see “Wireline Logging” section, this chapter).

The mcd scale grows, relative to the mbsf scale, for Holes 982B and 982C by about 10% over the range of the composite section (Fig. 3). This growth is presumably caused by physical expansion of the cores after recovery, and by stretching of the sequence during the coring process. Hole 982A offsets grew by about 13% with depth. The growth rates within each hole are relatively constant compared to the differences between holes, demonstrating that not only decompression and warming from in situ conditions, but also the coring process itself, are causes of expansion.

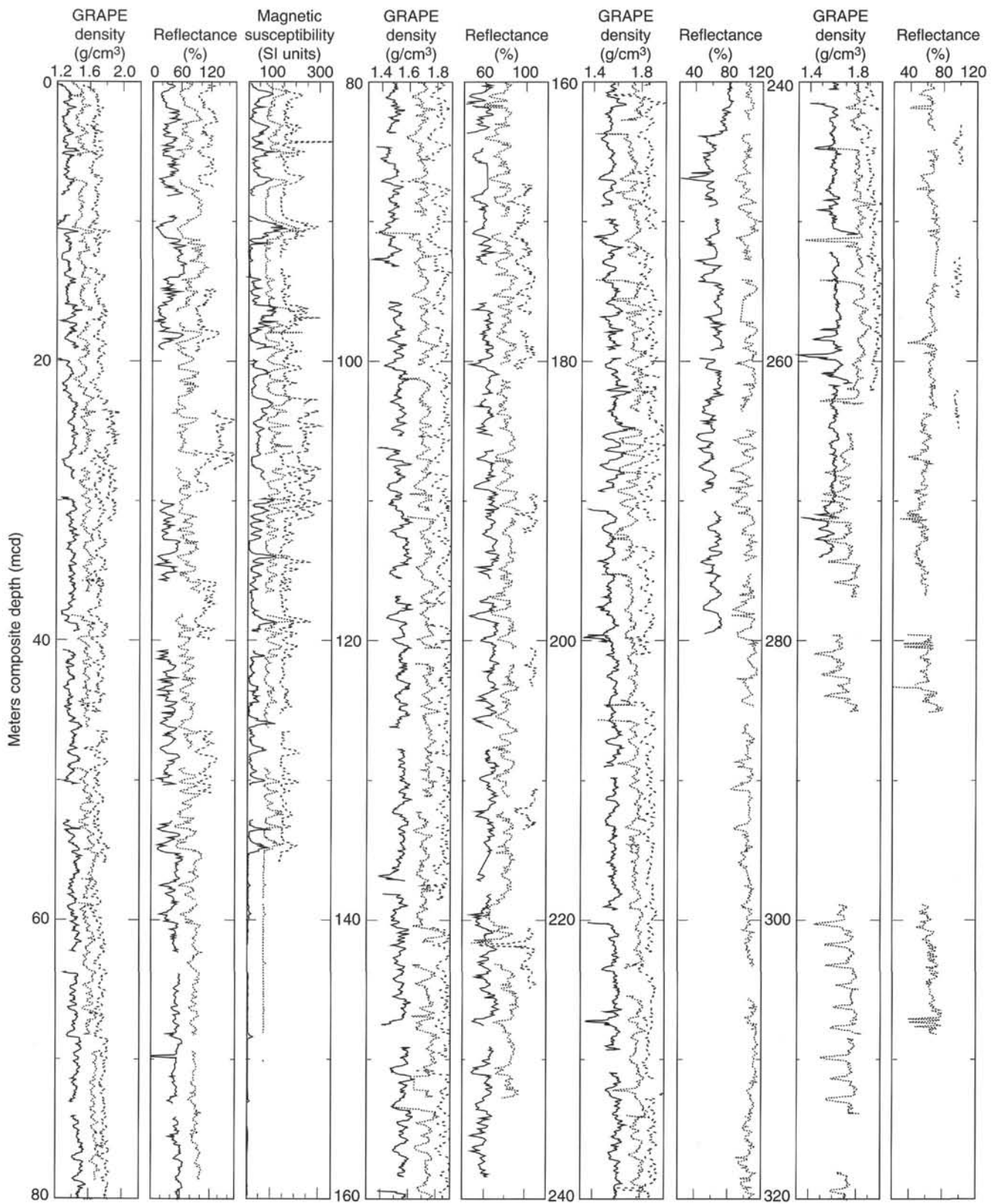


Figure 2. GRAPE density, spectral reflectance (650–700 nm), and magnetic susceptibility data from Site 982 on the mcd (meters composite depth) scale. Lines for Holes 982B (dotted), 982C (dashed), and 982D (long dashed, 24–32 mcd) have been horizontally offset from line for Hole 982A (solid) for better display; therefore, values given on horizontal scale are the true values only for Hole 982A. (See also back pocket.)

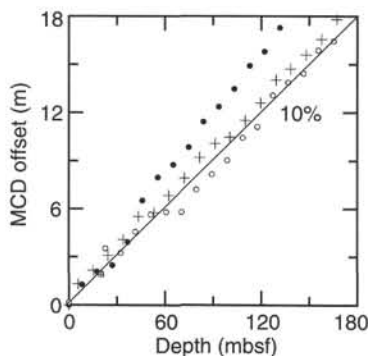


Figure 3. Depth offsets of the Site 982 meters composite depth scale relative to meters below seafloor depth, indicating the "growth" of the composite depth scale. Solid circles = Hole 982A, crosses = Hole 982B, open circles = Hole 982C, square with cross = Hole 982D.

After construction of the composite depth section for Site 982, a single spliced record was developed as discussed in the "Explanatory Notes" chapter (this volume). Although continuity of the sedimentary sequence was confirmed through 255 mcd, the exact alignment of events between adjacent holes was locally ambiguous below 245 mcd. Therefore, the spliced record was assembled only to that depth. The tie points between the cores used to construct the splice are given in Table 3. The spliced reflectance and GRAPE data are shown in Figure 4.

LITHOSTRATIGRAPHY

Four holes were drilled at Site 982, with a maximum penetration of 614.9 mbsf. The sediments have an average calcium carbonate content of around 86%. Nannofossil ooze and chalk dominate the sequence. Shallow intervals (<57 m) also contain variable amounts of clay, clayey nannofossil mixed sediments, and clays with variable amounts of nannofossils and silt. Authigenic components include the minor but ubiquitous presence of iron sulfides primarily in the form of disseminated pyrite.

The primary lithostratigraphic units for the Site 982 sedimentary sequence are defined on the basis of data obtained from eight sources: (1) visual observation of color, (2) smear slide examination, (3) bulk calcium carbonate measurements (three per core selected to represent the extremes of color), (4) spectral reflectance measurements, (5) magnetic susceptibility measurements, (6) natural gamma-ray measurements, (7) X-ray diffraction analysis, and (8) discrete velocity measurements. A distinct boundary dividing the sequence into two units occurs at approximately 57 mbsf. The boundary is marked by sharp downcore decreases in siliciclastic sediments and magnetic susceptibility (see "Physical Properties" section, this chapter) and sharp downcore increases in calcium carbonate content and spectral reflectance (Fig. 5). More subtle changes in the above data are used to divide both units into subunits (Table 4). All unit and subunit boundary depths are given for Hole 982B.

Description of Lithostratigraphic Units

Unit I

Intervals:

- Core 162-982A-1H through Section 7H-5
- Core 162-982B-1H through Section 7H-3
- Cores 162-982C-1H through Section 7H-5
- Core 162-982D-1H

Age: Holocene to late Pliocene

Depth: 0 to 57.4 mbsf

Table 3. Site 982 splice tie points.

Hole, core, section (cm)	Depth (mbsf)	Depth (mcd)		Hole, core, section (cm)	Depth (mbsf)	Depth (mcd)
162-982-				162-982-		
A-1H-6, 17	7.68	7.68	tie to	B-2H-1, 8	56.36	7.68
B-2H-7, 1	14.52	15.84	tie to	C-3H-2, 105	15.86	15.84
C-3H-4, 89	18.70	18.68	tie to	B-3H-2, 1	16.52	18.68
B-3H-5, 140	22.40	24.56	tie to	D-1H-2, 113	22.63	24.56
D-1H-5, 22	26.22	28.15	tie to	B-4H-1, 58	25.07	28.15
B-4H-6, 73	32.74	35.82	tie to	C-5H-1, 25	32.56	35.82
C-5H-3, 57	35.88	39.14	tie to	B-5H-1, 105	35.06	39.14
B-5H-6, 89	42.40	46.48	tie to	C-6H-1, 9	41.90	46.48
C-6H-3, 65	45.46	50.04	tie to	B-6H-1, 102	44.53	50.04
B-6H-6, 97	51.98	57.49	tie to	A-6H-4, 25	50.96	57.49
A-6H-5, 97	53.18	59.71	tie to	B-7H-1, 93	53.94	59.71
B-7H-5, 145	60.46	66.23	tie to	A-7H-2, 105	58.26	66.23
A-7H-4, 137	61.58	69.55	tie to	B-8H-1, 21	62.72	69.55
B-8H-5, 2	68.53	75.36	tie to	A-8H-1, 137	66.58	75.36
A-8H-5, 97	72.18	80.96	tie to	B-9H-1, 101	73.02	80.96
B-9H-6, 130	80.81	88.75	tie to	C-10H-2, 25	81.56	88.75
C-10H-7, 3	88.84	96.03	tie to	B-10H-4, 81	86.82	96.03
B-10H-6, 25	89.26	98.47	tie to	A-10H-2, 133	87.04	98.47
A-10H-6, 81	92.52	103.95	tie to	B-11H-2, 137	93.88	103.95
B-11H-6, 73	99.24	109.31	tie to	A-11H-3, 25	96.96	109.31
A-11H-5, 23	99.94	112.29	tie to	B-12H-1, 129	101.80	112.29
B-12H-7, 11	109.62	120.11	tie to	A-12H-3, 41	106.62	120.11
A-12H-5, 124	110.45	123.94	tie to	B-13H-2, 89	112.40	123.94
B-13H-6, 73	118.24	129.78	tie to	A-13H-2, 65	114.86	129.78
A-13H-4, 121	118.42	133.34	tie to	B-14H-1, 123	120.74	133.34
B-14H-7, 33	128.44	141.04	tie to	C-15H-1, 65	127.96	141.04
C-15H-3, 25	130.56	143.64	tie to	B-15H-1, 57	129.58	143.64
B-15H-6, 49	137.00	151.06	tie to	A-15H-2, 57	133.78	151.06
A-15H-5, 73	138.44	155.72	tie to	B-16H-2, 97	140.98	155.72
B-16H-6, 82	146.82	161.56	tie to	A-16H-1, 74	143.44	161.56
A-16H-6, 84	149.54	167.66	tie to	B-17H-3, 107	152.07	167.66
B-17H-6, 18	155.68	171.27	tie to	A-17H-2, 7	152.27	171.27
A-17H-6, 51	158.71	177.71	tie to	B-18H-3, 63	161.13	177.71
B-18H-6, 58	165.58	182.16	tie to	A-18H-2, 96	162.66	182.16
A-18H-6, 139	169.09	188.59	tie to	B-19H-3, 80	170.80	188.59
B-19H-6, 122	175.72	193.51	tie to	C-20H-1, 30	175.10	193.51
C-20H-4, 7	179.37	197.78	tie to	B-20H-2, 112	179.12	197.78
B-20H-5, 142	183.92	202.58	tie to	A-20H-3, 4	182.24	202.58
A-20H-6, 23	186.93	207.27	tie to	C-21H-3, 7	187.37	207.27
C-21H-6, 4	191.84	211.74	tie to	A-21H-2, 49	190.69	211.74
A-21H-7, 28	197.98	219.03	tie to	C-22H-5, 35	200.15	219.03
C-22H-6, 91	202.21	221.09	tie to	A-22H-1, 96	199.16	221.09
A-22H-6, 88	206.58	228.51	tie to	B-23H-3, 9	208.09	228.51
B-23H-5, 44	211.44	231.86	tie to	A-23H-1, 96	208.66	231.86
A-23H-4, 14	212.34	235.54	tie to	B-24H-2, 9	216.09	235.54
B-24H-7, 12	223.62	243.07	tie to	A-24H-2, 18	218.88	243.07
A-24H-5, 90	224.10	248.29	tie to	B-25H-3, 70	227.70	248.29
B-62X-1, 39	576.79	597.38				

Unit I sediments are dominated by variable amounts of calcareous nannofossils, clay, and, to a lesser extent, silt and foraminifers. Trace amounts of biogenic silica are present with abundances in the following order: sponge spicules, diatoms, radiolarians, and silicoflagellates. Calcium carbonate averages 57.7%, ranging from 8.3% to 94.2% and having a standard deviation of 29.8%. These variations are responsible for the considerable color contrast observed between the oozes and clays within the unit, which are similar to those observed at Sites 980 and 981. The compositional changes form distinct high-amplitude cyclic variations which occur on an 0.5- to 3-m scale and that are mainly related to fluctuations in the proportions of biogenic carbonate, detrital clay minerals, and, to a lesser extent, detrital silt. Color bands and mottles of green, gray, and black hues are present throughout the unit and appear to be in response to the extensive bioturbation and associated reducing conditions.

Two subunits are defined. Subunit IA (0–49.4 mbsf) exhibits the most compositional variation recovered at this site. Carbonate values and spectral reflectance are high throughout the entire site. It is only in the dark layers of Subunit IA that carbonate values drop as low as 8.3%. Spectral reflectance is commonly as low as 20% (Fig. 6A). The subunit consists of alternating intervals of four lithofacies: (1) very light gray, light gray, gray, pale yellow, and very light brown nannofossil ooze, and nannofossil ooze with foraminifers, (2) gray to dark gray clayey nannofossil mixed sediment, nannofossil clayey mixed sediment with foraminifers and quartz, and silty clayey nannofossil

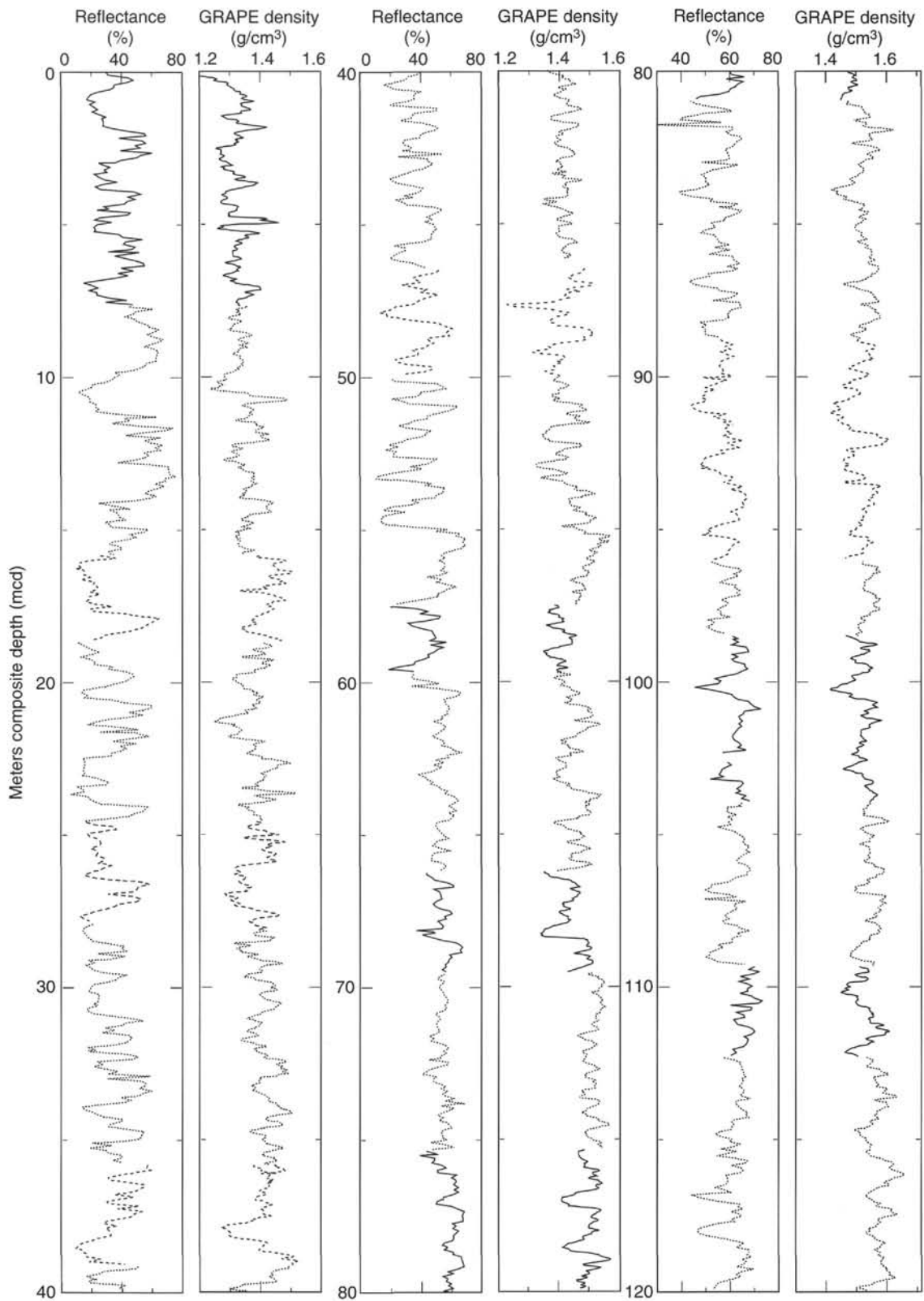


Figure 4. Spliced record of GRAPE density and spectral reflectance (650–700 nm) from Site 982. Tie points for forming the splice are given in Table 3. Holes are: 982A (solid), 982B (dotted), 982C (dashed), and 982D (long dashed).

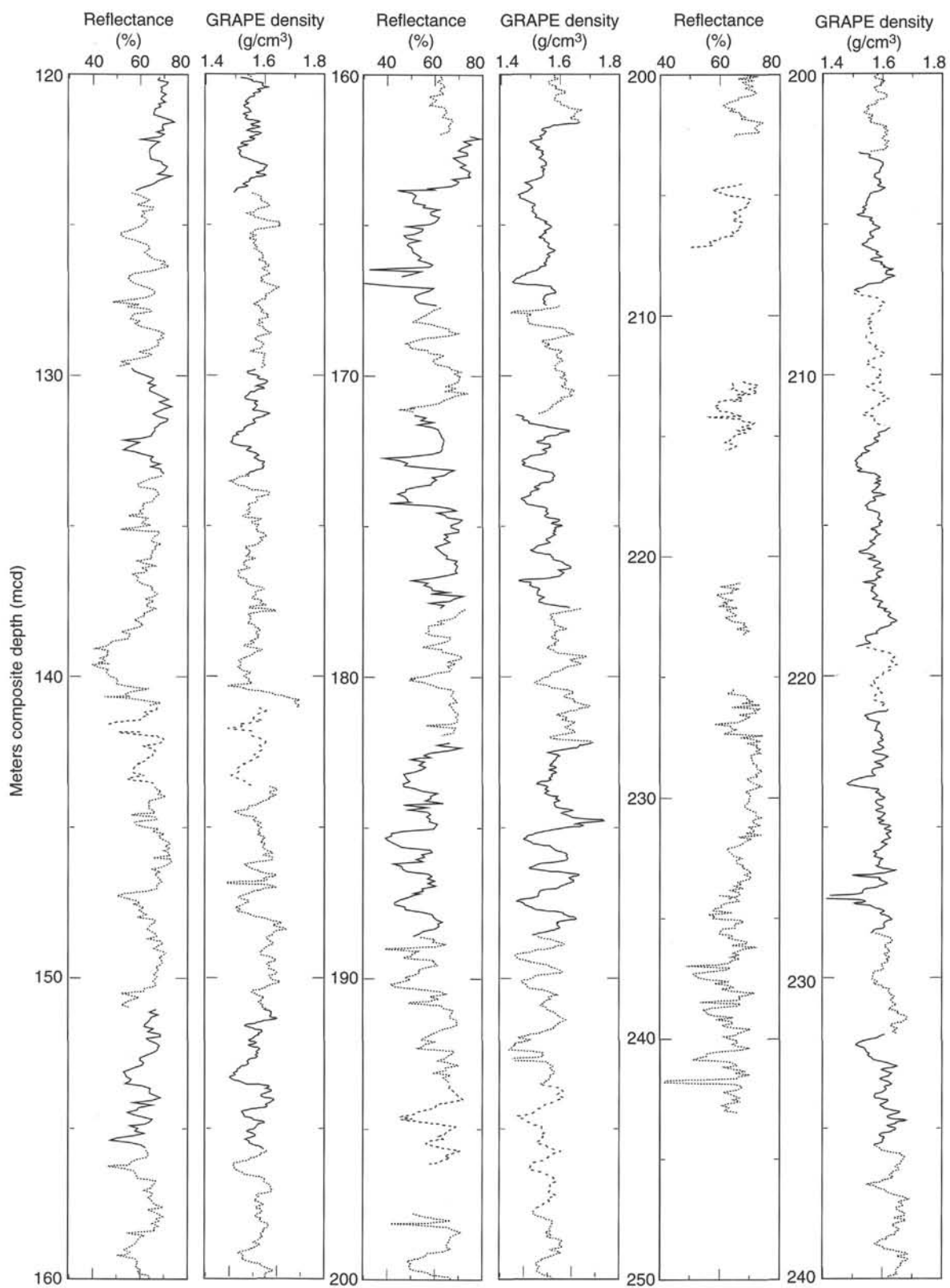


Figure 4 (continued).

Table 4. Summary table of lithostratigraphic units and subunits at Site 982.

Unit	Subunit	Depth (mbsf)	Thickness (m)	Age	Dominant lithologies/criteria	Calcium carbonate (%)			
						Mean	Min.	Max.	St. dev.
I		0–57.4	57.4	Pleist.–late Plio.	High-amplitude, cyclic (0.5 to 3 m) lithologic changes	57.5	8.3	94.2	29.8
	IA	0–49.4	49.4	Pleist.–late Plio.	Nannofossil ooze, nannofossil clay, silty clay/high-variation lithologic changes, terrigenous and biogenic components about equal				
	IB	49.4–57.4	8.0	late Pliocene	Nannofossil ooze, nannofossil clay/lower variation lithologic changes, more biogenic than terrigenous material				
II		57.4–614.9	557.5	late Plio.–mid. Mio.	Dominantly nannofossil ooze and chalk, low-amplitude lithologic changes at varying frequencies	90.8	69.6	95.0	3.7
	IIA	57.4–166.5	109.1	late Plio.–early Plio.	Nannofossil ooze/minor lithologic variation on meter scale (>2 m), ash layers common	90.6	87.0	93.9	2.0
	IIB	166.5–195.5	29.0	late Miocene	Nannofossil ooze, nannofossil ooze with clay/larger lithologic variation (1–3 m scale)	89.1	83.4	94.3	3.5
	IIC	195.5–480.0	284.5	late Mio.–mid. Mio.	Nannofossil ooze to chalk transition/minor lithologic variation, ash layers common	92.6	88.4	95.0	1.5
	IID	480.0–614.9	134.9	mid. Miocene	Nannofossil chalk/downcore increase in lithologic variability, poor recovery, especially in lower section	84.7	69.6	93.0	7.0

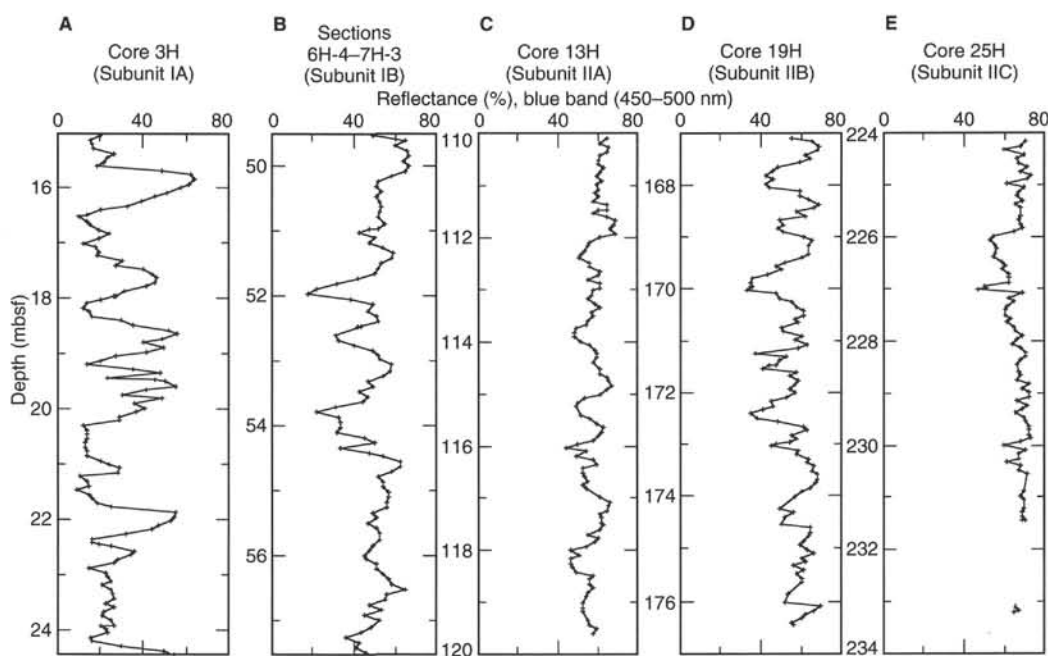


Figure 6. A–E. Percentage reflectance (blue band, 450–500 nm) for selected sections representative of lithostratigraphic units and subunits, Hole 982B.

mixed sediment, (3) light gray, gray, and dark gray, nannofossil silty clay, silty clay with nannofossils, and silty clay with nannofossils and sand, and (4) brown, grayish brown, and very dark gray silty clay. Thin layers (1 mm) of sandy silt are present in some of the more siliciclastic rich layers. XRD and smear slide analyses reveal that quartz, inorganic calcite, and feldspar dominate the detrital silt component found in the silty dark gray clay layers, with trace amounts of mica and glauconite.

In Subunit IA, cyclic dark (low carbonate) to light (high carbonate) color changes occur at submeter to meter scales, with color boundaries ranging from gradational to sharp, with bioturbation common at both types of color boundaries. They correspond with the 5- to 10-m-scale cycles observed at Sites 980 and 981, and like the cycles at those sites, higher frequency color and spectral reflectance variations are superimposed on these cycles. Upsection transitions from light to dark are commonly sharper than the more gradual tran-

sitions from dark to light. There are roughly equal proportions of siliciclastic-rich and biogenic-rich sediment.

Like Subunit IA, Subunit IB (49.4–57.4 mbsf) contains cyclic lithologic changes. The lithologies, however, are dominated by biogenic sediments, particularly light to very light gray nannofossil ooze with foraminifers, with only minor amounts of gray nannofossil clay. The dominance of the biogenic component is well displayed in the high spectral reflectance pattern for this subunit (Fig. 6B).

All dropstones observed in Site 982 sediments occur in Unit I. In all, 18 dropstones greater than 1 cm in size were identified (Table 5; Fig. 5). As at Sites 980 and 981, most occur in the dark- and medium-colored intervals within Unit I, suggesting that these darker sediments accumulated under the influence of ice rafting. The dropstones are dominated by subangular crystalline rocks, although the two oldest dropstones are sedimentary. The first dropstone appears at 52.51 mbsf (about 2.6 Ma; see “Sedimentation Rates” section, this chapter)

Table 5. Summary table of dropstones greater than 1 cm in size found in lithostratigraphic Unit I at Site 982.

Core, section, interval top (cm)	Depth (mbsf)	Size (cm)	Composition	Sediment color	Shape
162-982A-					
1H-2, 145	2.95	1.0	Quartzite	Medium	Subangular
1H-3, 124	4.24	2.0	Granite	Light	Angular
1H-5, 78	6.78	2.3	Basalt	Medium	Subangular
2H-5, 32	14.52	2.5	Biotite gneiss	Light	Subrounded
2H-5, 84	15.04	1.3	Pink feldspar	Dark	Subangular
5H-2, 136	39.56	2.3	Greenish quartzite	Dark	Subrounded
6H-1, 72	46.92	3.0	Quartz-rich igneous rock	Dark	Angular
162-982B-					
2H-3, 135	9.85	3.0	Schist	Dark/light	Angular
2H-CC, 18	15.30	1.0	Basalt	Dark	Angular
5H-6, 146	42.96	3.0	Greenish gray crystalline	Medium	Angular
162-982C-					
2H-3, 67	7.47	4.0	Schist	Dark	Subangular
2H-5, 106	10.86	1.3	Black, crystalline	Medium	Subangular
4H-3, 98	26.78	1.8	Chert	Dark	Subangular
4H-6, 32	30.62	3.9	Granite	Light	Angular
4H-6, 106	31.36	3.0	Sandstone	Medium	Subangular
5H-2, 148	35.28	1.0	Black, crystalline	Dark	Rounded
6H-3, 61	45.41	1.8	Black and gray, quartz conglomerate	Dark	Subangular
6H-4, 61	46.91	1.7	Tan, chert	Medium	Subangular

and occurs within the oldest of two concentrated ice-rafted debris (IRD) intervals, one between 52.51 and 32.38 mbsf and the other between 15.30 and 2.95 mbsf.

Unit II

Intervals:

Section 162-982A-7H-5 through Core 27H

Section 162-982B-7H-3 through Core 65H

Section 162-982C-7H-5 through Core 27H

Age: late Pliocene to middle Miocene

Depth: 57.4 to 614.9 mbsf

Unit II sediments are dominated by biogenic carbonate, primarily nanfossil ooze, with only minor amounts of clay, and, to an even lesser extent, biogenic silica. The mean carbonate content of Unit II, at 90.8% (standard deviation 3.7%) is considerably higher than that of Unit I and the low standard deviation attests to the homogeneity of these sediments. Disseminated pyrite and mottles and color bands of gray, greenish gray, green, and tan are present throughout. Four subunits have been defined on the basis of color, percentage carbonate content, and degree of consolidation (Table 5).

Subunit IIA occupies the upper 109.1 m of Unit II (57.4–166.5 mbsf). It is predominantly composed of very light greenish gray to light greenish gray nanfossil ooze, with minor amounts of light gray and light greenish gray nanfossil ooze with foraminifers, and light gray to gray nanfossil ooze with clay. Carbonate content averages 90.6%, with a standard deviation of 2.0%. A further indication of the homogeneity of this sediment can be seen in the low-amplitude spectral reflectance pattern (Fig. 6C).

At 57.44 mbsf (Section 982B-7H-3, 145 cm), 58.3 mbsf (Section 982B-7H-4, 70–71 cm), and 72.6 mbsf (Section 982B-9H-1, 64–67 cm), pockets (burrow fills?) and/or layers of spicule nanfossil ooze are present. Because the spicules clump together when the core is split, the original texture and location are destroyed. A dark gray, 2-cm-long, rough-textured celestite concretion was recovered at 164.6 mbsf (Section 982B-18H-6, 61 cm). Four ash layers were identified in this subunit, ranging from a highly disseminated layer at approximately 140 mbsf, to a 4-cm-thick layer at 128 mbsf (Fig. 7). The glass is predominantly clear and remarkably fresh, showing little indications of alteration.

Subunit IIB (166.5–195.5 mbsf) is composed of apparently cyclically varying very light gray, light gray, and light greenish gray nanfossil oozes, with minor light greenish gray nanfossil oozes with clay. Although the mean carbonate content of 89.1% is essentially the same as the adjacent subunits, the standard deviation (3.5%) is slight-

ly greater and there is higher variation in the spectral reflectance, which is more regular (cyclic) and ranges from 32% to 70% (Fig. 6D). There are only a few carbonate measurements for this unit and they may not have been taken in the more clay-rich layers.

Subunit IIC (195.5–480.0 mbsf) consists of homogeneous very light gray, light gray, and very light greenish gray nanfossil ooze with a mean calcium carbonate content of 92.6% (1.5%). The homogeneity of this unit can also be seen in the spectral reflectance plot from Core 982B-25H (Fig. 6E). Within this 284.5-m-thick Miocene interval the sediments become harder, approaching chalk, although this degree of induration is not evident in the physical properties data until approximately 480 mbsf, which is used as the lower boundary of this unit (see "Physical Properties" section, this chapter). Due to coring disturbance (XCB-created "biscuits") and poor recovery, spectral reflectance measurements were intermittent in the interval between 260 and 314 mbsf and were discontinued below 314 mbsf. The degradation of core quality is indicated by increased noise in the gamma-ray attenuation porosity (GRAPE) and natural gamma radiation records.

Although this subunit is very homogenous, some submeter scale variation can be seen in visual core inspection (Fig. 8), and meter- to decimeter-scale variations can be seen in the reflectance, GRAPE, and natural gamma radiation data. Although there are >20% variations in spectral reflectance amplitude, variations in carbonate content are only a few percent. This suggests that reflectance is more sensitive to the noncarbonate component when carbonate values exceed 80% (see "Lithostratigraphy" section, "Sites 980/981" chapter, this volume).

In addition to continuous nanfossil ooze, and alternating nanfossil ooze and chalk, several minor lithologies are present. Six ash layers were identified. As in Subunit IIA, they are composed of mostly fresh, clear glass. At 280 mbsf (Section 982A-24H-3, 20–38 cm), a 14-cm-thick, graded foraminifer ooze with nanfossils, sponge spicules, and micrite (Fig. 9) contains many broken planktonic foraminifers of roughly the same size and appears to be a turbidite. At approximately 377 mbsf (Section 982B-41X-2, 140–143 cm), a blue-gray, rounded nodule was identified by XRD analysis as celestite.

Core 982B-30X (268.5–278.2 mbsf) recovered a single piece of silica-cemented foraminifer sand. The foraminifers are similar to those found in chalk and ooze samples above and below, suggesting *in situ* lithification. However, the planktonic/benthic (P/B) ratio is 4:1. This is a much lower P/B ratio than found elsewhere in this subunit (e.g., 14:1 in Core 982B-40X), suggesting either a shallow-water origin and/or dissolution of the cemented assemblage (see "Biostratigraphy" section, this chapter). Logging results show a turbidite

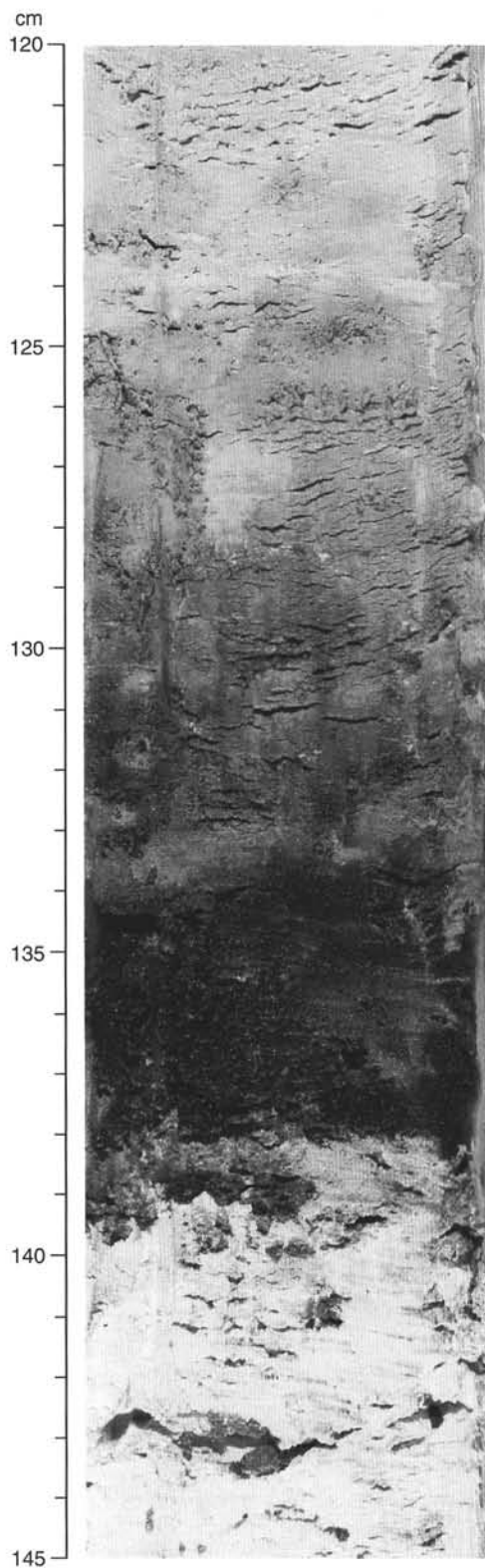


Figure 7. Well-defined ash layer in Subunit IIA from Section 162-982C-15H-1, 120–145 cm. Note the sharp bottom contact and disseminated ash in the overlying nannofossil ooze.

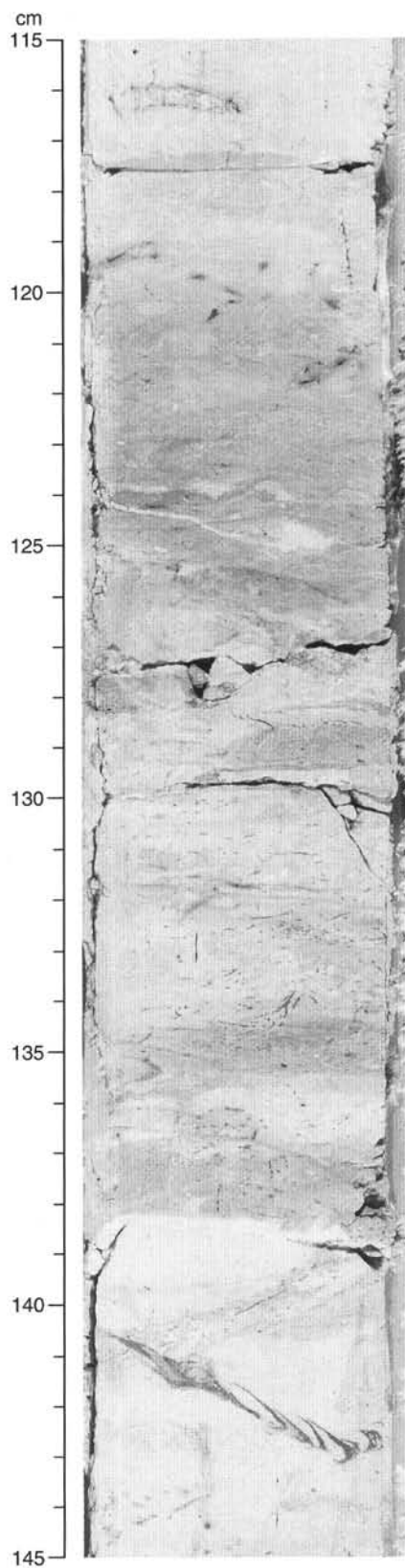


Figure 8. Minor color variations and bioturbation from Section 162-982B-45X-1, 115–145 cm, in Subunit IIC.

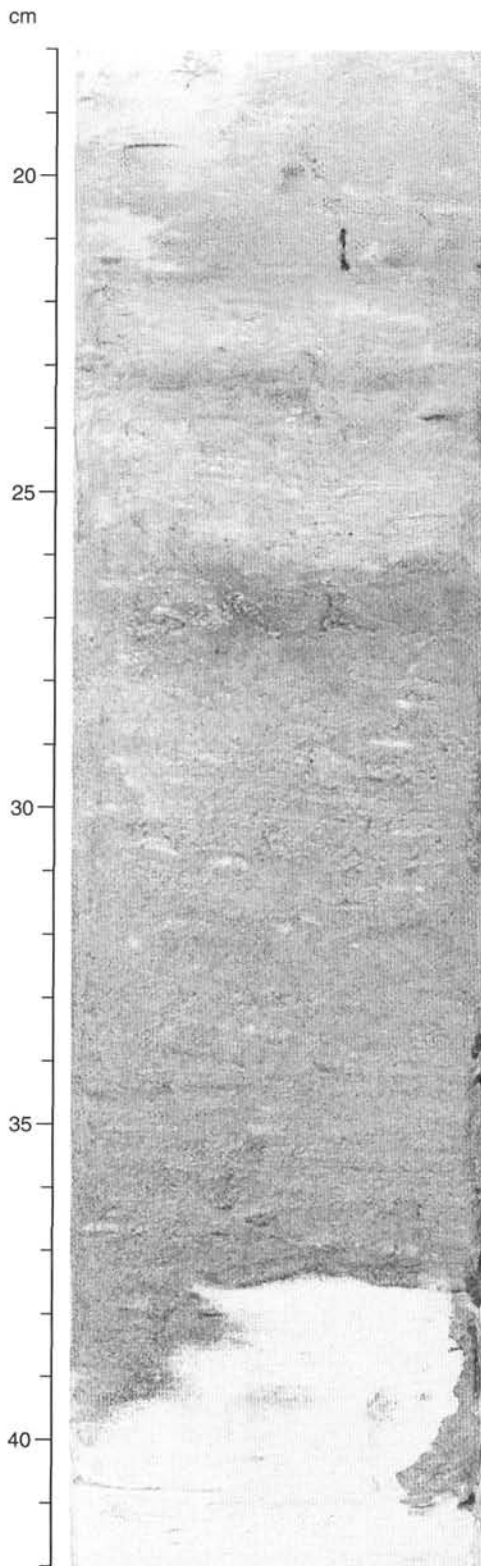


Figure 9. Graded foraminifer ooze with nanofossils and micrite (Section 982A-24H-3, 20–38 cm) in Subunit IIC.

at this depth interval (see “Wireline Logging” section, this chapter) and the rock was recovered at a depth similar to Reflector R1 (see “Seismic Stratigraphy” section, this chapter). It appears that this specimen may be part of a regionally widespread semipermeable cap rock (see “Inorganic Geochemistry” section, this chapter).

In Subunit IID (480–614.9 mbsf), severely biscuitized sediment was recovered. This unit is dominated by nanofossil chalk characterized by a high mean calcium carbonate content of 84.7% with a slightly higher standard deviation of 7%, indicating increasing variability, particularly lower in the section. For example, in Core 982B-60X (557.0–566.7 mbsf) there is a distinct color cyclicity and calcium carbonate concentration varies from 69.6% to 88.4%.

Four other minor lithologies are present. Between 500 and 515 mbsf, three 50-cm-thick layers of light gray nanofossil chalk with spicules and foraminifers were identified. At 538 mbsf (Section 982B-58X-3, 0–40 cm), several pieces of a partially lithified, dark greenish gray foraminifer ooze were recovered. The topmost piece contains a color contact between dark greenish gray and light greenish gray. Thin-section analysis of the rock reveals mostly rounded forms of foraminifers with a P/B ratio of 26:1. Chert was recovered as small nodule fragments at 567.0 and 567.1 mbsf in Section 982B-61X-1, 134–136 cm, and 140–143 cm, and as a 7-cm-thick layer at 569.2 mbsf (Section 982B-61X-2, 100–107 cm). A single, black, 4-cm-thick ash layer occurs at 485 mbsf (Section 982B-55X-3, 146 cm).

Interpretation

The two lithostratigraphic units recovered at Site 982 depict two very different modes of variability. Unit I exhibits persistent submeter- to meter-scale changes in color, spectral reflectance, and lithology which appear to be related to repetitive glacial-interglacial changes in sediment input. The onset of these changes took place rather abruptly at around 2.9 Ma.

Throughout Unit II, depositional conditions produced relatively homogeneous sediment for over 550 m of the section, an interval representing well over 15 m.y. (see “Biostratigraphy” section, this chapter). Despite this homogeneity, low-amplitude meter- to decimeter-scale changes can be observed in all of the measured parameters. These changes are most pronounced in Subunit IIB, which may represent a precursor to the subsequent ice age world.

BIOSTRATIGRAPHY

Site 982 on the Hatton Rockall Plateau yielded a relatively continuous sedimentary sequence of late early Miocene to Holocene age (~18.8 to 0 Ma). Calcareous microfossils are generally abundant and well-preserved, and provide the primary basis for Site 982 biostratigraphy. Siliceous microfossils exhibit variable preservation, and provide useful stratigraphic information in some intervals. Biostratigraphic zones for calcareous nanofossils, planktonic foraminifers, diatoms, and siliceous flagellates are summarized in Figure 10. Age information is not entirely consistent between calcareous and siliceous microfossil groups, possibly due to the relatively lower abundance of siliceous microfossils. Age boundaries (Fig. 10) are therefore based on nanofossil data. The biostratigraphic datums presented in Table 6 are also integrated with magnetic polarity data to estimate sedimentation rates (see “Sedimentation Rates” section, this chapter).

Calcareous Nanofossils

Calcareous nanofossils are generally abundant throughout the 610-m-thick sequence cored at Site 982. Preservation is good in the Pliocene–Pleistocene and moderate in the Miocene. Most zonal

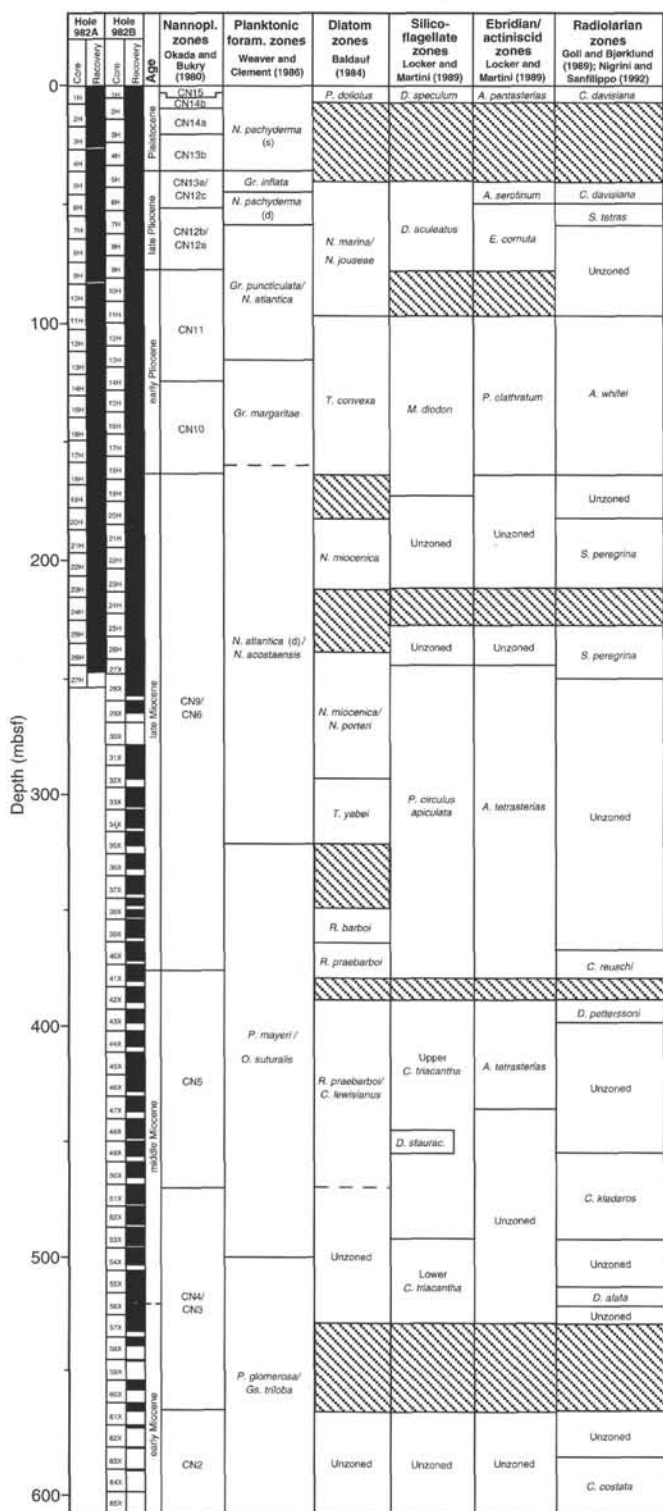


Figure 10. Biostratigraphic summary, Site 982. Hatched intervals indicate absence of fossils. Age boundaries are based on nannofossil datums, which provided the primary age control for this site. Dashed line indicates uncertainty in exact placement of a boundary.

markers plus some nontraditional datums have been located within about 1.5 m, and are listed in Table 6.

All the Pleistocene nannofossil zones are recognized (Fig. 10). Biostratigraphic resolution is lower in the older sediment due to the scarcity or absence of many index species. It is interesting to note that some warm-water marker species (*Sphenolithus heteromorphus* and *S. belemnos*) are present in the middle and lower Miocene, and they provide important age information (see Fig. 14, "Sedimentation Rates" section, this chapter). The presence of *S. belemnos* from Core 162-982B-61X through the last Core 65X indicates that the deepest sediment cored at Site 982 has an age between 18.4 and 19.2 Ma (early Miocene).

Planktonic Foraminifers

Planktonic foraminifers are generally abundant from the top of the section to Sample 982A-20H-CC, common from Sample 982A-21H-CC to 982B-53X-CC, and few from Sample 982B-54X-CC to 65X-CC. Preservation is good from the top of the section to Sample 982A-20H-CC, and moderate from Sample 982A-21H to 982B-65X-CC. Most of the planktonic foraminifer zones of Weaver and Clement (1986), based on North Atlantic DSDP Leg 94 sites, are recognized. The *Neogloboquadrina pachyderma* (sinistrally coiling) Zone marks the Pleistocene. The Pliocene is subdivided into four zones, the uppermost Pliocene *Gr. inflata* Zone, the upper Pliocene *N. pachyderma* (dextrally coiling) Zone, the middle Pliocene *Gr. puncticulata*/*N. atlantica* Zone and the lower Pliocene *Gr. margaritae* Zone (Fig. 10). The upper Miocene is subdivided into the *Gr. conoidea* Zone, the *N. atlantica* (sinistrally coiling)/*N. acostaensis* Zone, and the upper part of the *Paragloborotalia mayeri* Zone. The middle Miocene includes the lower part of the *Paragloborotalia mayeri* Zone and the *Orbulina suturalis* Zone. Lastly, the lower Miocene is marked by the *Praeorbulina/Globigerinoides triloba* Zone (undifferentiated).

Planktonic foraminifer datums found in the Site 982 sequence are tabulated in Table 6. In addition to core-catcher material from Holes 982A and 982B, samples were analyzed aboard ship within individual cores in Hole 982B to refine biostratigraphic datums to within 1.5 m. Several of these datums are integrated with calcareous nannofossil datums and magnetic polarity stratigraphy in order to calculate sedimentation rates (see "Sedimentation Rates" section, this chapter).

Benthic Foraminifers

Benthic foraminifers were present in all the core-catcher samples from this site, generally constituting less than 5% of the total foraminiferal fauna from the >63-µm sieve fraction studied. Semiquantitative estimates of relative species abundance were made with counts of >100 individuals per sample. Diversity is variable, with up to about 30 species counted in some samples (162-982A-4H-CC and 12H-CC), but tends to decrease downhole, with fewer than 15 species present in Sample 162-982B-64X-CC. Preservation is generally good throughout, showing some deterioration downhole, particularly below about 220 mbsf. Rhombic overgrowths of calcite, possibly associated with *Bolboforma*, are observed at certain intervals and are particularly well developed in Sample 162-982B-29X-CC.

The Pleistocene sediments are characterized by variable assemblages, presumably responding to glacial/interglacial cycles, and the most common taxa include *Bolivina* spp., *Cassidulina teretis*, *Epistominella exigua*, *Nonionella* spp., *Pullenia bulloides*, *Sigmoilopsis schlumbergeri*, *Stainforthia fusiformis*, and *Trifarina angulosa*. The Pliocene sequence is characterized by increased abundance of *Cassidulina* spp., *Cibicidoides* spp., *Globocassidulina subglobosa*, and *Uvigerina* spp. The early Pliocene and late Miocene sediments generally exhibit greater abundance of *Cibicidoides kullenbergi* and *Uvigerina* spp. *Ehrenbergina trigona* occurs together with *Laticarinina pauperata* during the early Pliocene, although the latter is not restrict-

Table 6. Depth range of biostratigraphic datums, Site 982.

Datum	Age (Ma)	Core, section, interval (cm)	Depth (mbsf)	Depth (mcd)	Datum	Age (Ma)	Core, section, interval (cm)	Depth (mbsf)	Depth (mcd)
FO <i>E. huxleyi</i> (N)	0.26	162-982B-1H-3, 10 1H-4, 10	3.10 4.60	3.10 4.60	LO <i>D. quinqueramus</i> (N)	5.30	982A-18H-4, 10 18H-5, 10	164.80 166.30	184.30 185.80
LO <i>P. lacunosa</i> (N)	0.46	2H-2, 124 2H-3, 144	8.24 9.94	9.56 11.26	FO <i>T. oestrupii</i> (D)	5.60	11H-CC, 15-17 14H-CC, 18-20	103.31 131.94	115.66 147.76
FO <i>Gephyrocapsa</i> spp. C/D (N)	0.78	3H-3, 65 3H-4, 10	18.65 19.60	20.81 21.76	LO <i>M. diodon</i> (S)	5.93	10H-CC, 13-14 11H-CC, 15-17	94.01 103.31	105.44 115.66
LO <i>Gephyrocapsa</i> spp. A/B (N)	1.23	3H-6, 12 4H-1, 10	22.62 24.60	24.78 27.68	LO <i>N. miocenica</i> (D)	6.14	17H-CC, 16-18 18H-CC, 18-20	160.32 170.02	179.32 189.52
LO <i>C. macintyreii</i> (N)	1.59	4H-2, 124 4H-3, 110	27.24 28.60	30.32 31.68	d. to s. <i>N. atlantica</i> (F)	6.40	982B-26H-3, 19-21 26H-4, 19-21	236.69 238.19	257.28 258.78
FO <i>Gephyrocapsa</i> spp. A/B (N)	1.70	4H-6, 100 5H-1, 100	33.00 35.00	36.08 39.08	LO <i>P. apiculata</i> (S)	6.59	26H-CC, 18-20 27X-CC, 16-21	242.94 249.46	263.53 270.05
S, acme <i>N. pachyderma</i> s. (F)	1.80	982A-4H-CC, 8-13 982A-5H-CC, 15-20	36.96 46.51	39.46 50.44	FO <i>A. delicatus</i> (N)	6.90	982A-20H-CC, 15-18 982A-21H-1, 10	188.86 188.80	209.20 209.85
S, acme <i>N. pachyderma</i> s. (F)	1.80	982B-3H-6, 12-14 982B-4H-2, 124-126	22.62 27.24	24.78 30.32	FO <i>D. surculus</i> (N)	7.30	982B-26H-CC, 18-20 27X-CC, 16-21	242.94 249.46	263.53 270.05
LO <i>A. serotinum</i> (E)	2.00	982A-4H-CC, 8-13 5H-CC, 15-20	36.96 46.51	39.46 50.44	LO <i>D. hustedtii</i> (D)	8.40	30X-CC, 8 31X-CC, 16-21	268.58 287.73	289.17 308.32
FO <i>Gr. inflata</i> (F)	2.09	4H-CC, 8-13 5H-CC, 15-20	36.96 46.51	39.46 50.44	LO <i>N. cylindrica</i> (D)	8.33	31X-CC, 16-21 32X-CC, 34-36	287.73 293.62	308.32 314.21
FO <i>Gr. inflata</i> (F)	2.09	982B-5H-5, 110-112 982B-5H-6, 104-106	41.10 42.54	45.18 46.62	FO <i>N. fossilis</i> (D)	8.83	32X-CC, 34-36 33X-CC, 35-37	293.62 305.54	314.21 326.13
LO <i>N. atlantica</i> (F)	2.41	982A-4H-CC, 8-13 982A-5H-CC, 15-20	36.96 46.51	39.46 50.44	FO <i>N. acostaensis</i> (F)	10.03	35X-CC, 35-36 36X-1, 19	323.05 326.49	343.64 347.08
LO <i>N. atlantica</i> (F)	2.41	982B-6H-2, 54 982B-6H-3, 65-67	45.54 47.15	51.05 52.66	LO <i>Gr. mayeri</i> (F)	10.30	35X-CC, 35-36 36X-1, 19	323.05 326.49	343.64 347.08
LO <i>Gr. puncticulata</i> (F)	2.41	982A-5H-CC, 15-20 982A-6H-CC, 21-26	46.51 55.97	50.44 62.50	LO <i>C. miopelagicus</i> (N)	10.90	41X-2, 10 41X-3, 10	376.10 377.60	396.69 398.19
LO <i>Gr. puncticulata</i> (F)	2.41	982B-7H-3, 18 7H-4, 18	56.18 57.68	61.95 63.45	FO <i>H. cuneiformis</i> (D)	11.44	38X-CC, 33-35 40X-CC, 34-36	353.80 372.29	374.39 392.88
LO <i>D. surculus</i> (N)	2.59	7H-1, 18 7H-2, 18	53.18 54.68	58.95 60.45	LO <i>C. floridanus</i> (N)	11.60	49X-1, 10 49X-2, 10	451.50 453.00	472.09 473.59
LO <i>E. cornuta</i> (E)	2.61	982A-5H-CC, 15-20 6H-CC, 21-26	46.51 55.97	50.44 62.50	LO <i>C. depressus</i> (S)	12.39	41X-CC, 35-38 42X-CC, 31-34	381.54 390.62	402.13 411.21
LO <i>D. tamalis</i> (N)	2.78	7H-5, 18 7H-6, 18	61.88 63.38	69.85 71.35	LO <i>D. stauracanthus</i> (S)	13.25	47X-CC, 44-47 48X-CC, 37-40	438.64 450.12	459.23 470.71
LO <i>Gr. cf. crassula</i> (F)	3.30	8H-CC, 11-13 9H-CC, 22-24	74.96 83.60	83.74 93.43	LO <i>S. heteromorphus</i> (N)	13.60	51X-1, 10 51X-2, 10	470.70 472.20	491.29 492.79
FO <i>P. lacunosa</i> (N)	3.70	9H-3, 10 9H-4, 10	77.80 79.30	87.63 89.13	FO <i>D. hustedtii</i> (D)	14.20	49X-CC, 25-30 52X-CC, 35-40	458.35 488.65	478.94 509.24
FO <i>Gr. puncticulata</i> (F)	4.50	12H-CC, 18-20 13H-CC, 13-15	112.90 122.36	126.39 137.28	FO <i>M. diodon</i> (S)	14.64	52X-CC, 35-40 53X-CC, 33-37	488.65 498.60	509.24 519.19
FO <i>Gr. puncticulata</i> (F)	4.50	982B-12H-7, 20-22 982B-13H-1, 30-32	109.70 110.30	120.19 121.84	FO <i>O. suturalis</i> (F)	15.10	53X-CC, 33-37 54X-1, 40-42	498.60 499.70	519.19 520.29
LO <i>N. cylindrica</i> (D)	4.67	982A-7H-CC, 15-17 8H-CC, 11-13	65.30 74.96	73.27 83.74	FO <i>C. wuellerstorfi</i> (F)	15.20	53X-CC, 33-37 54X-1, 40-42	498.60 499.70	519.19 520.29
LO <i>A. primus</i> (N)	4.70	14H-3, 10 14H-4, 10	125.30 126.80	141.12 142.62	FO <i>A. ingens</i> (D)	15.37	55X-CC, 20-25 56X-CC, 41-45	518.52 528.31	539.11 548.90
FO <i>N. jouseae</i> (D)	4.91	7H-CC, 15-17 8H-CC, 11-13	65.30 74.96	73.27 83.74	LO <i>C. dissimilis</i> (F)	17.30	57X-CC, 32-36 58X-CC, 28-33	535.70 541.56	556.29 562.15
LO <i>N. acostaensis</i> (F)	5.29	16H-CC, 25-27 17H-CC, 16-18	151.01 160.32	169.13 179.32	FO <i>S. heteromorphus</i> (N)	18.20	60X-CC, 31-36 61X-CC, 27-32	561.15 570.20	581.74 590.79
LO <i>N. acostaensis</i> (F)	5.29	982B-18H-3, 24-26 982B-18H-4, 24-26	160.74 162.24	177.32 178.82	LO <i>S. belemnos</i> (N)	18.40	60X-CC, 31-36 61X-1, 10	561.15 566.80	581.74 587.39

Notes: FO = first occurrence; LO = last occurrence; S = start. In parentheses: N = calcareous nannofossil, F = planktonic foraminifer, D = diatom, S = silicoflagellate, E = ebridian, d. = dextral, and s. = sinistral.

ed to this interval and has its first occurrence in Sample 162-982B-46X-CC, near the end of the middle Miocene. Taxa that range down to the middle Miocene include *Bolivina* spp., *Bulimina striata*, *Cibicoides kullenbergi*, *Epistominella exigua*, *Globocassidulina subglobosa*, *Melonis barleeanus*, and *Uvigerina* spp. The early middle Miocene and early Miocene are characterized by the presence of *Siphonia tenuicarinata* (last occurrence = Sample 162-982B-52X-CC) and absence of *Cibicoides wuellerstorfi* (first occurrence = Sample 162-982B-50X-CC). The early Miocene faunas exhibit a low diversity.

Diatoms

Diatoms found at Site 982 are few in abundance, and samples are intermittently barren. However, when diatoms are found, they are typically well preserved, allowing the determination of several datums and assignment to the North Atlantic diatom zonation of Baldauf (1984) (Fig. 10). Barren intervals of relatively long duration occur between Samples 162-982B-34X-CC and 37X-CC, representing the middle to late Miocene and encompassing the *Denticulopsis praedimorpha* diatom zone, and between Samples 162-982B-57X-CC to 60X-CC, representing an unzoned interval of early to middle Miocene age.

Silica immediately below a resistant layer in Sample 162-982B-30X-CC was quite well-preserved, and sediments contained the species *Denticulopsis hustedtii* and *Nitzschia cylindrica*, suggesting an age of about 8 Ma.

Radiolarians

A set of 25 samples was selected from Holes 982A and 982B to study radiolarians. Samples that were recognized as nearly or totally barren during the study of siliceous flagellates were omitted. The frequency of radiolarians changes from abundant in the Pleistocene through uppermost Miocene to few in the upper Miocene to common in the middle and lower Miocene. The preservation of skeletons is usually moderate to good, but is often poor in the lower part of the section.

It is difficult to assign the radiolarian assemblages of Site 982 to an established zonation. The mid-latitude zonation of Nigrini and Sanfilippo (1992) was introduced primarily for the Pacific Ocean and the high-latitude zonation of Goll and Björklund (1989) for the Norwegian-Greenland Sea. Certain zones of both zonation schemes can, however, be recognized in the northern Atlantic. In the Pleistocene and Pliocene mainly the zonation of Goll and Björklund (1989) can be applied, and in the Miocene mainly the zonation of Nigrini and Sanfilippo (1992).

Samples 162-982A-1H-CC and 5H-CC include both *Botryostrobus aquilonarius* and *Cycladophora davisiana* and are placed in the Pleistocene to latest Pliocene *Cycladophora davisiana* Zone. Sample 162-982A-6H-CC contains *Spongaster tetras* and is assigned to the upper Pliocene *Spongaster tetras* Zone. Due to the occurrence of common *Antarctissa whitei*, Samples 162-982A-11H-CC through 17H-CC are referred to the lower Pliocene *Antarctissa whitei* Zone. The most common species of the Pleistocene to Pliocene radiolarian assemblages are *Lithelius spiralis* and *Spongodiscus resurgens*, but in certain intervals *Lithomitra lineata*, *Porodiscus* sp., and *Stylocdictya validispina* are common as well.

In Samples 162-982A-20H-CC to 982B-27X-CC *Stichocorys peregrina* is found, which indicates the upper Miocene *Stichocorys peregrina* Zone. Below, an unzoned interval follows between Samples 162-982B-31X-CC and 38X-CC. Sample 162-982B-40X-CC probably marks the base of the *Eucoronis fridjofnansenii*/*Corythospyris reuschi* Zone because *Corythospyris reuschi* has its first occurrence here. Sample 162-982B-42X-CC is placed in the middle Miocene *Diartus pettersoni* Zone, since *Cyrtocapsella japonica*,

which has its first and last occurrence in this zone (Nigrini and Sanfilippo, 1992), is recorded. The presence of *Cyrtocapsella cladaros* in Samples 162-982B-49X-CC and 52X-CC indicates the *Cyrtocapsella cladaros* Zone. Sample 162-982B-55X-CC is assigned to the lower middle Miocene *Dorcadospyrus alata* Zone, due to the occurrence of the nominate species. Samples 162-982B-63X-CC and 64X-CC are attributed to the *Calocyctella costata* Zone, based on the presence of *Eucyrtidium diaphanes*, which has its last occurrence in this zone (Nigrini and Sanfilippo, 1992). The most common species of the Miocene radiolarian assemblages are *Lithelius spiralis* and *Lithomitra lineata*, but in certain intervals *Spongodiscus resurgens* and *Porodiscus* sp. are common as well.

The radiolarian study from Site 982 demonstrates that certain zones of the zonation schemes of Goll and Björklund (1989) and of Nigrini and Sanfilippo (1992) can be applied in this area. The *Cycladophora davisiana*, *Spongaster tetras*, and *Antarctissa whitei* Zones of the Quaternary to Pliocene time interval are subdivisions of the high-latitude zonation of Goll and Björklund (1989). The *Stichocorys peregrina*, "*Diartus pettersoni*," *Dorcadospyrus alata*, and *Calocyctella costata* Zones of the Miocene time interval are subdivisions of the mid-latitude zonation of Nigrini and Sanfilippo (1992). Within these mid-latitude zones of the Miocene, two high-latitude zones of Goll and Björklund (1989) were recognized, that is, the *Eucoronis fridjofnansenii*/*Corythospyris reuschi* and *Cyrtocapsella cladaros* Zones. The occurrence of both middle- and high-latitude marker species in Miocene to Pliocene sediments at Site 982 reflects strongly changing paleoenvironmental conditions in the northern Atlantic Ocean during that time interval.

Siliceous Flagellates

Siliceous flagellates (including silicoflagellates, ebridians, and actiniscidians) display scattered occurrences downsection in Holes 982A and 982B, with the abundance of these microfossils varying from trace to common. Preservation of silicoflagellates is usually moderate, and of ebridians and actiniscidians good.

Silicoflagellates

Sample 162-982A-1H-CC represents the Pleistocene *Distephanus speculum* Zone. After a barren interval, Samples 162-982A-5H-CC to 8H-CC can be placed in the upper to lower Pliocene *Distephanus aculeatus* Zone. From Sample 162-982A-11H-CC to 18H-CC the *Mesocena diodon* Zone follows, straddling the Pliocene/Miocene boundary. The lower part of the section between Samples 162-982A-20H-CC and 22H-CC remains unzoned, due to rare occurrences of nondiagnostic silicoflagellate species.

Samples 162-982B-27X-CC to 40X-CC are assigned to the *Paramesocena circulus apiculata* Zone, which has an upper age of 6.59 Ma. Between Samples 162-982B-42X-CC and 52X-CC, the Upper *Corbisema triacantha* Zone is present, interrupted by the *Distephanus stauracanthus* Subzone in Sample 162-982B-48X-CC. The LAD of *Distephanus stauracanthus* is calculated to 13.25 Ma. The interval from Sample 162-982B-55X-CC to 64X-CC is assigned to the Lower *Corbisema triacantha* Zone, which lies above the distinct LAD of all *Naviculopsis* species in the early Miocene.

Ebridians and Actiniscidians

Sample 162-982A-1H-CC belongs to the Pleistocene *Actiniscus pentasterias* Zone. Below a barren interval, Sample 162-982A-5H-CC can be placed in the *Ammochium serotinum* Zone and Samples 162-982A-6H-CC to 8H-CC in the *Ebriopsis cornuta* Zone. Both zones characterize the upper and lower Pliocene. The LAD of *Ammochium serotinum* occurs at 2.00 Ma and the LAD of *Ebriopsis cornuta* at 2.61 Ma. Samples 162-982A-11H-CC to 17H-CC are

assigned to the *Parathranium clathratum* Zone. The section between Samples 162-982A-18H-CC and 22H-CC remains unzoned due to rare occurrences of nondiagnostic ebridian and actiniscidian species. Samples 162-982B-27X-CC to 46X-CC are assigned to an *Actiniscus tetrasterias* Zone, which correlates, in general, with the *Paramesocena circulus apiculata* Zone of silicoflagellates. The lower part of the section between Samples 162-982B-48X-CC and 64X-CC cannot be placed in any zone.

PALEOMAGNETISM

At Site 982, the magnetic polarity stratigraphy could be resolved down to the upper part of the Gauss polarity chron. Below this level, magnetization intensities were within the noise of the shipboard pass-through cryogenic magnetometer. Archive halves of Cores 982A-1H through 10H and some sections from Cores 982A-11H through 19H were measured using the shipboard cryogenic magnetometer. Archive halves of Cores 982B-1H through 8H and Cores 982C-1H through 8H were also measured (Table 7). The data from levels below Cores 982A-7H, 982B-7H, and 982C-7H are considered unreliable due to weak magnetization intensities. Time constraints and the necessity to keep pace with core flow permitted only a single alternating field (AF) demagnetization step for the majority of core sections. Only Cores 982C-3H through 7H were oriented using the Tensor tool.

At Site 982, a peak AF demagnetization of 25 mT was used on all sections which were measured on the cryogenic magnetometer, with additional demagnetization steps at 15 or 30 mT for a few sections (Table 7). Progressive AF demagnetization of discrete samples indicated that a very strong, steeply inclined drill-string magnetic (viscous) overprint was removed by alternating fields in the 15–30 mT range.

Natural remanent magnetization (NRM) intensities are in the 1–20 mA/m range down to 40 mbsf. Below this depth NRM intensities decrease quite abruptly. After partial demagnetization, the magnetization intensities reach magnetometer noise level just below 50 mbsf (Fig. 11) and the Gauss/Matuyama polarity chron boundary.

The Brunhes/Matuyama boundary, Jaramillo Subchron, Olduvai Subchron, Reunion Subchron, and Gauss/Matuyama boundary are reasonably well defined in Holes 982B and 982C (Fig. 12). Sub-bottom depths of polarity chron boundaries are given in Table 8. In Hole 982A, the magnetic stratigraphy is undefined from the base of the Brunhes Chron to the top of the Olduvai Subchron due to coring disturbance in Cores 983A-3H and 4H. In Hole 982C, the anomalously thick Reunion Subchron and anomalous inclinations at the base of the Matuyama Chron are probably artifacts of coring disturbance (and resulting drill-string remagnetization) in Core 982C-6H. In many cores, the upper 50% (at least) of Section 1 appears to have a high coercivity (drill-string) remagnetization which was not removed at peak alternating fields of 25 or 30 mT.

SEDIMENTATION RATES

A sedimentary section 605 m thick was recovered from the four holes drilled at Site 982, representing an interval from the early Miocene to the Holocene. Sedimentation rates were determined on the basis of magnetostratigraphy and calcareous nannofossil biostratigraphy (Table 9; see "Paleomagnetism" and "Biostratigraphy" sections, this chapter). Sedimentation rate reconstructions (Fig. 13) were based on biostratigraphic data from Hole 982B and paleomagnetic data from all holes, and related to a common depth through the Site 982 composite depth section (see "Composite Depths" section, this chapter). To facilitate comparison between sites, sedimentation rates were

Table 7. Summary of pass-through cryogenic magnetometer measurements at Site 982.

Measurement	Core sections
15 mT	162-982A- 11H-4, 11H-6, 12H-3, 12H-6, 13H-4, 14H-4, 15H-2, 15H-5, 16H-5, 16H-6, 17H-4
25 mT	1H-1 through 10H-6, 11H-2, 11H-3, 11H-4, 11H-6, 13H-2, 14H-3, 15H-5, 16H-2, 16H-4 through 16H-6, 17H-3 through 17H-5, 18H-2, 18H-4, 18H-6, 19H-3, 19H-4
25 mT	162-982B- 1H-1 through 8H-6
30 mT	3H-7, 5H-1, 6H-6, 7H-4
25 mT	162-982C- 2H-1 through 8H-6
30 mT	3H-6, 4H-3, 5H-2

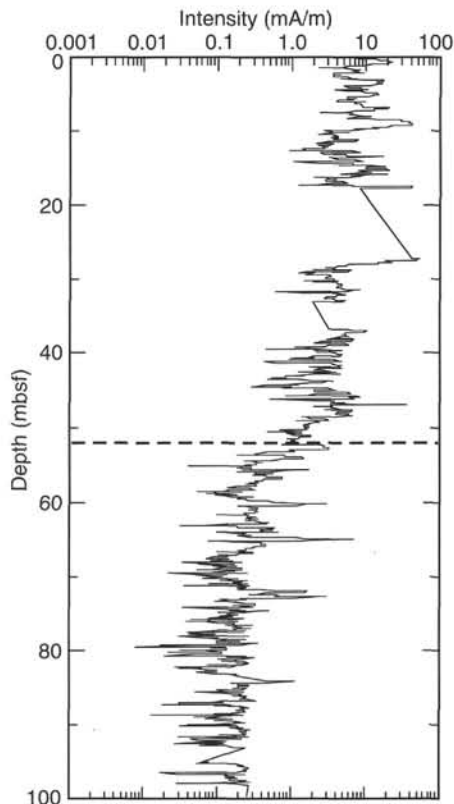


Figure 11. Magnetization intensity from Hole 982A after demagnetization in peak alternating fields of 25 and 15 mT. The shift in intensity at about 50 mbsf (dashed line) corresponds approximately to the Gauss/Matuyama polarity chron boundary.

estimated from age vs. depth plots by drawing straight-line segments (uniform sedimentation rate) between selected datums (Fig. 14).

Sedimentation rates were calculated for both the meters below seafloor (mbsf) depth scale and the meters composite depth (mcd) depth scale. Figure 13 presents sedimentation rates as a function of age and composite depth. Magnetic polarity age control points include the Brunhes/Matuyama and Matuyama/Gauss Chron boundaries, and the Jaramillo and Olduvai Subchrons. Eight calcareous nannofossil datums are used, from the FO of *Emilianii huxleyi* at 0.26 Ma to the FO of *Sphenolithus heteromorphus* at 18.2 Ma (Table 9). These datums are considered synchronous from low to middle latitudes (e.g., Takayama and Sato, 1987).

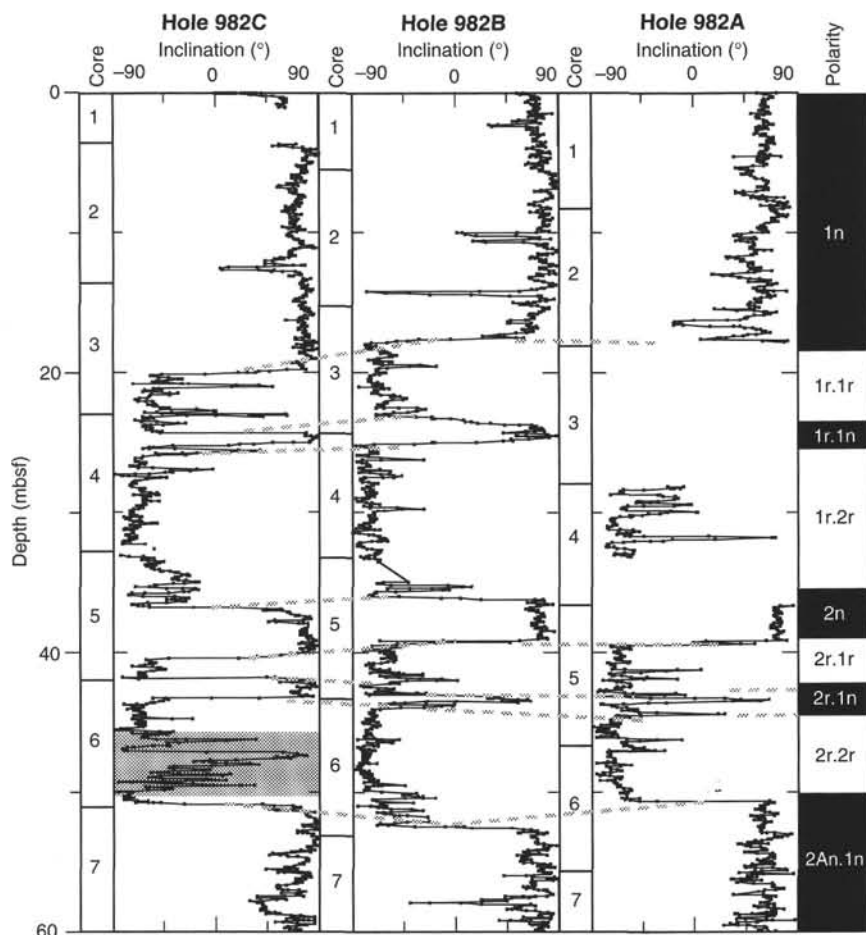


Figure 12. Inclination of the magnetization vector vs. depth (mbsf) for Site 982, after AF demagnetization at peak fields of 25 mT. The shaded area in Core 982C-6H corresponds to anomalous inclinations attributed to drilling disturbance. Gray dashed line = correlative horizons.

Table 8. Preliminary positions of polarity chron boundaries at Site 982.

Core, section, interval (cm)	Depth (mbsf)	Interpreted boundary	Age (Ma)	Comments
162-982A-5H-2, 130	39.50	Olduvai (bottom)	1.95	
5H-5, 60	43.30	Reunion (top)	2.14	Poorly defined
5H-6, 25	44.45	Reunion (bottom)	2.15	Poorly defined
6H-4, 0	50.70	Matuyama/Gauss	2.60	Section break
162-982B-3H-2, 110	17.60	Brunhes/Matuyama	0.78	
3H-6, 90	23.40	Jaramillo (top)	0.99	
4H-1, 50	25.00	Jaramillo (bottom)	1.07	
5H-2, 65	36.15	Olduvai (top)	1.77	
5H-4, 65	39.15	Olduvai (bottom)	1.95	
5H-7, 15	43.15	Reunion (top)	2.14	
6H-1, 0	43.50	Reunion (bottom)	2.15	Core break
6H-7, 0	52.55	Matuyama/Gauss	2.60	Section break
162-982C-3H-5, 80	20.10	Brunhes/Matuyama	0.78	
4H-2, 0	24.30	Jaramillo (top)	0.99	Section break
4H-2, 140	25.70	Jaramillo (bottom)	1.07	
5H-4, 5	36.85	Olduvai (top)	1.77	
5H-6, 70	40.50	Olduvai (bottom)	1.95	
6H-1, 0	41.85	Reunion (top)	2.14	Section break
6H-1, 135	43.20	Reunion (bottom)	2.15	
7H-1, 0	51.30	Matuyama/Gauss	2.60	Core break

Sedimentation rates increase from approximately 20 m/m.y. in the early to middle Miocene and are highest during the late Miocene and early Pliocene, reaching ~50 m/m.y. from ~7 to 4 Ma. Rates drop in the early Pliocene at ~4 Ma, after which they vary between about 12 and 36 m/m.y. (Fig. 13).

ORGANIC GEOCHEMISTRY

The shipboard organic geochemistry program at Site 982 consisted of analyses of volatile hydrocarbons, determinations of inorganic carbon, total nitrogen, total carbon, and total sulfur, and pyrolysis measurements (for methods, see "Explanatory Notes" chapter, this volume).

Volatile Hydrocarbon

As part of the shipboard safety and pollution monitoring program, concentrations of methane (C_1) and ethane (C_2) gases were measured on every core using the standard ODP headspace-sampling technique. Sixty-one sediment samples were collected from Hole 982A (6.0–242.2 mbsf) and Hole 982B (247.5–576.4 mbsf). Throughout the sediment sequence at Site 982, the methane content remained very low (2–7 ppm; Table 10; Fig. 15). Ethane was not detected.

Carbon, Nitrogen, and Sulfur Concentration

Determinations of inorganic carbon, carbonate, total carbon, total nitrogen, and total sulfur in Hole 982B are summarized in Table 11. According to the carbonate content data, the sediment sequence of Hole 982B can be divided into two intervals (Fig. 15). The upper interval (0–57.4 mbsf; Holocene to late Pliocene), which corresponds to lithostratigraphic Unit I (see "Lithostratigraphy" section, this chapter), is characterized by high amplitude variations of carbonate percentages ranging from 8.3% to 94.2%, with an average value of

Table 9. Age control points, Site 982.

Event	Age (Ma)	982A (mbsf)	982A (mcd)	982B (mbsf)	982B (mcd)	982C (mbsf)	982C (mcd)	Avg. depth (mbsf)	Avg. depth (mcd)	Rate (mbsf/m.y.)	Rate (mcd/m.y.)
Core top	0.00	0.00	0.00	0.00	0.00	0.00	0.15	0.00	0.00		
FO <i>E. huxleyi</i> (N)	0.26			3.85	3.85			3.85	3.85	14.81	14.81
LO <i>P. lacunosa</i> (N)	0.46			9.09	10.41			9.09	10.41	26.20	32.80
Brunhes/Matuyama	0.78			17.60	19.76	20.10	20.08	18.85	19.92	30.50	29.72
Jaramillo top	0.99			23.40	25.56	24.30	27.82	23.85	26.69	23.81	32.24
Jaramillo bottom	1.07			25.00	28.08	25.70	29.22	25.35	28.65	18.75	24.50
Olduvai top	1.77			36.15	40.23	36.85	40.11	36.50	40.17	15.93	16.46
Olduvai bottom	1.95	39.50	43.43	39.15	43.23	40.50	43.76	39.72	43.47	17.87	18.35
Reunion II top	2.14			43.15	47.23	41.85	46.43	42.50	46.83	14.65	17.67
Matuyama/Gauss	2.58	50.70	57.23	52.55	58.06	51.30	56.95	51.52	57.41	20.50	24.05
FO <i>P. lacunosa</i> (N)	3.70			78.55	86.49			78.55	86.49	24.13	25.96
LO <i>A. primus</i> (N)	4.70			126.05	138.65			126.05	138.65	47.50	52.16
FO <i>D. surculus</i> (N)	7.30			246.20	266.79			246.20	266.79	46.21	49.28
LO <i>C. miopelagicus</i> (N)	10.90			376.85	397.44			376.85	397.44	36.29	36.29
LO <i>S. heteromorphus</i> (N)	13.60			471.45	492.04			471.45	492.04	35.04	35.04
FO <i>S. heteromorphus</i> (N)	18.20			565.68	586.27			565.68	586.27	20.48	20.48

Notes: Ages are from Berggren et al. (1995). N = calcareous nannofossil.

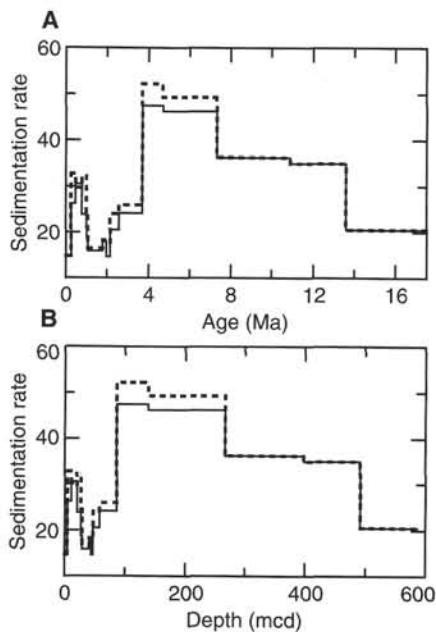


Figure 13. Site 982 sedimentation rates vs. age (A) and vs. composite depth (B). Solid lines indicate rates in mbsf/m.y.; dashed lines indicate rates in mcd/m.y.

56.1%. The concentration of carbonate in sediment is primarily controlled by dilution of biogenic carbonate by ice-rafted debris. These high amplitude variations are similar to those recorded and described in detail in DSDP Leg 94 sites (e.g., Ruddiman, Kidd, Thomas, et al., 1987) and in DSDP Hole 552A from the Hatton Drift in the North Atlantic (Zimmerman et al., 1984). The carbonate cycles in the upper interval of Hole 982B undoubtedly reflect glacial/interglacial fluctu-

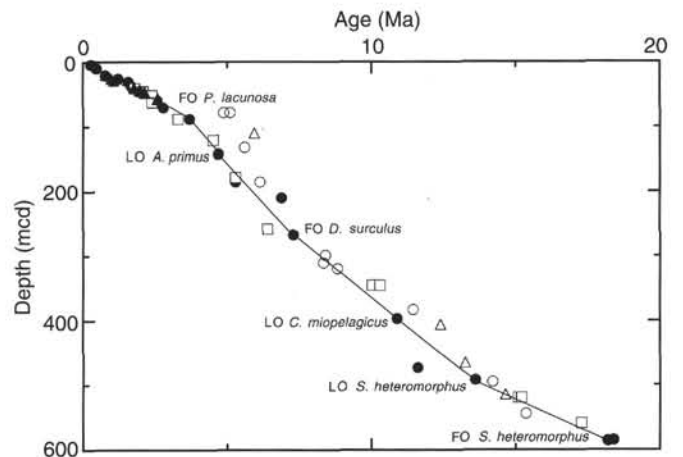


Figure 14. Site 982 age vs. depth (mcd) curve based on integrated magnetostratigraphic and biostratigraphic datums. Solid circles = nannofossils; open circles = diatoms; open squares = foraminifers; solid triangles = siliceous flagellates; open triangles = magnetostratigraphic datums.

ations. The lower interval (57.4–614.9 mbsf; late Pliocene to middle Miocene) corresponds to lithostratigraphic Unit II (see “Lithostratigraphy” section, this chapter), and the carbonate content is high throughout, with the average concentration being 90.7%.

Total organic carbon (TOC) contents vary between 0% and 0.36%, with an average value of 0.11% (Fig. 15; Table 11). This average is lower than the average of 0.2% calculated from DSDP Legs 1 through 31 by McIver (1975). The average of TOC content is 0.16% in the upper interval and 0.05% in the lower interval. A maximum TOC value of 0.36% occurs in the upper part of the sedimentary record of Hole 982B (Sample 162-982B-5H-1, 28–29 cm; 34.29 mbsf). Total nitrogen contents are generally very low (Fig. 15; Table 11; 0.02%–0.04%). Total sulfur values vary between 0% and 0.20% with an average value of 0.02% (Fig. 15; Table 11).

Table 10. Results of headspace gas analysis of Holes 982A and 982B samples using the Hewlett Packard 5890 Series II gas chromatograph.

Core, section, interval (cm)	Depth (mbsf)	C ₁ (ppm)
162-982A-		
1H-5, 0-5	6.03	2
2H-5, 0-5	14.23	2
3H-5, 0-5	23.73	3
4H-5, 0-5	33.23	3
5H-5, 0-5	42.73	3
6H-5, 0-5	52.23	2
7H-5, 0-5	61.73	3
8H-5, 0-5	71.23	3
9H-5, 0-5	80.73	3
10H-5, 0-5	90.23	3
11H-5, 0-5	99.73	4
12H-5, 0-5	109.23	3
13H-5, 0-5	118.73	3
14H-5, 0-5	128.23	3
15H-5, 0-5	137.73	3
16H-5, 0-5	147.23	3
17H-5, 0-5	156.73	3
18H-5, 0-5	166.23	3
19H-5, 0-5	175.73	3
20H-5, 0-5	185.23	3
21H-5, 0-5	194.73	3
22H-5, 0-5	204.23	3
23H-5, 0-5	213.73	3
24H-5, 0-5	223.23	3
25H-4, 0-5	231.23	3
26H-5, 0-5	242.23	3
162-982B-		
27X-4, 0-5	247.53	3
28X-3, 0-5	252.33	4
29X-3, 0-5	261.93	3
31X-5, 0-5	284.23	3
32X-2, 0-5	289.33	3
33X-4, 0-5	301.93	3
34X-5, 0-5	313.13	2
35X-3, 0-5	319.73	3
36X-4, 0-5	330.83	4
37X-5, 0-5	342.03	3
38X-5, 0-5	351.63	3
39X-4, 0-5	359.73	3
40X-4, 0-5	369.43	3
41X-4, 0-5	379.03	3
42X-4, 0-5	388.63	3
43X-3, 0-5	396.83	3
44X-4, 0-5	407.93	3
45X-4, 0-5	417.53	4
46X-5, 0-5	428.63	3
47X-4, 0-5	436.73	4
48X-4, 0-5	446.33	4
49X-4, 0-5	455.93	3
50X-4, 0-5	465.53	3
51X-4, 0-5	475.13	3
52X-5, 0-5	486.23	3
53X-4, 0-5	494.23	3
54X-4, 0-5	503.83	2
55X-6, 0-5	516.43	2
56X-5, 0-5	524.53	3
57X-4, 0-5	532.63	2
58X-2, 0-5	539.23	3
59X-CC, 15-20	546.08	6
60X-2, 0-5	558.53	7
61X-3, 3-8	569.76	5
62X-1, 0-5	576.43	3

Note: C₁ = methane

Composition of Organic Matter

The type of the organic matter in the sediments of Hole 982B has been characterized using organic carbon/nitrogen (C/N) ratios. The average C/N ratio of marine zoo- and phytoplankton is between 5 and 8, whereas higher land plants have ratios between 20 and 200 (Borodovskiy, 1965; Emerson and Hedges, 1988). Due to the organic-carbon-poor nature of the sediments, pyrolysis analyses were not made (Katz, 1983; Peters, 1986). C/N ratios vary between 0.6 and 8.5 in the sediments of Hole 982B (Fig. 15; Table 11). These data indicate a predominance of marine organic material (Fig. 16).

Further qualitative and quantitative organic geochemical data, such as detailed records of flux rates of terrigenous and marine organic carbon, as well as biomarker data, are required before a detailed pa-

leoceanographic interpretation of the organic carbon data can be made.

INORGANIC GEOCHEMISTRY

Interstitial Water

The pore-water profiles of Site 982 are unusual in that most parameters show a break in Core 162-982-30X at a depth of about 280 mbsf. The depth of this break generally corresponds with recovery in Core 162-982B-30X (268.5–278.2 mbsf) of a single clast of silica-cemented foraminifer sand containing quartz and glauconite (see "Lithostratigraphy" section, this chapter), which is estimated to be 8 Ma in age (see "Biostratigraphy" section, this chapter). Logging results indicate that this clast is from a dense layer approximately 4 m thick (see "Wireline Logging" section, this chapter), which has apparently impeded diffusion of pore fluids, resulting in the observed anomalies in interstitial water profiles. Silicification has previously been observed to result in a large decrease in porosity and a subsequent large decrease in diffusion, thereby creating a "diffusion barrier" (Gieskes, 1983). If silicification of this unit occurred before the Messinian Stage of the late Miocene and diffusion has been completely impeded by this layer, it opens the intriguing possibility that pore waters below this "barrier" may preserve a record of pre-Messinian seawater, whereas pore waters above would have been influenced by the removal of dissolved salts during the Salinity Crisis.

In the upper sediments, the sulfate, ammonium, and alkalinity profiles are indicative of sulfate reduction. Sulfate decreases from 26.4 to 14.3 mM between 6 and 280 mbsf (Fig. 17A; Table 12). Across the lithified horizon, sulfate concentrations drop slightly from 16.5 to 14.3 mM. Below 280 mbsf, sulfate values vary between 12 and 14 mM. Ammonium concentrations increase rapidly in the top 100 m of sediment, the zone of sulfate reduction, and then level off at 225 mM between 150 and 284 mbsf (Fig. 17C; Table 12). Below the lithified horizon, ammonium concentrations increase again from 225 mM to a maximum of 343 mM near the base of the core. Alkalinity increases rapidly in the top 100 m of section from about 3.6 mM near the surface to more than 6 mM and then remains nearly constant at about 6.5 mM between 150 and 284 mbsf (Fig. 17D; Table 11). Below the lithified horizon, alkalinity shows a decreasing trend from 6.7 to 3.3 mM.

Similar to Sites 980 and 981, the magnesium profile at Site 982 resembles that of sulfate and the inverse of the ammonium profile (Fig. 17B; Table 11). From the core top to 280 mbsf, magnesium decreases from 50 to 32 mM, with the largest changes occurring in the top 50 m of sediment, the same interval in which the largest changes in sulfate and ammonium are observed. The rapid decline in the top 50 m appears to be linked with sulfate reduction, whereby hydrogen sulfide reacts with iron in clay minerals to produce iron sulfides, which is accompanied by replacement of magnesium for iron (Drever, 1971). Decreases in magnesium below 280 mbsf may reflect chemical alteration of volcanic material in the sediment column.

Calcium concentrations increase rapidly downhole in the top 150 m of sediment from 11 mM near the surface to 16 mM at 200 mbsf (Fig. 17E; Table 11). There is a small increase in calcium across the lithified layer at 280 mbsf, and then values slowly increase toward the base of the core. The increase in calcium in the upper 180 m may reflect carbonate dissolution, although the increase in alkalinity during sulfate reduction usually results in carbonate saturation of pore waters. The slow increase in calcium below 180 mbsf may reflect exchange of magnesium for calcium during alteration of volcanic material.

Silica concentrations increase downhole in the upper 250 m from 306 to 1172 μ M. In the sample closest to the lithified zone, dissolved silica drops 116 μ M (Fig. 17F; Table 11); this may be related to silicification of the foraminifer sand unit. Below this lithified layer, silica concentrations increase and remain high until 530 mbsf where

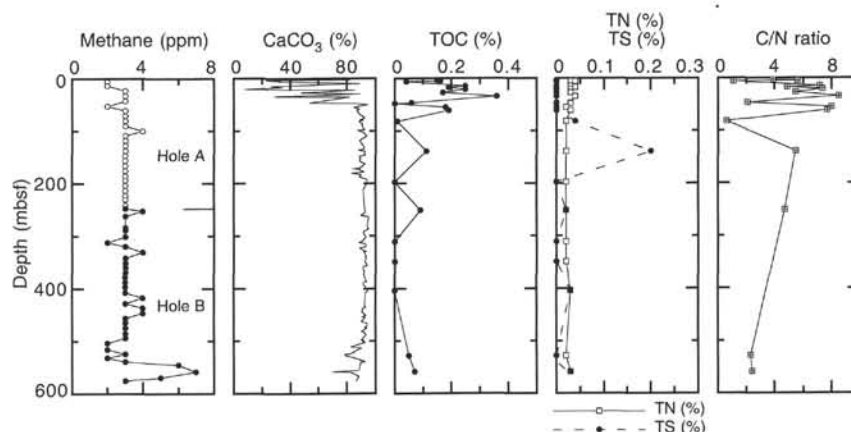


Figure 15. Methane concentration in Holes 982A (open circles) and 982B (solid circles). Calcium carbonate (CaCO_3), total organic carbon (TOC), total nitrogen (TN), and total sulfur (TS) contents, and TOC/TN (C/N) ratio in Hole 982B.

they decrease abruptly. This decrease is associated with chertification of the sediments below 500 mbsf (see “Lithostratigraphy” section, this chapter).

Phosphate concentrations are low and generally less than 4 μM throughout Site 982 (Fig. 17G). A decrease is observed at about 350 mbsf, and phosphate values are lower below this level. Potassium concentrations show a steady decline from as high as 12 mM near the surface to a low of about 8 mM near the bottom of the hole (Fig. 17H; Table 11). This decrease may be due to reactions in the sediment, such as formation of smectite.

The profiles of sodium and especially chloride display the most abrupt changes across the lithified layer (Fig. 17I, 17J; Table 11). Sodium concentrations average 496 mM above and increase to 508 mM below, resulting in a net mean difference of 12 mM (Fig. 17J). Chloride concentrations average 567 mM above and increase to 572 mM below, resulting in a net mean difference of 5 mM (Fig. 17I). The change in sodium and chloride across the lithified horizon may reflect the decrease in oceanic salinity caused by the removal of halite in the Messinian evaporites. The relationship between sodium and chloride is linear (Fig. 17O), but the slope is significantly greater than the 1:1 predicted slope if halite precipitation was removing these elements from seawater. Considering the unexpected slope of about 2:1, we speculate that sodium may not be conservative and there must be an additional source of sodium to the pore waters. Shore-based work is needed to test the assumption that chloride is conservative and has not been affected by diagenetic reactions (e.g., hydrolysis of clays during alteration of volcanic material).

With the exception of the top sample, salinity is constant at 34 for the top 220 m of core. Salinity shows more variation below this level and slightly lower mean values occur below 400 mbsf (Fig. 17K; Table 11). The pH values are about 7.5 at the top of the core and generally decrease downhole in the upper 260 m. A modest increase occurs across the lithified layer at 280 mbsf and then values decrease sharply at 340 mbsf followed by a gradual increase toward the base of the core (Fig. 17L; Table 11).

Dissolved lithium at Site 982 is relatively constant in the upper 250 mbsf, ranging from 12 to 14 μM , with slightly higher values in the upper 20 m (from 14 to 28 μM). Below 250 mbsf, lithium increases with depth from 14 to 113 μM , suggesting that lithium is being released during alteration of volcanic material in the sediments (Fig. 17M; Table 11). The small decrease observed in the very bottom of the profile could also represent some uptake of lithium during chertification.

Interstitial water profiles of strontium increase from 290 to 1159 μM in the top 100 m and then remain relatively constant (Fig. 17N; Table 11). At 250 mbsf there is a small minimum in dissolved strontium that may have some relation to the silicified foraminiferal sand at this depth. The strontium profile implies that some recrystallization of biogenic calcite has occurred to enrich the pore waters in

strontium (Baker et al., 1982). In addition, two nodules of celestite (SrSO_4) were found at this site, at 165 and 377 mbsf (see “Lithostratigraphy” section, this chapter). Although there is no apparent change in the strontium concentrations at these depths, celestite is a very significant sink for this element (Baker, 1986), and decreases in dissolved strontium associated with the precipitation of authigenic celestite must have been modified by diffusion.

PHYSICAL PROPERTIES

The shipboard physical properties program at Site 982 included nondestructive, near-continuous measurements of bulk density, bulk magnetic susceptibility, compressional-wave (*P*-wave) velocity, and natural gamma radiation on whole-round sections of all cores from each hole using the multisensor track (MST) (see “Explanatory Notes” chapter, this volume).

Index properties (gravimetric density) measurements were made on one or two (10-cm³) samples per working section in all cores (see “Explanatory Notes” chapter, this volume). Method C for calculating index properties was used at this site; all discrete measurements were made on samples from Hole 982B. Index properties data are presented in Table 13.

Discrete compressional velocity and undrained vane-shear-strength measurements were made at a resolution of about one measurement per section (Tables 14, 15). The sonic transducers of the digital sound velocimeter (DSV) were inserted into the sediment along the core axis until about 20 mbsf; below this depth the sediment became too consolidated to use the DSV and the Hamilton Frame velocimeter was used to make sonic measurements through the core liner.

Geotechnical Stratigraphy

Five geotechnical units are defined at Site 982. These units are defined in terms of inflections, reversals, or discontinuities in the prevailing trends of physical properties measured at this site (Figs. 18, 19).

Geotechnical Unit G1, which extends from the seafloor to 20 mbsf, is defined by relatively low mean shear strengths (13.4 kPa) and compressional velocities (1541 m/s); this unit is also marked by low-frequency fluctuations in magnetic susceptibility and natural gamma radiation. The shear strength measurements in geotechnical Unit G1 show little scatter, except for two peaks just above the base of the unit (Fig. 18). The upper surface of a prominent peak in both magnetic susceptibility and natural gamma radiation defines the boundary between geotechnical Units G1 and G2.

Geotechnical Unit G2 (20–49.5 mbsf) exhibits higher frequency fluctuations in susceptibility and natural gamma radiation, which de-

Table 11. Summary of organic geochemical analyses in Hole 982B samples.

Core, section, interval (cm)	Depth (mbsf)	IC (%)	CaCO ₃ (%)	TC (%)	TOC (%)	TN (%)	TS (%)	C/N
160-982B-								
1H-2, 102-103	2.5	9.86	82.1					
1H-3, 31-32	3.3	2.78	23.2	2.93	0.15	0.04	0.00	3.9
1H-4, 55-56	5.1	3.99	33.2	4.15	0.16	0.03	0.00	5.6
2H-1, 44-45	5.9	3.88	32.3	3.92	0.04	0.04	0.00	1.1
2H-3, 102-103	9.5	10.69	89.0					
2H-7, 45-46	15.0	3.13	26.1	3.38	0.25	0.03	0.00	7.2
3H-2, 65-66	17.2	4.08	34.0	4.27	0.19	0.04	0.00	4.9
3H-4, 113-114	20.6	1.00	8.3	1.25	0.25	0.03	0.00	7.4
3H-5, 104-105	22.0	10.28	85.6					
4H-2, 98-99	27.0	5.71	47.6	5.88	0.17	0.03	0.00	5.5
4H-4, 98-99	30.0	10.73	89.4					
5H-1, 28-29	34.3	3.48	29.0	3.84	0.36	0.04	0.00	8.5
5H-2, 28-29	35.8	9.78	81.5					
6H-3, 30-31	46.8	6.40	53.3	6.46	0.06	0.03	0.00	2.1
6H-3, 80-81	47.3	10.41	86.7	10.38	0.00	0.03	0.00	
6H-5, 30-31	49.8	11.31	94.2					
7H-2, 100-101	55.5	10.16	84.6	10.34	0.18	0.02	0.00	8.0
7H-4, 100-101	58.5	10.67	88.9					
7H-6, 100-101	61.5	10.45	87.0	10.64	0.19	0.03	0.00	7.7
8H-3, 116-117	66.7	10.60	88.3					
9H-2, 116-117	74.7	11.10	92.5					
9H-5, 117-118	79.2	10.72	89.3					
9H-6, 37-38	79.9	10.98	91.5					
10H-1, 36-37	81.9	10.62	88.5	10.63	0.01	0.02	0.04	0.6
10H-4, 117-118	87.2	10.88	90.6					
10H-6, 36-37	89.4	10.87	90.5					
11H-2, 134-135	93.8	10.94	91.1					
11H-5, 43-44	97.4	11.08	92.3					
11H-6, 33-34	98.8	10.45	87.0					
12H-2, 43-44	102.4	11.00	91.6					
12H-4, 116-117	106.2	11.07	92.2					
12H-6, 27-28	108.3	11.27	93.9					
13H-1, 86-87	110.9	11.19	93.2					
13H-4, 74-75	115.2	10.85	90.4					
13H-6, 74-75	118.2	10.67	88.9					
15H-2, 30-31	130.8	11.02	91.8					
15H-4, 30-31	133.8	11.05	92.0					
15H-6, 30-31	136.8	10.58	88.1					
16H-1, 101-102	139.5	11.13	92.7	11.24	0.11	0.02	0.20	5.5
16H-5, 100-101	145.5	11.04	92.0					
16H-6, 100-101	147.0	11.22	93.5					
17H-1, 90-91	148.9	10.68	89.0					
17H-4, 83-84	153.3	10.75	89.5					
17H-6, 76-77	156.3	10.65	88.7					
18H-2, 136-137	160.4	10.83	90.2					
18H-4, 85-86	162.9	11.14	92.8					
18H-6, 128-129	166.3	11.00	91.6					
19H-3, 92-93	170.9	10.72	89.3					
19H-4, 86-87	172.4	10.13	84.4					
19H-5, 87-88	173.9	10.61	88.4					
20H-2, 45-46	178.5	11.01	91.7					
20H-3, 128-129	180.8	10.01	83.4					
20H-5, 83-84	183.3	10.81	90.0					
21H-2, 68-69	188.2	10.69	89.0					
21H-5, 68-69	192.7	11.32	94.3					
22H-2, 77-78	197.8	11.33	94.4	11.14	0.00	0.02	0.00	
22H-4, 77-78	200.8	11.27	93.9					
23H-5, 90-91	211.9	11.00	91.6					
28X-2, 83-84	251.6	11.07	92.2	11.16	0.09	0.02	0.02	4.7
28X-4, 108-109	254.9	11.18	93.1					
29X-2, 83-84	261.2	10.76	89.6					
29X-4, 61-62	264.0	11.40	95.0					
31X-4, 84-85	283.5	11.29	94.0					
31X-6, 62-63	286.3	11.40	95.0					
32X-2, 61-62	289.9	11.17	93.0					
32X-4, 67-68	293.0	11.00	91.6					
33X-2, 70-71	299.6	11.07	92.2					
33X-4, 90-91	302.8	11.20	93.3					
34X-3, 92-93	311.0	10.84	90.3	10.82	0.00	0.02	0.00	
34X-4, 73-74	312.3	10.61	88.4					
34X-6, 12-13	314.7	11.17	93.0					
35X-2, 64-65	318.8	11.22	93.5					
35X-3, 94-95	320.6	11.14	92.8					
35X-4, 68-69	321.9	10.68	89.0					
36X-2, 33-34	328.1	11.06	92.1					
36X-3, 73-75	330.0	11.27	93.9					
36X-3, 53-54	329.8	11.05	92.0					
37X-2, 53-54	338.0	11.20	93.3					
37X-3, 73-74	339.7	11.13	92.7					
37X-5, 121-122	343.2	11.23	93.5					
38X-3, 43-44	349.0	11.09	92.4	11.01	0.00	0.02	0.00	
38X-4, 91-92	351.0	11.21	93.4					
39X-1, 104-105	356.2	11.33	94.4					
39X-3, 63-64	358.8	10.91	90.9					
40X-2, 52-53	366.9	11.02	91.8					
40X-5, 60-61	371.5	11.00	91.6					
42X-2, 104-105	386.6	11.26	93.8					
42X-3, 57-58	387.7	11.09	92.4					

Table 11 (continued).

Core, section, interval (cm)	Depth (mbsf)	IC (%)	CaCO ₃ (%)	TC (%)	TOC (%)	TN (%)	TS (%)	C/N
42X-4, 27-28	388.9	10.97	91.4					
43X-1, 62-63	394.4	11.04	92.0					
43X-3, 38-39	397.2	11.22	93.5					
43X-4, 88-89	399.2	11.21	93.4					
44X-1, 72-73	404.1	11.35	94.5	11.24	0.00	0.03	0.03	
44X-3, 68-69	407.1	11.20	93.3					
44X-4, 128-129	409.2	11.15	92.9					
47X-1, 73-74	432.9	11.11	92.5					
47X-3, 88-89	436.1	11.23	93.5					
47X-4, 134-135	438.0	10.93	91.0					
48X-3, 62-64	445.4	10.90	90.8					
48X-4, 107-109	447.4	10.97	91.4					
49X-1, 78-80	452.2	11.21	93.4					
49X-2, 77-79	453.7	10.86	90.5					
49X-3, 101-103	455.4	11.16	93.0					
50X-2, 17-19	462.7	10.82	90.1					
50X-3, 94-96	465.0	11.06	92.1					
50X-4, 70-72	466.2	11.32	94.3					
51X-2, 78-80	472.9	11.25	93.7					
51X-3, 44-46	474.1	11.09	92.4					
51X-4, 101-103	476.1	11.26	93.8					
52X-2, 14-16	481.9	10.84	90.3					
52X-3, 99-101	484.2	11.07	92.2					
52X-6, 31-33	488.0	11.20	93.3					
53X-4, 99-101	495.2	10.95	91.2					
53X-5, 127-129	497.0	10.98	91.5					
53X-6, 64-66	497.9	10.77	89.7					
54X-1, 77-79	500.1	11.03	91.9					
54X-2, 143-145	502.2	10.94	91.1					
54X-3, 84-86	503.2	11.15	92.9					
55X-2, 75-77	511.2	9.98	83.1					
55X-4, 83-85	514.2	10.80	90.0					
55X-6, 79-81	517.2	10.44	87.0					
56X-3, 27-29	521.8	10.13	84.4					
56X-5, 83-85	525.3	9.88	82.3					
56X-6, 45-47	526.5	9.39	78.2					
57X-1, 59-60	528.7	9.49	79.1	9.54	0.05	0.02	0.00	2.3
57X-3, 59-60	531.7	10.17	84.7					
58X-2, 70-71	539.9	11.16	98.0					
58X-3, 41-42	541.1	10.77	89.7					
60X-1, 15-16	557.2	10.61	88.4					
60X-2, 33-34	558.8	8.36	69.6	8.43	0.07	0.03	0.03	2.4
60X-2, 133-134	559.8	9.92	82.6					
61X-1, 55-56	567.3	10.62	88.5					
62X-1, 19-20	576.6	10.38	86.5					

Notes: IC = Inorganic carbon, CaCO₃ = calcium carbonate, TC = total carbon, TOC = total organic carbon, TN = total nitrogen, TS = total sulfur, and C/N = total organic carbon/total nitrogen ratios.

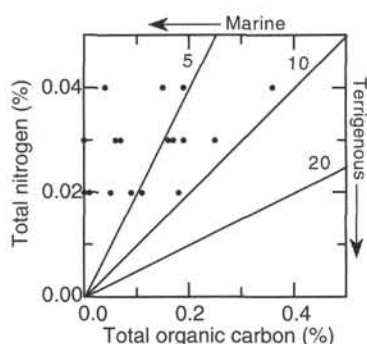


Figure 16. Total organic carbon vs. total nitrogen in Hole 982B. Lines show C/N ratios of 5, 10, and 20.

crease in amplitude toward the base of the unit (Figs. 18, 19); bulk density (mean = 1.78 g/cm³) and velocity (mean = 1589 m/s) values increase downhole in this unit, while mean shear strengths are higher (22.4 kPa) and show more scatter than those measured in geotechnical Unit G1.

These upper two units correlate with similarly defined units at Sites 980 and 981 (see "Physical Properties" section, "Sites 980/981" chapter, this volume). The natural gamma radiation data (total

counts/second) in the upper two units exhibit fluctuations which are similar in character to those observed in the magnetic susceptibility record (Fig. 18); these fluctuations seem to correspond to variations in the amount of terrigenous material in the sediment (see "Lithostratigraphy" section, this chapter).

Geotechnical Unit G3 (49.5–166.5 mbsf) is defined by relatively constant mean shear strength (14.1 kPa), bulk density (1.74 g/cm³), and velocity (1565 m/s) values. Shear strength declines in the upper part of geotechnical Unit G3 and then maintains fairly constant, low values (mean = 14.1 kPa) to the base of this unit. The magnetic susceptibility of the sediment in this unit is very low to absent. The natural gamma radiation exhibits a step increase at around 75 mbsf, remains fairly constant until about 140 mbsf, and then decreases to a lower but fairly constant level; it does not increase again until geotechnical Unit G5 (Fig. 19).

Geotechnical Unit G4 (166.5–480 mbsf) exhibits an increased velocity gradient relative to the overlying unit (see Fig. 19), and a scatter in peak strength values. The highest shear strengths in Hole 982B were measured in this unit, but the range of values is highly variable (2.9–68.5 kPa). The scatter in the deeper values is due to the "biscuiting" of the cores in the XCB section of the hole and the presence of more lithified sediment, approaching chalk.

Geotechnical Unit G5 (480 mbsf to total depth in Hole 982B) is defined by large increases in measured compressional velocity and an increase in lithification (see "Lithostratigraphy" section, this chap-

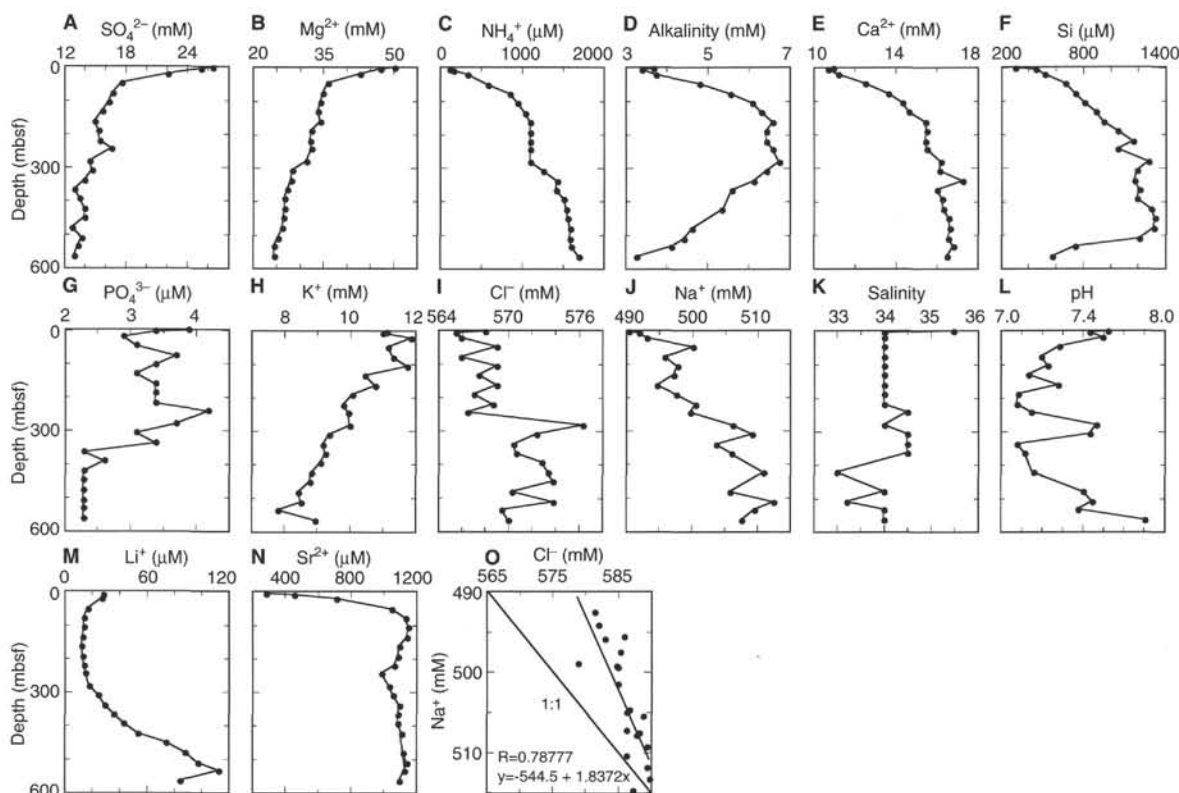


Figure 17. Vertical profiles of interstitial sulfate (A), magnesium (B), ammonium (C), alkalinity (D), calcium (E), silica (F), phosphate (G), potassium (H), chloride (I), sodium (J), salinity (K), pH (L), lithium (M), strontium (N), and the relationship between sodium and chloride (O).

Table 12. Composition of interstitial waters in Holes 982A and 982B.

Core, section, interval (cm)	Depth (mbsf)	Na (mM)	K (mM)	Mg (mM)	Ca (mM)	Cl (mM)	SO ₄ (mM)	NH ₄ (μM)	Si (μM)	PO ₄ (μM)	pH	Alkalinity (mM)	Salinity	Sr (μM)	Li (μM)
162-982A-															
1H-4, 145-150	5.95	490	11.1	50.5	11.0	567	26.4	121.9	306	3.9	7.53	3.639	35.5	290	28
2H-2, 145-150	11.15	491	11.0	47.6	10.6	565	25.3	176.3	449	3.4	7.44	3.365	34.0	456	28
3H-4, 145-150	23.65	493	11.9	43.1	11.2	565	22.0	346.9	517	2.9	7.50	3.724	34.0	720	27
6H-4, 145-150	52.15	500	11.1	36.2	12.5	568	17.5	597.4	672	3.1	7.29	4.800	34.0	1056	17
9H-4, 145-150	80.65	495	11.3	35.0	13.6	565	16.6	862.3	747	3.7	7.20	5.536	34.0	1144	14
12H-4, 145-150	109.15	497	11.7	34.6	14.3	568	16.3	956.7	813	3.4	7.23	6.089	34.0	1159	14
15H-4, 145-150	137.65	497	10.4	34.0	14.7	567	15.7	1047.5	894	3.1	7.14	6.304	34.0	1149	13
18H-4, 145-150	166.15	494	10.8	34.4	15.5	568	14.9	1112.8	954	3.4	7.28	6.571	34.0	1102	12
21H-4, 145-150	194.65	497	10.1	32.6	15.5	566	15.3	1123.7	1058	3.4	7.09	6.415	34.0	1097	13
24H-4, 140-150	223.10	500	9.8	32.3	15.5	568	15.4	1123.7	1172	3.4	7.08	6.435	34.0	1069	14
162-982B-															
27X-3, 140-150	247.40	499	9.9	32.7	15.5	566	16.6	1112.8	1056	4.2	7.15	6.585	34.5	944	15
31X-4, 140-150	284.15	506	10.0	31.5	16.2	576	14.3	1120.1	1279	3.7	7.47	6.724	34.0	1044	18
34X-4, 145-150	313.05	509	9.3	28.5	16.2	572	14.6	1276.2	1193	3.1	7.44	6.415	34.5	1068	25
37X-4, 145-150	341.95	503	9.2	28.3	17.3	570	13.8	1443.1	1176	3.4	7.08	6.092	34.5	1101	29
40X-4, 140-150	369.30	506	9.3	27.3	16.0	570	12.9	1439.5	1214	2.3	7.12	5.580	34.5	1100	36
43X-2, 140-150	396.70		9.1	26.9	16.3	572	13.4	1519.5	1197	2.6				1099	44
46X-4, 140-150	428.50	511	8.8	26.9	16.3	573	13.9	1555.6	1299	2.3	7.16	5.335	33.0	1118	54
49X-3, 140-150	455.80		8.8	26.4	16.6	573	13.9	1581.1	1334	2.3				74	
52X-4, 135-150	486.05	505	8.4	26.2	16.7	570	12.6	1602.8	1321	2.3	7.41	4.607	34.0	1132	89
55X-5, 135-150	516.25	512	8.5	25.5	16.6	573	13.6	1606.5	1217	2.3	7.45	4.404	33.2	1153	98
58X-1, 135-150	539.05	509	7.8	24.5	16.8	569	13.3	1624.6	740	2.3	7.38	4.085	34.0	1138	113
61X-3, 8-23	569.78	507	8.9	24.6	16.5	569	12.8	1719.0	572	2.3	7.71	3.259	34.0	1106	85

ter). The velocities also show a wider scatter, with high velocities measured in thin, indurated intervals.

Discussion

Mean gravimetric bulk density values are consistently higher than the mean GRAPE bulk density values in the upper two geotechnical units by approximately 0.25 and 0.23 g/cm³, respectively; this relationship is also observed at Site 981 (see "Physical Properties" section, "Sites 980/981" chapter, this volume). The mean offset between

these two sets of density measurements decreases to about 0.19 g/cm³ in the middle two geotechnical Units G3 and G4, but in the lower-most geotechnical Unit G5, this offset increases again to about 0.28 g/cm³ (Figs. 18, 19).

In situ bulk densities, measured using the Hostile-Environment Litho-Density Tool (HLDT) of the "Quad combination" standard logging run, are on the average about 10% greater than the main trend of the GRAPE density measurements (see "Wireline Logging" section, this chapter) and are similar to the gravimetric bulk density measurements. Corrections to the laboratory values for the removal of the

Table 13. Index properties of samples from Hole 982B.

Core, section, interval (cm)	Depth (mbsf)	Water content		Bulk density	Grain density	Dry density	Porosity	Void ratio
		(wet %)	(dry %)	Method C (g/cm ³)	Method C (g/cm ³)	Method C (g/cm ³)	Method C (%)	Method C
162-982B-								
1H-1, 39-41	0.39	49.9	99.4	1.50	2.77	0.75	72.9	2.69
1H-2, 98-100	2.48	50.8	103.3	1.50	2.85	0.74	74.2	2.87
1H-3, 63-65	3.63	40.6	68.2	1.66	2.86	0.99	65.6	1.91
1H-4, 53-55	5.03	36.5	57.4	1.72	2.82	1.09	61.3	1.58
2H-1, 43-45	5.93	40.4	67.7	1.62	2.66	0.96	63.7	1.75
2H-2, 85-87	7.85	43.6	77.2	1.54	2.52	0.87	65.5	1.90
2H-3, 99-101	9.49	40.0	66.7	1.65	2.77	0.99	64.3	1.80
2H-4, 99-101	10.99	44.7	80.8	1.56	2.72	0.86	68.2	2.14
2H-5, 46-48	11.96	43.1	75.7	1.57	2.62	0.89	65.9	1.93

Only part of this table is reproduced here. The entire table appears on the CD-ROM (back pocket).

Table 14. Compressional-wave velocity measurements from Hole 982B.

Core, section, interval (cm)	Depth (mbsf)	Velocity (m/s)	Temperature (°C)	Direction
162-982B-				
1H-1, 38	0.38	1520	18.5	z
1H-2, 95	2.45	1516	18.9	z
1H-3, 63	3.63	1563	19.4	z
1H-3, 110	4.10	1552	17.1	z
1H-4, 50	5.00	1562	19.7	z
2H-1, 40	5.90	1540	19.4	z
2H-1, 106	6.56	1521	19.0	z
2H-2, 89	7.89	1508	18.8	z
2H-3, 32	8.82	1497	19.5	z

Note: For explanation of measurement directions, see "Explanatory Notes" chapter (this volume).

Only part of this table is reproduced here. The entire table appears on the CD-ROM (back pocket).

Table 15. Undrained shear strength measurements from Hole 982B.

Core, section, interval (cm)	Depth (mbsf)	Undrained shear strength (kPa)	Spring no.
162-982B-			
1H-1, 39	0.39	10.1	1
1H-2, 98	2.48	4.7	1
1H-3, 78	3.78	18.9	1
1H-3, 113	4.13	6.7	1
1H-4, 52	5.02	10.9	1
2H-1, 52	6.02	11.9	1
2H-2, 92	7.92	7.1	1
2H-3, 98	9.48	11.0	1
2H-4, 99	10.99	10.5	1

Only part of this table is reproduced here. The entire table appears on the CD-ROM (back pocket).

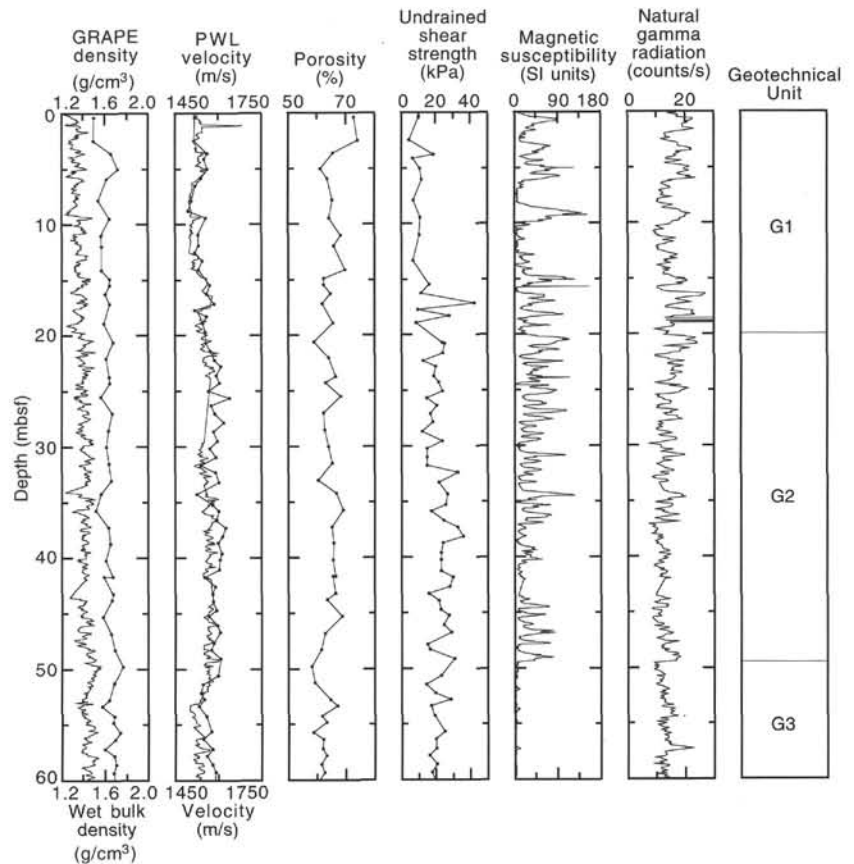


Figure 18. GRAPE bulk density (thin line) superimposed with gravimetric bulk density (Method C; line with solid circles). PWL velocity (thin line) superimposed with split-core velocity (line with solid circles), porosity, undrained shear strength, magnetic susceptibility, and natural gamma radiation vs. sub-bottom depth for the upper 60 mbsf of Hole 982B. Also shown are the boundaries of geotechnical units.

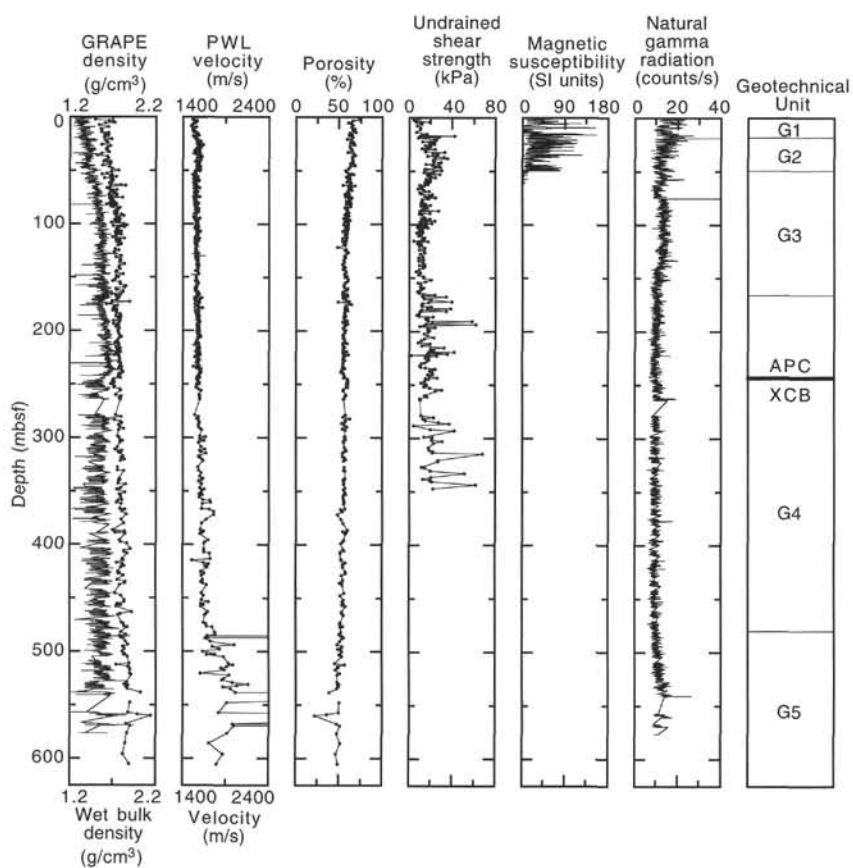


Figure 19. GRAPE bulk density (thin line) superimposed with gravimetric bulk density (Method C; line with solid circles), PWL velocity (thin line) superimposed with split-core velocity (line with solid circles), porosity, undrained shear strength, magnetic susceptibility, and natural gamma radiation vs. sub-bottom depth in Hole 982B. Also shown are the boundaries of geotechnical units.

in situ overburden pressure (i.e., to correct for the expansion of sediment upon recovery) would tend to increase the laboratory values further, by a few percent. The overall trend of the values measured by these different methods are, however, quite similar.

The change in the character of the magnetic susceptibility data within the upper two geotechnical units may be explained by changes in the relative accumulation of terrigenous material derived from the continents surrounding the North Atlantic. High values of magnetic susceptibility and natural gamma radiation (total counts/second) are positively correlated with clay-rich zones, whereas higher weight percentages of calcium carbonate result in decreased magnetic susceptibility (Robinson, et al., 1995; Grousset et al., 1993) and natural gamma radiation values (see "Lithostratigraphy" section, this chapter).

In Figures 18 and 19 split-core velocities and those measured with the PWL are superimposed to show that the two sets of values coincide well. Below the APC/XCB transition at 243 mbsf, only discrete velocity data are available; the PWL was turned off below this depth due to attenuation of the acoustic pulse by air between the sediment and the liner. Mean values of split-core velocity measurements increased from 1541 m/s in geotechnical Unit G1 to 1589 m/s in Unit G2, but declined in Unit G3 to 1565 m/s. Mean velocity values increased again in Unit G4 to 1612 m/s. Below 480 mbsf (Unit G5), some of the sediments were markedly more indurated and measured velocity values were high, averaging 1853 m/s (Fig. 19). Selected lithified samples had measured velocities of 2950 to 4550 m/s. These values were not included in calculating the mean value for geotechnical Unit G5.

The in situ velocities collected by the Sonic Digital Tool (SDT-C) are discussed in "Wireline Logging" section (this chapter). The velocities on the recalculated sonic log are close to those predicted by the empirical function of Hamilton (1979), but are typically considerably higher than the laboratory velocities measured on split cores.

The laboratory values are reported as uncorrected values. For quantitative work, corrections should be applied laboratory measurements for in situ temperatures and the effects of porosity increase due to the release of overburden pressure. Both of these effects tend to decrease the magnitude of velocities measured in the shipboard laboratory.

WIRELINE LOGGING

Operations

At Site 982, downhole wireline logging measurements were conducted using the Quad combination (Quad combo) and Formation MicroScanner (FMS) tool strings in Hole 982B (Table 16). The Quad combo consists of seismic stratigraphy tools and lithoporosity tools with the Lamont temperature tool (TLT) attached to its base. Drilling of Hole 982B was completed at ~615 mbsf (1760 mbrf) and the hole was conditioned by a "wiper trip" to remove drilling debris prior to logging. The wiper trip for this hole consisted of lowering drill string to bottom of hole and flushing with seawater.

Wireline heave compensator was used to counter ship heave. Refer to "Explanatory Notes" chapter (this volume) for complete description of all tool strings and associated acronyms.

Hole conditions during logging were very good. No obstacles were encountered and only a meter of drilling debris remained at the bottom of the hole. Caliper data from both tool strings indicated that hole diameter varied between 30 and 38 cm, with very few "washed out" zones in excess of 40 cm. The bottom of the drilling pipe was set at 98 mbsf (1242 mbrf) and was raised 15 m to ~80–83 m during the uphole logging of both the Quad combo and the FMS to allow for additional log measurements. The natural gamma-ray tool (NGT), which is used with every tool string, was used to determine the mudline through the drill pipe. The mudline was measured at ~1144 mbrf by running the NGT very slowly near estimated driller's depth and

Table 16. Logged depth intervals in Hole 982B for Quad combination and FMS runs.

String	Run	Depth interval logged		Tools
		(mbsf)	(mbrf)	
Quad combo:	Down	98.0–615.0	1242.0–1759.0	NGT/SDT/CNT-G/HLDT/DIT/TLT
	Up	614.0–83.0	1758.0–1227.0	NGT/SDT/CNT-G/HLDT/DIT/TLT
	Up*	206.0–131.0	1350.0–1275.0	NGT/SDT/CNT-G/HLDT/DIT/TLT
Start time:	1320 hr			
Stop time:	1730 hr			
Logging speeds:	375 m/hr down log 275 m/hr up log			
(Mudline measured at ~1144 mbrf with NGT)				
String	Run	Depth interval logged		Tools
		(mbsf)	(mbrf)	
FMS:	Up	610.0–80.0	1754.0–1224.0	NGT/FMS/GPIT
	Up	610.0–471.0	1754.0–1615.0	NGT/FMS/GPIT
	Up#	505.0–83.0	1649.0–1227.0	NGT/FMS/GPIT
Start time:	1900 hr			
Stop time:	2300 hr			
Logging speed:	460 m/hr			
New wireline heave compensation testing:				
Start time:	2330 hr			
Stop time:	0130 hr			
Wiper trip: Hole conditioning prior to logging				
Start time:	0400 hr			
Stop time:	1130 hr			
Total logging time: 21.5 hr				
Estimated time: ~20 hr				

Notes: Depths are in meters below seafloor (mbsf) and meters below rig floor (mbrf). * = repeat section for quality control. # = overlapped run on second pass due to MAXIS computer problem. NGT = Natural Gamma-ray Tool, SDT = Sonic Digital Tool (Array), CNT-G = Dual Porosity Compensated Neutron Tool, HLDT = High-temperature Litho-Density Tool, DIT = Phasor Dual Induction Tool, TLT = Lamont Temperature Logging Tool, FMS = Formation MicroScanner, GPIT = General Purpose Inclinerometry Cartridge.

recording where a spike occurs when seawater is encountered. This mudline value was used to depth-shift all raw data from both tool strings to mbsf from mbrf. Due to the homogeneous nature of the sediments observed from Hole 982A and 982B, the geochemical logging tool (GLT) string was not used. Table 16 provides a complete summary of logged depth intervals, tools used, and logging times.

Log Quality and Initial Results

The wireline logging measurements from both tool strings were generally very good due to good borehole conditions. No major differences were noted in the borehole conditions between the APC section (0–245 mbsf) and the XCB section (245–615 mbsf), as indicated by the calipers. In fact, the best recorded section, especially with the FMS resistivity imaging, was from the lower 150 m of the hole. Preliminary comparison of logging results with core measurements of gravimetric density and natural gamma radiation show good correlations. Porosity measurements in the logs appear on average to be in agreement with the core data, but the signal for all three types of porosity (neutron, epithermal, and high-resolution thermal neutron) measured by the lithoporosity tool string appears noisy and not well calibrated. Sonic velocity logs were more consistent at longer receiver spacings (10 and 12 ft) than at the shorter spacings, where sensitivity to changing borehole conditions caused cycle skipping problems. Computed wireline log velocities were generally greater than laboratory *P*-wave velocities (see “Physical Properties” section, this chapter). Log bulk density measurements matched very well with gravimetric wet bulk density data in cores.

Depth: Core-to-Log Comparison

One of the core-to-log data comparisons was made using laboratory core natural gamma radiation (NGR) measurements (1 sample per 10 cm) vs. continuous log electrical resistivity (SFLU) and NGR

measurements (Fig. 20). The average vertical resolution of log NGR and SFLU within the hole is ~40–45 cm and 15–20 cm, respectively. By comparing the curve patterns of NGR and SFLU from the logging data and using the location of known lithologic features in the core and the logs as tie points, the core NGR was matched to the log NGR and SFLU curves. The primary features of the core curve are easy to match with the log NGR and SFLU curves (Fig. 20). The major tie points used are displayed, but because of the compressed scale of Figure 20, finer scale correlations may not be obvious. Observed ash layers, concretions or nodules, and discolored intervals in the cores often serve as good tie points as they have significant resistivity and/or NGR peaks associated with them. The chemistry of ash layers also may vary, however, so the resistivity or other logs may sometimes correlate better with a specific feature than NGR.

The purpose of this analysis was to not only compare data values but to assess how well the core depth (mbsf) relates to log depth (mbsf). To first order, the higher resolution of the discrete measurements allows a good approximation of log depth and constrains the maximum offset of composite core depth to log depth to no more than 2 m at any point in this hole.

Velocity: Core-to-Log Comparison

In order to obtain continuous downhole estimates of seismic velocities, for correlation with seismic reflection data, for comparison with core physical properties measurements, and for computation of a synthetic seismogram, a provisional attempt was made to correct problems in data from the individual source-receiver spacings. Initial inspection of the raw data indicated that the most straightforward path to obtaining an improved depth-derived, borehole-compensated transit-time series would be to edit the data from the 12-ft and the two 10-ft source-receiver spacings. After these corrections were made, a new borehole-compensated transit-time series was calculated from the edited data for 10- and 12-ft source-receiver spacings (DTLF).

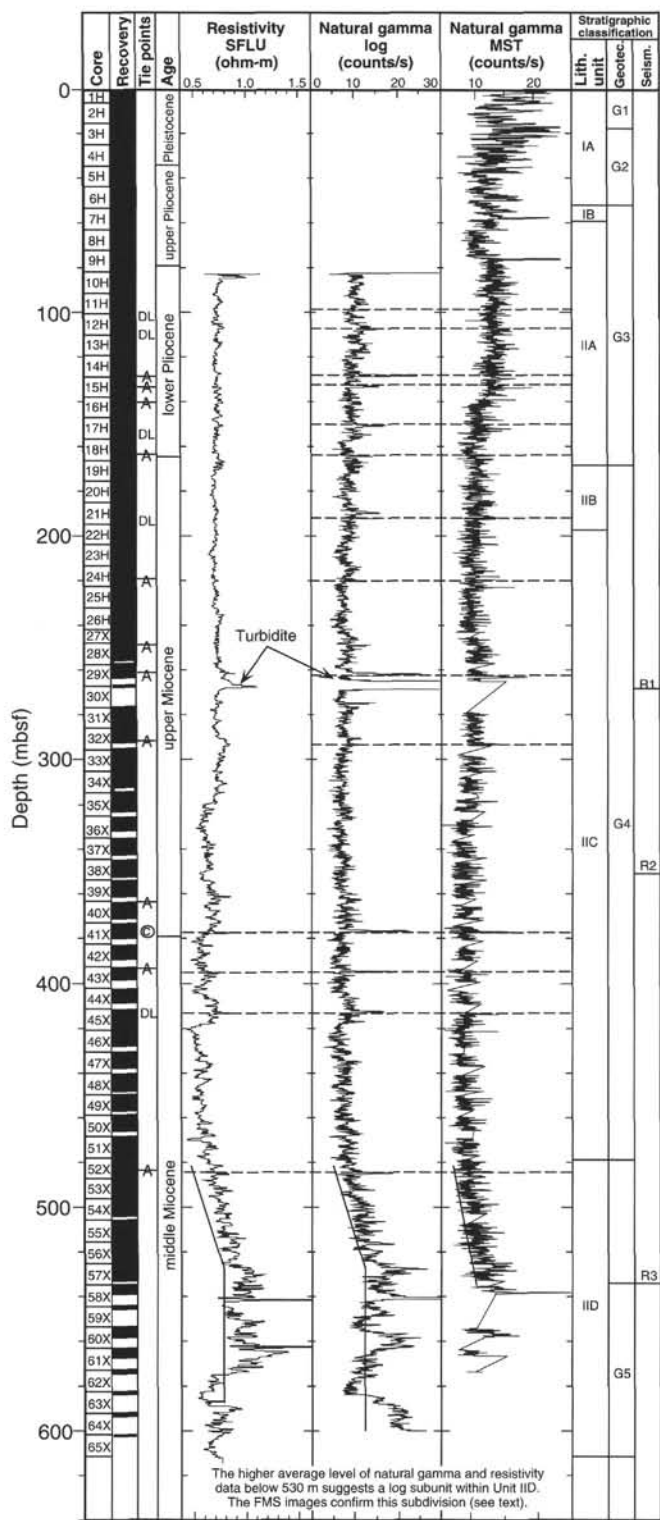


Figure 20. Comparison of log (SFLU) resistivity and natural gamma (NGT) data with natural-gamma-ray core measurements from Hole 982B. Also indicated are relevant lithologic, geotechnical, and seismic units that correlated with log data throughout the 80–610-m interval. See “Lithostratigraphy,” “Seismic Stratigraphy,” and “Physical Properties” sections (this chapter) for full descriptions of all units. Crossed A’s = ash layer, DL = dark layer, and © = nodular concretion.

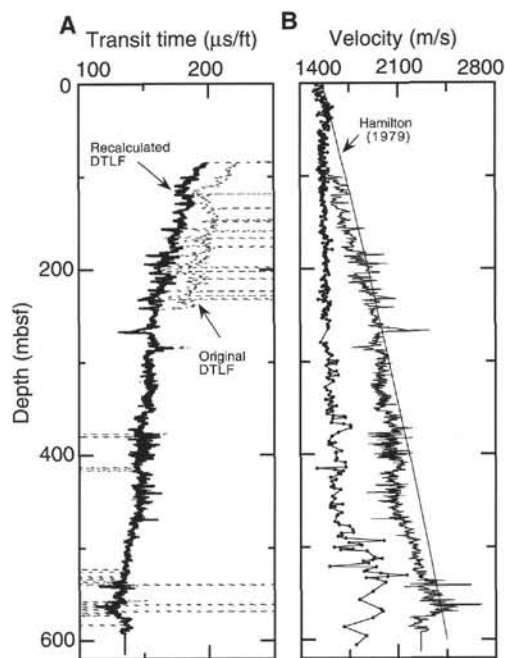


Figure 21. A. Comparison of original depth-derived borehole-compensated sonic log (DTLF), computed during logging, with the same log recalculated after removal of spikes from the original transit-time data and provisional corrections for cycle skipping. Dashed line is the original log and solid line is the recalculated log. B. Comparison of seismic velocities from recalculated sonic log with laboratory velocity measurements on core samples (line with solid circles) from Hole 982B. Also shown is the empirical velocity vs. depth function for calcareous deep-sea sediments from Hamilton (1979).

Figure 21A shows a comparison of the recalculated log with the original DTLF transit times computed during logging.

The recalculated log shows the general steady decrease in transit time with depth that is expected for such a uniform sedimentary succession. The transit times were converted into velocities, and these are shown together with laboratory measurements from the same hole (Fig. 21B). An empirical velocity-vs.-depth function for deep-sea calcareous sediments is also shown (Fig. 21B). The velocities on the recalculated sonic log are close to those predicted by the empirical function of Hamilton (1979), but at most depths they are considerably higher than the laboratory measurements. The *P*-wave logger was used only on cores from Hole 982B down to 242 mbsf, and above this depth the *P*-wave logger and laboratory measurements are very similar (see “Physical Properties” section, this chapter). It is expected that the seismic velocity measured in situ by logging should be significantly higher than laboratory measurements on the cores because of core expansion upon recovery. However, the magnitude of the difference over a large part of this hole is surprising. Between 241 and 493 mbsf, the interval over which the sonic log data are thought to be most reliable, the velocity derived from the sonic log is more than 20% greater than that from laboratory measurements at most depths. Below about 460 mbsf, in the chalk encountered in the deeper part of the hole, both laboratory and downhole velocity measurements show a steeper velocity gradient.

The sharp velocity peak on the recalculated sonic log at 266–267 mbsf, reaching a peak velocity of greater than 2300 m/s, occurs within the interval covered by Core 162-982B-30X, from which only a few centimeters of core was recovered. The layer containing this velocity peak is interpreted as the source of Reflector R1 of Roberts et al. (1970) and of the present study (see “Seismic Stratigraphy” section, this chapter). The high velocity does not in itself explain the permeability barrier inferred from pore-water chemistry studies (see

“Inorganic Geochemistry” section, this chapter), but the silica cementation observed in the small core sample retrieved may help explain density and velocity increases. Although the log shows velocities that are higher than background values over an interval of 4 m, velocities greater than 2100 m/s only occur within 1.2 m at the base of this interval. FMS images at the base of this layer show a sharp contact with the sediments below.

Density: Core-to-Log Comparison

Bulk density data were collected by the HLDLT, which was run as part of the standard Quad combo. Measurements from this tool were run in high-resolution mode at 2.5-cm spacing, which allowed a vertical resolution of ~15–20 cm. The wireline log bulk density data are shown with laboratory GRAPE data and wet bulk density measurements (Fig. 22). The logging data show bulk densities that are mainly between 1.75 and 1.9 g/cm³, and in general increase gradually with depth, like the sonic log. The density log shows a steeper gradient in the chalk below 460 mbsf. The high-velocity layer at 264–268 mbsf is also observed as a high-density layer, with a peak bulk density greater than 2.0 g/cm³, corresponding to the depth of Reflector R1 (see “Seismic Stratigraphy” section, this chapter). Downhole log densities correspond well with gravimetric densities from the cores. The systematically too low GRAPE densities from cores are due to instrument problems (see “Exploratory Notes” chapter, this volume).

In Figure 20, we have noted the major lithostratigraphic (e.g., “IIA”), seismic (e.g., “R1”), and geotechnical (e.g., “G1”) stratigraphic classification schemes (see “Seismic Stratigraphy,” “Lithostratigraphy,” and “Physical Properties” sections, this chapter). Physical properties measurements and FMS imaging in this hole was used for the identification of two major seismic reflectors (R1 and R3). The FMS data (Fig. 23) from Reflector R1 at ~268 mbsf shows a ~4-m-thick interval interpreted as a turbidite deposit. This “turbidite” deposit exhibits fining-upward structure from 268 to 264 mbsf with 5–10-cm diameter clasts in the basal section. Layering within surrounding sediment can be observed above and below, with a prominent ash layer ~2–4 m above. Several physical properties and geochemical logs also clearly identify this “turbidite” feature (Fig. 23).

Information on the density increase and the mineralogy of this “turbidite” layer is provided by the photoelectric effect log. This log is a good indicator of lithology; it measures a sedimentary unit’s electron density by measuring the output of low-energy electrons resulting from neutron collisions induced in the formation by the gamma-ray energy source in the tool. The basic assumption behind the photoelectric effect is that most major rock-forming elements have an atomic number per proton (A/Z) ratio of ~2. This “turbidite” layer has a photoelectric effect value of >6 (for reference, sandstone = 1.5, dolomite = 3, and limestone = 5), which may be the result of silicification. This would also help explain the increase in the density measurements. Silica cementation was observed in the one rock sample recovered from this interval. The photoelectric log value can also be cross-plotted with a calculated Th (ppm)/K (wt%) ratio from the NET data to provide information on clay mineral content. The Th/K ratio in this layer is 2.5, which, combined with a photoelectric value of >6, would indicate the possible presence of glauconite in this layer.

Downhole Temperature Measurements

Borehole fluid temperature measurements were recorded in Hole 982B using the Lamont temperature logging tool (TLT). The TLT was run at the base of the Quad combo string, which was run first. A downhole and an uphole profile were acquired. Figure 24 shows the fast (T_F) and the slow (T_S) thermistor temperatures for the downhole and the uphole runs. Because the logging operation follows immediately behind the drilling, the presence of seawater used to flush debris

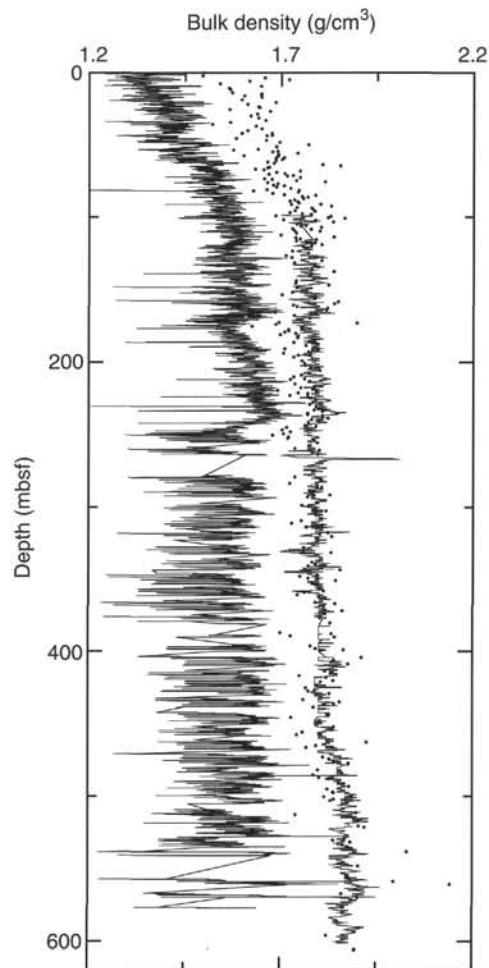


Figure 22. Comparison of wireline log bulk density measurements (right side) with GRAPE bulk density measurements (left side) and wet bulk density measurements on core samples (solid circles).

from the hole can result in values that are not in equilibrium. All values should be interpreted with caution. The bottom-hole temperature (BHT) recorded from both thermistors varies between 18°C and 20°C. No thermal anomalies were noted.

SEISMIC STRATIGRAPHY

The pre-cruise site survey data for Site 982 consisted of high-resolution multichannel seismic data acquired in 1990, using GPS and Loran C navigation. Accurate positioning of these lines was therefore expected, and later verified by the present survey. The pre-cruise data show a near-horizontal seafloor with underlying sequences of parallel strata, without apparent unconformities within the proposed drilling depth in the vicinity of the site. A short survey of approximately 9 nmi was therefore carried out. Two seismic lines were run (Fig. 25), using the 80-in.³ water gun and 3.5- and 12-kHz PDR systems, respectively (See “Underway Geophysics” section, “Explanatory Notes” chapter, this volume). Line S1 follows the pre-cruise survey Line MH90-02 (University of Aarhus and Geological Survey of Denmark, unpubl. data), and features in the pre-cruise data were easily recognizable in the analog seismic records. However, as it became apparent that the sedimentary section was disturbed by numerous small faults, a crossing line, S2, was run over the proposed site. Based

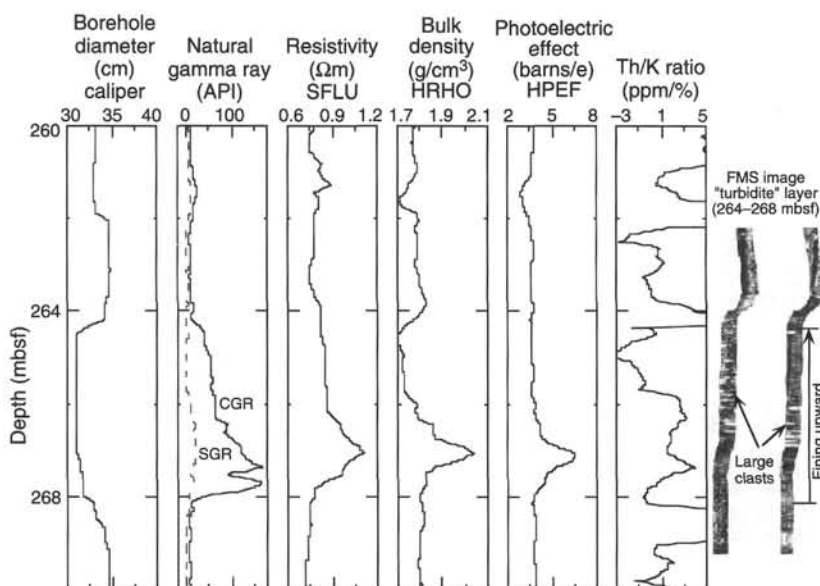


Figure 23. Gray-scale FMS resistivity image of turbidite layer that constitutes Reflector R1 at depth of 264–268 mbsf, at far right. Also shown are major wireline log physical property responses across Reflector R1. Note the lack of borehole deviation from original borehole size, as exhibited by caliper data across this layer. Th/K ratio curve was calculated from natural-gamma-ray log data. Caliper = measures downhole width (inches) with the High-temperature Litho-Density Tool (HLDT); SGR = Spectroscopy Gamma Ray (API units); CGR = Computed Gamma Ray (API units); HRHO = High-Resolution Bulk Density (g/cm^3); HPEF = High-Resolution Photoelectric Effect (barns/electron).

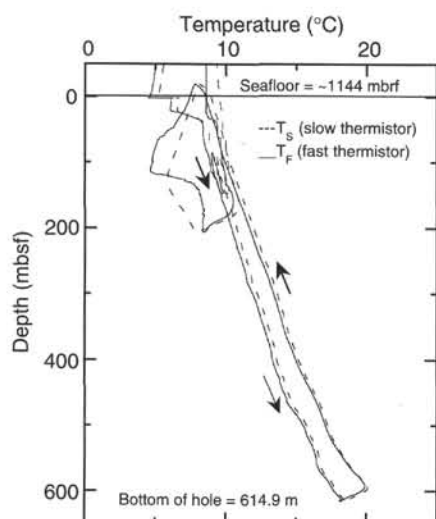


Figure 24. Borehole fluid temperature profile recorded in Hole 982B using the Lamont temperature logging tool (TLT).

on the two lines, the site was moved approximately 500 m to the northeast of the proposed site (NAMD-1) location. Site 982 is located at shotpoint (SP) 961 of Line S2 (Fig. 25).

In addition to the seismic data from 1990, DSDP Leg 12 drilled Site 116 within 2 km of the originally proposed NAMD site (Shipboard Scientific Party, 1972). They report a seismic stratigraphic interpretation based on site survey during Leg 12, as well as on regional pre-cruise seismic lines between the Rockall and Hatton Banks. The results of Leg 12 will be discussed in relation to the results of the present survey later in this section.

Because Hole 982B was logged (see “Wireline Logging” section, this chapter), interval velocities used for depth conversion of seismic reflectors have been derived from the logging results rather than from the shipboard laboratory measurements (see “Physical Properties” section, this chapter), with the exception of the upper 80 mbsf, where there is no log data. The main reason for this is that the velocities derived from the logging are measured in situ; another reason is the relatively low core recovery in the lower parts of Hole 982B (see “Operations” section, this chapter).

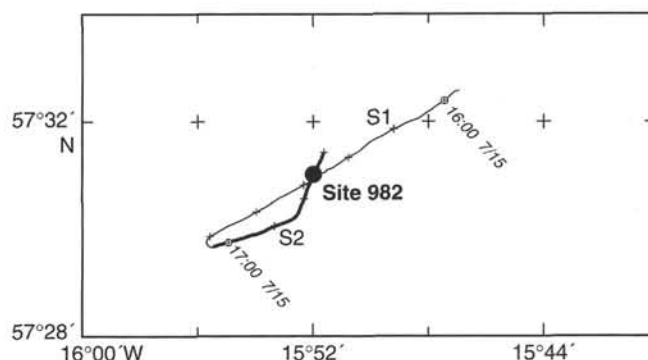


Figure 25. Navigation map of the site survey at Site 982. Location of the profile in Figure 26 is marked by heavy lines.

Description of Seismic Stratigraphy

During DSDP Leg 12, five seismic reflectors were identified, R1 to R5 (Shipboard Scientific Party, 1972), partly based on earlier work by Roberts et al. (1970). During the present survey, the same reflectors were identified, and we have therefore adopted the reflector notations of Shipboard Scientific Party (1972). We have also assigned names to three additional reflectors in order to relate the seismic record to the drilling results. Hence, our seismic stratigraphy at Site 982 is defined by Reflectors R0, R1, R1A, R1B, R2, R3, R4, and R5 (Fig. 26), of which R0, R1A, and R1B were not identified during Leg 12. Six seismic units, NA-I to NA-VI, were defined, mainly based on the difference in internal acoustic character, but partly also from the unconformable character of Reflectors R2 and R4 (Fig. 26). Reflector R1B does not define a unit boundary, but is nevertheless a distinct seismic reflector within the sedimentary section at Site 982.

Seismic Units NA-I to NA-V are all characterized by subhorizontal, parallel acoustic stratification. Normal faulting is frequently observed in these units. Individual faults can be identified throughout the sequence and form small depressions in the seafloor. Fault displacements are commonly in the order of 5–10 ms, and the faults seem to be associated with the relief of Reflector R4.

The exact position of the base of seismic Unit NA-I, Reflector R0, is uncertain, based only on the seismic record. However, based on differences in seismic character, and supported by 3.5-kHz data,

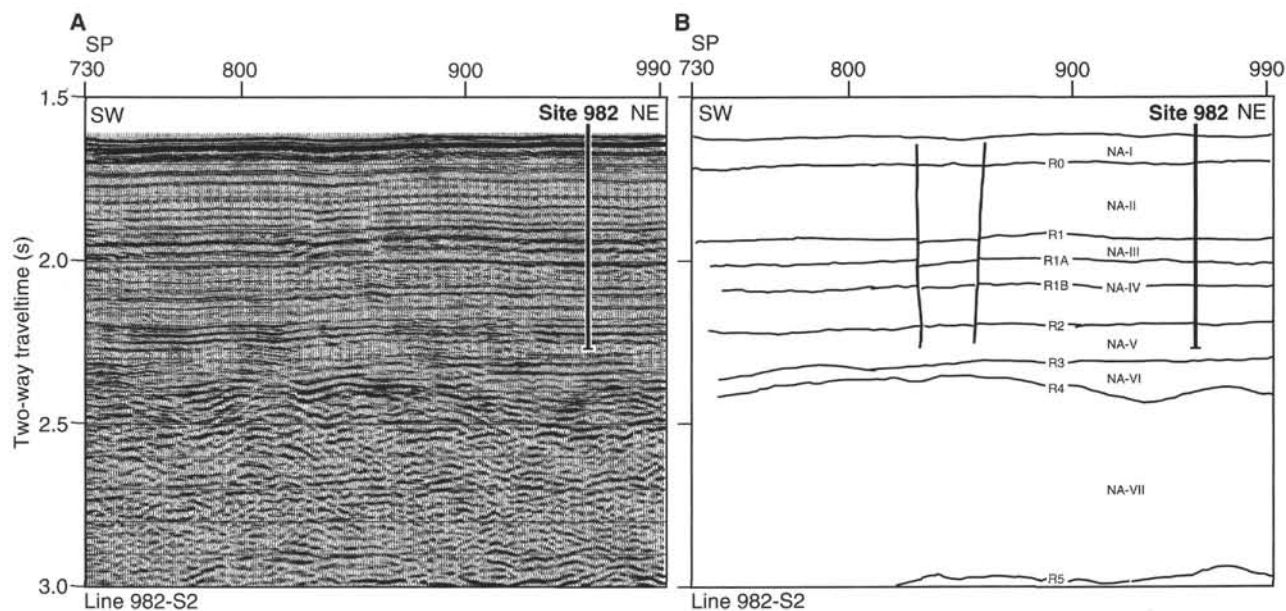


Figure 26. **A.** Seismic record along Line S2. **B.** Interpretation of seismic Line S2, with seismic reflectors and units shown. See Figure 25 for location.

which have a penetration of 30–40 ms and show acoustic stratification, the reflector is placed at 1.69 s two-way traveltime (TWT). Using an interval velocity of 1.57 km/s (see “Physical Properties” section, this chapter), the thickness of Unit NA-I is 63 m at Site 982.

Reflector R1 defines the base of Unit NA-II, and is identified at 1.93 s TWT at Site 982 (Fig. 26). Using interval velocities of 1.75 km/s below 0.08 s, this corresponds to a depth of 273 mbsf. Continuous, parallel acoustic stratification of medium amplitudes is characteristic of this unit. A slight, wavy pattern seems to be associated with the faulting. The middle part of this unit appears to have the least pronounced reflections, with the reflection strength increasing toward the lower part of the unit.

Seismic Unit NA-III is capped by Reflector R1, which has a sharp, high-amplitude character. The unit is only 0.080 s thick at Site 982, which at this depth corresponds to 80 m. Internally, the character of Unit NA-III appears to have less frequent stratification than that above, but this could be an effect of low seismic resolution. The base of this unit is defined by another pronounced reflector, R1A.

Unit NA-IV shows very weak and indistinct internal stratification, with the exception of Reflector R1B, which is distinct throughout the survey area (Fig. 26). At Site 982, Reflector R1B and Reflector R2, which forms the base of the unit, are observed at 2.08 and 2.185 s TWT respectively, corresponding to depths of 427 m and 538 mbsf using an interval velocity of 2.1 km/s.

Unit NA-V, defined between Reflectors R2 and R3, thins northeastward along Line S1. Reflector R2 becomes less pronounced toward the northeastern end of Line S1, but pinch-out of the unit is not observed. Based on the internal reflection pattern in Unit NA-V, the upper boundary, Reflector R2, is apparently erosional when traced 10–15 km farther northeast along pre-cruise seismic Line MH90-02. No truncations can be observed, however, near the site. At Site 982, Reflector R3 is identified at 2.31 s TWT, which corresponds to 678 mbsf, using a velocity of 2.2 km/s for the lowermost part of Hole 982B (see “Wireline Logging” section, this chapter) and extrapolating beyond the bottom of the hole at 615 mbsf.

Unit NA-VI fills in depressions in the highly undulating surface of Reflector R4 (Fig. 26). Weak internal structures seem to indicate southwestward-dipping strata with an erosional truncation beneath Reflector R3. At Site 982, this unit is approximately 0.08 s thick, corresponding to about 90 m, but its thickness varies between 0.05 and near 0.150 s over short distances.

Unit NA-VII has a thickness of 0.58 s at Site 982, between unconformities R4 and R5, the latter of which is defined as acoustic basement in the present survey. It should be noted, however, that Shipboard Scientific Party (1972) suggest an older sedimentary basin below Reflector R5, based on gravity data. Indistinct, but continuous internal reflectors, consisting of wide bands of individual reflections, have an apparent southwestward dip. Velocities are likely to be high in this unit, and the total depth to Reflector R5 probably exceeds 1.5 km.

Synthetic Seismogram

A synthetic seismogram was generated to facilitate correlation between seismic and lithostratigraphic units. The recalculated sonic log and edited density log (see “Wireline Logging” section, this chapter) were used to calculate reflection coefficients below 99 mbsf. Discrete measurements of density and compressional velocity on the recovered cores (see “Physical Properties” section, this chapter) were used to calculate reflection coefficients above 99 mbsf. The velocity and density at 99 mbsf obtained from the logs are similar to the discrete measurements at this depth, so the change from one type of data to the other does not produce a spurious reflection coefficient. A water velocity of 1480 m/s and density of 1.03 g/cm³ were assumed to calculate a reflection coefficient for the seafloor. Reflection coefficients were calculated as a function of both depth and two-way traveltime, to enable TWT on the synthetic seismogram to be related directly to depth.

The seismic line used for correlation is Line 982-S2 of the Site 982 site survey. More precise correlation would have been possible using the high-resolution pre-cruise site survey data, but unfortunately no digital data from this survey were available aboard ship. The seismic source signature of Line 982-S2 data was estimated by stacking the seafloor reflection on the 21 shots closest to Site 982 (see “Explanatory Notes,” this volume), and convolved with the reflection coefficient series (Fig. 27) to produce the synthetic seismogram (Fig. 28).

Figure 29 shows the synthetic seismogram inserted into Line 982-S2 at the location of the site. Most of the significant reflectors are clearly recognizable on the synthetic from their shape and amplitude. However, reflections on the synthetic lag a few milliseconds behind those on the survey data. The lag increases to about 10 ms in the first

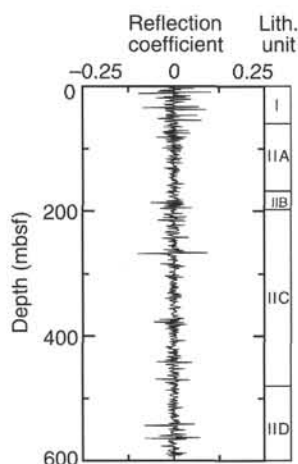


Figure 27. Reflection coefficients, calculated from log data (below 99 mbsf) and discrete measurements on cores (above 99 mbsf), plotted vs. depth. Also shown are the lithostratigraphic unit boundaries (see "Lithostratigraphy" section, this chapter).

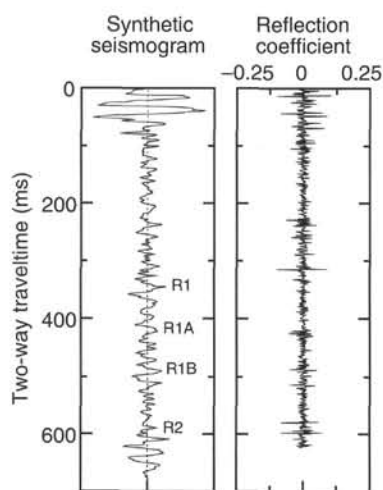


Figure 28. Synthetic seismogram and reflection coefficients plotted against two-way traveltime. Significant seismic reflectors, which have been identified by comparison with site survey Line S2, are labeled on the synthetic seismogram.

300 ms TWT below the seafloor reflection, indicating that the seismic velocities used for the upper part of the hole are on average about 3% too low. At greater TWT the lag remains constant at about 10 ms, confirming the accuracy of the log velocities from the deeper part of the hole.

The origin of the TWT axis in Figure 28 is at the start of the initial trough of the seafloor reflection. All other TWTs reported in this chapter are measured from just before the onset of the first peak of the seafloor reflection, so the TWTs of all reflectors in Figure 28 have an additional apparent lag of 10 ms. The estimated seismic source signature contains two main peaks and two main troughs 15–55 ms after its start. Therefore the main seismic response to each reflection coefficient in Figure 28 is delayed by 15–55 ms. This is well illustrated by Reflector R1, which is expressed as a large peak and trough between 340 and 360 ms on the synthetic seismogram in Figure 28. This peak and trough are mainly a response to the large reflection coefficients between 310 and 320 ms. The fact that the largest positive and

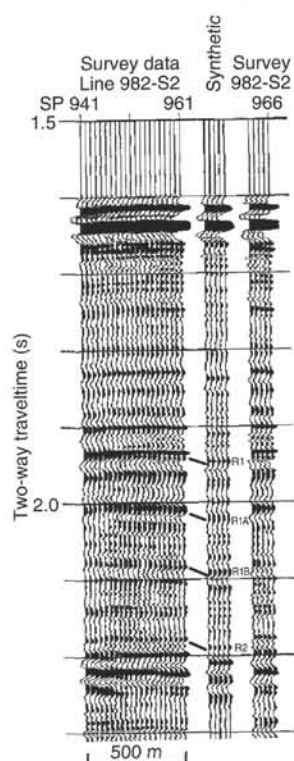


Figure 29. Part of site survey Line 982-S2, with five copies of the synthetic seismogram inserted at the location of Site 982.

negative reflection coefficients are very close together in this interval causes a lot of destructive interference, otherwise the amplitude of Reflector R1 would be much greater. If the thin, high-velocity layer that causes this pair of reflection coefficients varied in thickness laterally, we would expect changes in the amplitude and character of Reflector R1. Reflector R1A, the peak of which is at 422 ms in Figure 28, does not appear to be caused by any large, discrete reflection coefficients. Thus it is probably caused by constructive interference between reflections from several layer boundaries with small reflection coefficients. A large contribution to Reflector R1B (peak at 490 ms) probably comes from the isolated, positive reflection coefficient at 454 ms, which corresponds to a depth of 407 mbsf (Fig. 27). The large reflection coefficients that occur at approximately the same time as the peak of Reflector R2 (589 ms) in Figure 28 contribute to the large amplitude reflections between 600 and 640 ms, but not to Reflector R2 itself. Like Reflector R1A, Reflector R2 must be an interference composite caused by a number of small reflection coefficients. In the interpretation of the survey data, the delayed seismic response has been accounted for by always marking the reflectors well above the first peak. Still, this may explain some discrepancies between core and seismic data.

Correlation with Core Data

Hole 982B penetrated Reflector R2 and hence recovered sediments from seismic Units NA-I to NA-V. Most of the lithostratigraphic boundaries do not correspond directly to the seismic stratigraphy at this site, but the upper seismic Unit NA-I does, however, correspond to lithostratigraphic Unit I as well as to geotechnical Units G1 and G2 (Fig. 29). The lithostratigraphy is characterized by cyclic changes between intervals enriched with terrigenous and biogenic sediments, respectively (see "Lithostratigraphy" section, this

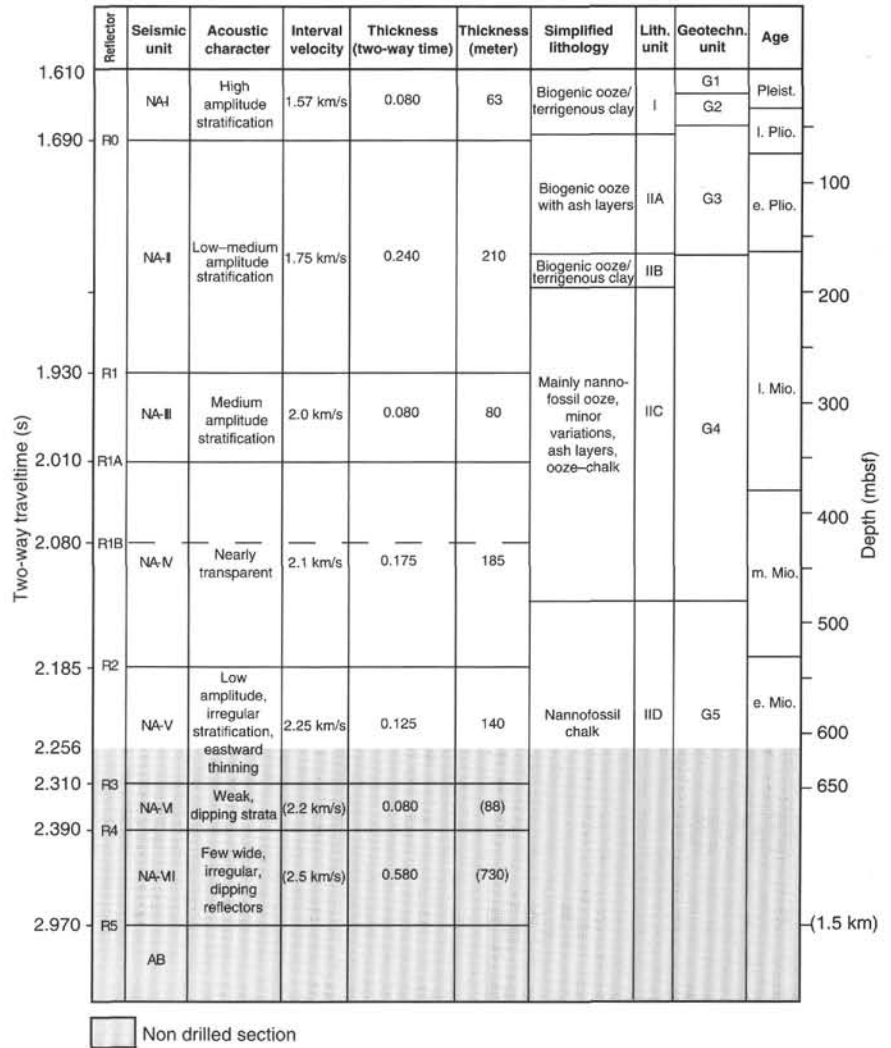


Figure 30. Relationship between seismic stratigraphy, lithostratigraphy, and geotechnical stratigraphy. Note that the depth scale in mbsf is linear but is not to scale below the drilled depth.

chapter). The slightly deeper level of Reflector R0 relative to the lithostratigraphic and geotechnical boundaries may be attributed to inadequate seismic resolution.

Lithostratigraphic Unit II is split into four subunits, IIA to IID, based on relatively small lithologic variations, abundance of ash layers, and varying degrees of lithification (see "Lithostratigraphy" section, this chapter). The average carbonate content, however, is above 80% throughout this lithostratigraphic unit. A possible increase in reflection strength in the lower part of seismic Unit NA-II (Fig. 26) may be related to the larger lithologic variability reported for lithostratigraphic Unit IIB (see "Lithostratigraphy" section, this chapter).

Reflector R1 corresponds to Core 162-982B-30X, which contained only one clast of silica-cemented foraminiferal sandstone (see "Lithostratigraphy" section, this chapter). Downhole logging results suggest this interval to consist of a 4-m-thick upward-fining bed, possibly a turbidite (see "Wireline Logging" section, this chapter). A transition from ooze to chalk takes place from about 350 mbsf (see "Lithostratigraphy" section, this chapter), and this is most likely the cause of seismic Reflector R1A (Fig. 30). Although no geotechnical unit boundary is defined at this level, the porosity and P-wave velocity show a small deviations at approximately 360 mbsf, which could be related to diagenetic effects. Severe core disturbance may, however, obscure the laboratory results.

No obvious change in lithology or physical properties is observed at the level of seismic Reflector R1B, at approximately 430 mbsf.

The downhole logging results, however, show a small velocity inversion at this level, which could be the reason for the reflector. The velocities below this level show an increased gradient of downhole velocity increase relative to intervals above (see "Wireline Logging" section, this chapter).

Seismic Reflector R2 corresponds approximately to the first appearance of hard, silicified chalks (with the exception of the single bed at 270 mbsf) (see "Lithostratigraphy" section, this chapter). Discrete measurements of P-wave velocity on rock fragments gave results of up to 4.5 km/s. Although these velocities are not representative for the unit as a whole, the overall physical character of the sediments most likely changes enough to cause a seismic boundary and a change in acoustic character. The synthetic seismogram suggests that several smaller impedance contrasts may interfere to form reflector R2.

Seismic Units NA-VI and NA-VII were not cored at Site 982. However, drilling of DSDP Site 116 showed Unit NA-VII to consist of chert and chalks with varying degrees of silicification. Reflector R4 was shown to be a major lower to upper Oligocene unconformity (Shipboard Scientific Party, 1972).

Although the seismic stratigraphy in the area of Site 982 consists of seven units, the changes in seismic character between the upper five units are relatively small. In the upper part of the drilled section, the changes are related to variations in the amount of terrigenous vs. calcareous material, whereas variations in degree of lithification of

carbonates seem to be most important in the lower parts of the cored interval.

Unit NA-VI differs from those above in that it fills depressions in the underlying surface and shows an apparent westward dip of internal reflectors. The base of this unit, Reflector R4, shows the characteristics of a true seismic sequence boundary (Vail et al., 1977). Both the two lowermost seismic units show evidence for an easterly source of sediments, most likely the Rockall Bank area. The seismic records from the study area do not show significant erosion within the cored interval.

REFERENCES

- Avery, O.E., Vogt, P.R., and Higgs, R.H., 1969. Morphology, magnetic anomalies and evolution of the Northeast Atlantic and Labrador Sea, Part II. Magnetic anomalies. *Eos*, 50:184. (Abstract)
- Baker, P.A., 1986. Pore-water chemistry of carbonate-rich sediments, Lord Howe Rise, Southwest Pacific Ocean. In Kennett, J.P., von der Borch, C.C., et al., *Init. Repts. DSDP*, 90: Washington (U.S. Govt. Printing Office), 1249–1256.
- Baker, P.A., Gieskes, J.M., and Elderfield, H., 1982. Diagenesis of carbonates in deep-sea sediments: evidence from $\text{Sr}^{2+}/\text{Ca}^{2+}$ ratios and interstitial dissolved Sr^{2+} data. *J. Sediment. Petrol.*, 52:71–82.
- Baldauf, J.G., 1984. Cenozoic diatom biostratigraphy and paleoceanography of the Rockall Plateau region, North Atlantic, Deep Sea Drilling Project Leg 81. In Roberts, D.G., Schnitker, D., et al., *Init. Repts. DSDP*, 81: Washington (U.S. Govt. Printing Office), 439–478.
- Berggren, W.A., Hilgen, F.J., Langereis, C.G., Kent, D.V., Obradovich, J.D., Raffi, I., Raymo, M.E., and Shackleton, N.J., 1995. Late Neogene chronology: new perspectives in high-resolution stratigraphy. *Geol. Soc. Am. Bull.*, 107:1272–1287.
- Bordovskiy, O.K., 1965. Accumulation and transformation of organic substances in marine sediment, 2. Sources of organic matter in marine basins. *Mar. Geol.*, 3:5–31.
- Cande, S.C., and Kent, D.V., 1995. Revised calibration of the geomagnetic polarity timescale for the Late Cretaceous and Cenozoic. *J. Geophys. Res.*, 100:6093–6095.
- Drever, J.I., 1971. Magnesium-iron replacement in clay minerals in anoxic marine sediments. *Science*, 172:1334–1336.
- Emerson, S., and Hedges, J.I., 1988. Processes controlling the organic carbon content of open ocean sediments. *Paleoceanography*, 3:621–634.
- Fronval, T., and Jansen, E., in press. Late Neogene paleoclimates and paleoceanography in the Iceland-Norwegian Sea: evidence from the Iceland and Vøring Plateaus. In Thiede, J., Myhre, A.M., Firth, J.V., Johnson, G.L., and Ruddiman, W.F. (Eds.), *Proc. ODP, Sci. Results*, 151: College Station, TX (Ocean Drilling Program).
- Gieskes, J.M., 1983. The chemistry of interstitial waters of deep-sea sediments: interpretation of deep-sea drilling data. In Riley, J.P., and Chester, R. (Eds.), *Chemical Oceanography* (Vol. 8): London (Acad. Press), 222–269.
- Goll, R.M., and Bjørklund, K.R., 1989. A new radiolarian biostratigraphy for the Neogene of the Norwegian Sea: ODP Leg 104. In Eldholm, O., Thiede, J., Taylor, E., et al., *Proc. ODP, Sci. Results*, 104: College Station, TX (Ocean Drilling Program), 697–737.
- Grousset, F.E., Labeyrie, L., Sinko, J.A., Cremer, M., Bond, G., Duprat, J., Cortijo, E., and Huon, S., 1993. Patterns of ice-rafted detritus in the glacial North Atlantic (40°–55°N). *Paleoceanography*, 8:175–192.
- Hamilton, E.L., 1979. Sound velocity gradients in marine sediments. *J. Acoust. Soc. Am.*, 65:909–922.
- Jansen, E., and Sjøholm, J., 1991. Reconstruction of glaciation over the past 6 Myr from ice-borne deposits in the Norwegian Sea. *Nature*, 349:600–603.
- Katz, B.J., 1983. Limitations of “Rock-Eval” pyrolysis for typing organic matter. *Org. Geochem.*, 4:195–199.
- Laughton, A.S., Berggren, W.A., et al., 1972. *Init. Repts. DSDP*, 12: Washington (U.S. Govt. Printing Office).
- Locker, S., and Martini, E., 1989. Cenozoic silicoflagellates, ebridians, and actiniscidians from the Vøring Plateau (ODP Leg 104). In Eldholm, O., Thiede, J., Taylor, E., et al., *Proc. ODP, Sci. Results*, 104: College Station, TX (Ocean Drilling Program), 543–585.
- McIver, R.D., 1975. Hydrocarbon occurrences from JOIDES Deep Sea Drilling Project. *Proc. Ninth Petrol. Congr.*, 269–280.
- Nigrini, C., and Sanfilippo, A., 1992. Cenozoic radiolarian stratigraphy for low and middle latitudes. Catalogue compiled for ODP. [Unpublished]
- Peters, K.E., 1986. Guidelines for evaluating petroleum source rock using programmed pyrolysis. *AAPG Bull.*, 70:318–329.
- Roberts, D.G., Bishop, D.G., Laughton, A.S., Ziolkowski, A.M., Scrutton, R.A., and Matthews, D.H., 1970. New sedimentary basin on Rockall Plateau. *Nature*, 225:170–172.
- Robinson, S.G., Maslin, M.A., and McCave, I.N., 1995. Magnetic susceptibility variations in late Pleistocene deep-sea sediments of the N.E. Atlantic: implications for ice-rafting and paleocirculation at the last glacial maximum. *Paleoceanography*, 10:221–250.
- Ruddiman, W.F., Kidd, R.B., Thomas, E., et al., 1987. *Init. Repts. DSDP*, 94 (Pts. 1 and 2): Washington (U.S. Govt. Printing Office).
- Shipboard Scientific Party, 1972. Sites 116 and 117. In Laughton, A.S., Berggren, W.A., et al., *Init. Repts. DSDP*, 12: Washington (U.S. Govt. Printing Office), 395–671.
- Takayama, T., and Sato, T., 1987. Coccolith biostratigraphy of the North Atlantic Ocean, Deep Sea Drilling Project Leg 94. In Ruddiman, W.F., Kidd, R.B., Thomas, E., et al., *Init. Repts. DSDP*, 94 (Pt. 2): Washington (U.S. Govt. Printing Office), 651–702.
- Vail, P.R., Mitchum, R.M., Jr., Todd, R.G., Wiedmier, J.M., Thompson, S., III, Sangree, J.B., Bubb, J.N., and Hatlelid, W.G., 1977. Seismic stratigraphy and global changes in sea level. In Payton, C.E. (Ed.), *Seismic Stratigraphy: Applications to Hydrocarbon Exploration*. AAPG Mem., 26:49–217.
- Weaver, P.P.E., and Clement, B.M., 1986. Synchronicity of Pliocene planktonic foraminiferal datums in the North Atlantic. *Mar. Micropaleontol.*, 10:295–307.
- Wolf, T.C.W., and Thiede, J., 1991. History of terrigenous sedimentation during the past 10 My in the North Atlantic (ODP Legs 104, 105, and DSDP 81). *Mar. Geol.*, 101:83–102.
- Wright, J.D., and Miller, K.G., 1993. Southern Ocean influences on late Eocene to Miocene deepwater circulation. *Antarct. Res. Ser.*, 60:1–25.
- Zimmerman, H.B., Shackleton, N.J., Backman, J., Kent, D.V., Baldauf, J.G., Kaltenback, A.J., and Morton, A.C., 1984. History of Plio-Pleistocene climate in the northeastern Atlantic, Deep Sea Drilling Project Hole 552A. In Roberts, D.G., Schnitker, D., et al., *Init. Repts. DSDP*, 81: Washington (U.S. Govt. Printing Office), 861–875.

Ms 162IR-104

Note: For all sites drilled, core description forms (“barrel sheets”) and core photographs can be found in Section 3, beginning on page 391. Forms containing smear slide data can be found in Section 4, beginning on page 1147. All processed logs (including FMS, dipmeter, temperature data, high-resolution density and neutron data, and sonic waveforms not shown in printed form) are on the CD-ROM enclosed in the back pocket of this volume. Also on the CD-ROM are all tables from this chapter (including an extended coring summary table) and shipboard measurements (files containing GRAPE density, *P*-wave velocity, natural gamma radiation, magnetic susceptibility, index properties, and spectral reflectance data).

SHORE-BASED LOG PROCESSING

Hole 982B

Bottom-hole Assembly

The following bottom-hole assembly (BHA) depths are as they appear on the logs after differential depth shift (see "Depth shift" section) and depth shift to the seafloor. As such, there may be a discrepancy with the original depths given by the drillers on board. Possible reasons for depth discrepancies are: ship's heave, use of wireline heave compensator, and drill string and/or wireline stretch.

DIT/SDT/HLDT/CNTG/NGT: BHA at ~82.5 mbsf.
 DIT/SDT/HLDT/CNTG/NGT: Pipe at ~15 mbsf.
 FMS/GPIT/NGT: Did not reach BHA (pass 1).
 FMS/GPIT/NGT: Did not reach BHA (pass 2).
 FMS/GPIT/NGT: BHA at ~82.5 mbsf (pass 3).

Processing

Depth shift: Original logs have been interactively depth-shifted with reference to NGT from DIT/SDT/HLDT/CNTG/NGT main run and to the seafloor (-1143.5 m). Note that the depth of the seafloor as seen on the logs differs from the "bottom felt" depth given by the drillers (-1.5 m).

Gamma-ray processing: Data have been processed to correct for borehole size and type of drilling fluid.

Acoustic data processing: The array sonic tool was operated in standard depth-derived borehole compensated mode, including long-spacing (8-10-10-12 ft) and short-spacing (3-5-5-7 ft) logs. The long-spacing sonic logs have been processed to eliminate some of the noise and cycle skipping experienced during the recording. Processing could not eliminate completely all the noise recorded in the 185-240, 380-393, and 420-430 mbsf intervals; caution is therefore suggested if using these data quantitatively.

Quality Control

Data recorded through bottom-hole assembly and pipe, such as the neutron porosity and gamma-ray logs above 83 mbsf, should be used qualitatively only because of the attenuation on the incoming signal. Invalid gamma-ray spikes were recorded at 56-61 and 78-84 mbsf.

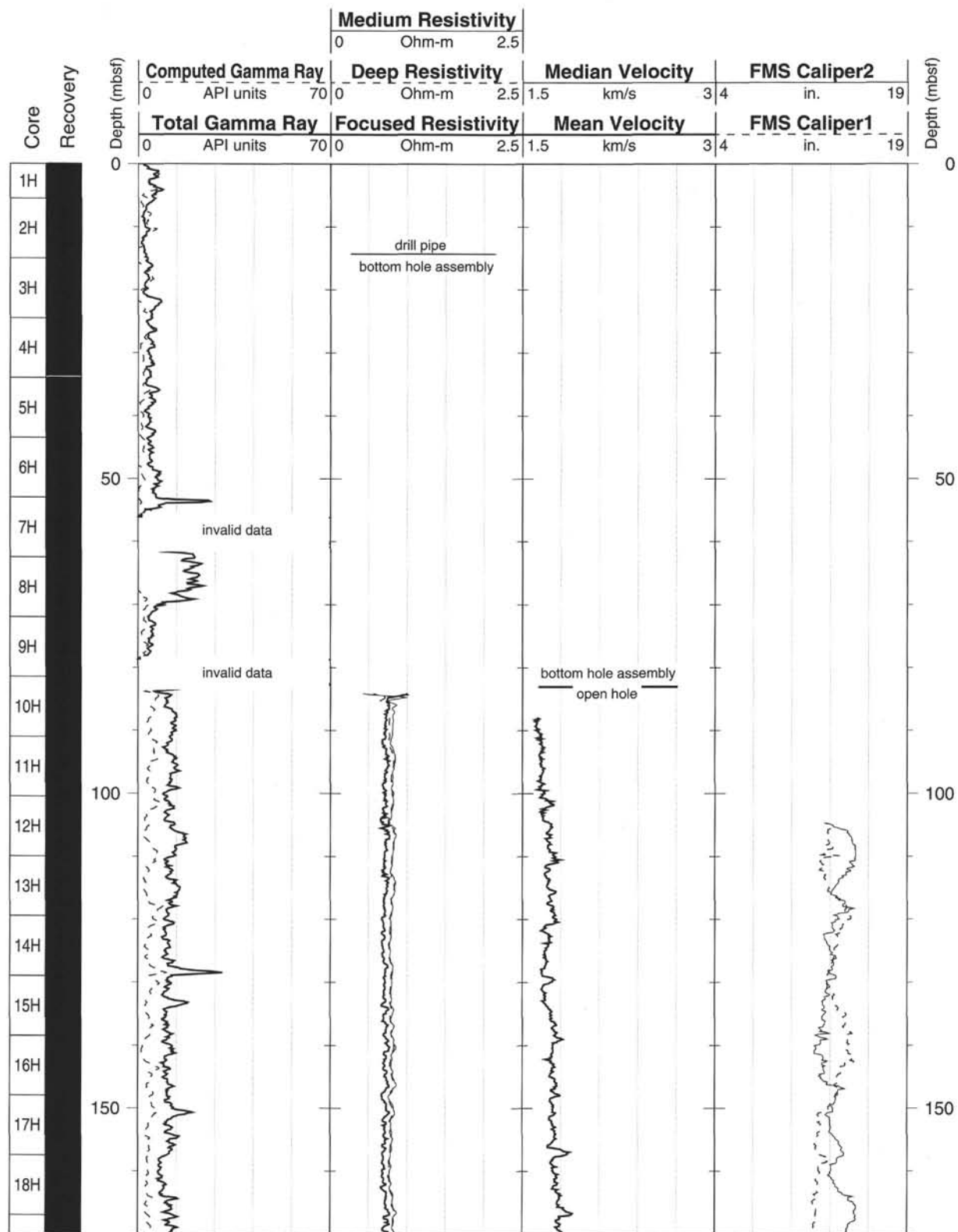
Hole diameter was recorded by the hydraulic caliper on the HLDT tool (CALI), and the caliper on the FMS string (C1 and C2).

Note: Details of standard shore-based processing procedures are found in the "Explanatory Notes" chapter (this volume). For further information about the logs, please contact:

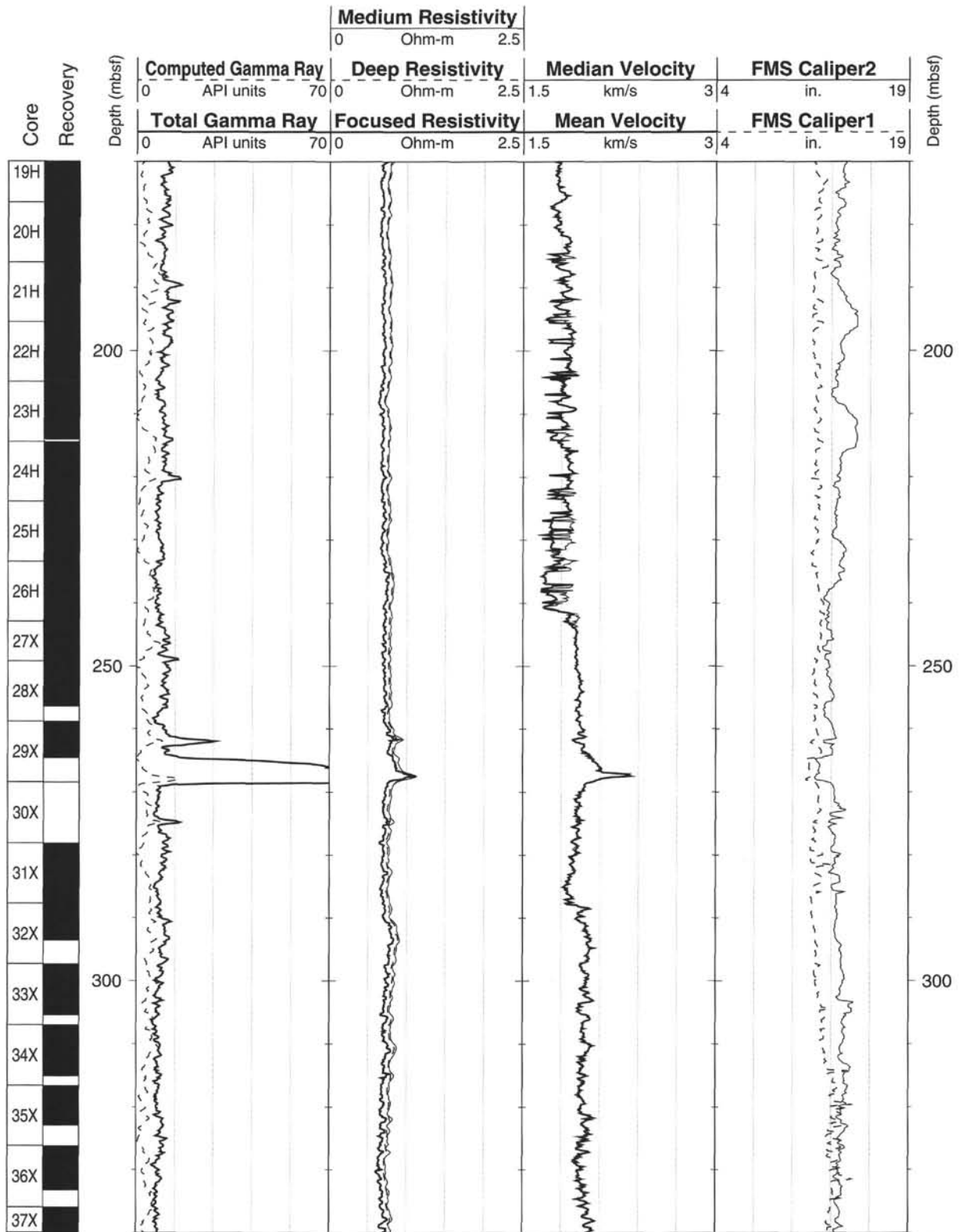
Cristina Broglia
 Phone: 914-365-8343
 Fax: 914-365-3182
 E-mail: chris@ldeo.columbia.edu

Elizabeth Pratson
 Phone: 914-365-8313
 Fax: 914-365-3182
 E-mail: beth@ldeo.columbia.edu

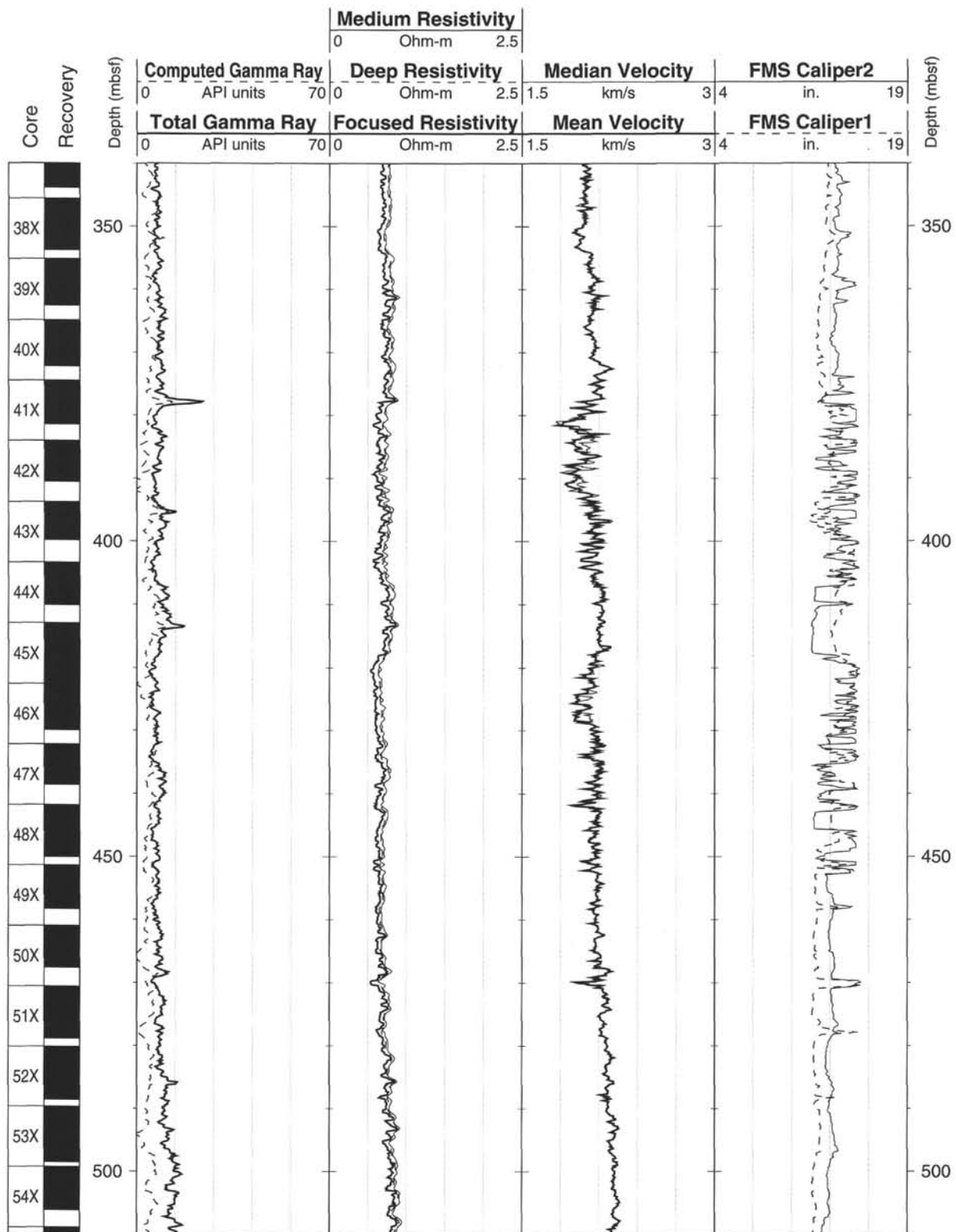
Hole 982B: Natural Gamma Ray-Resistivity-Sonic Logging Data



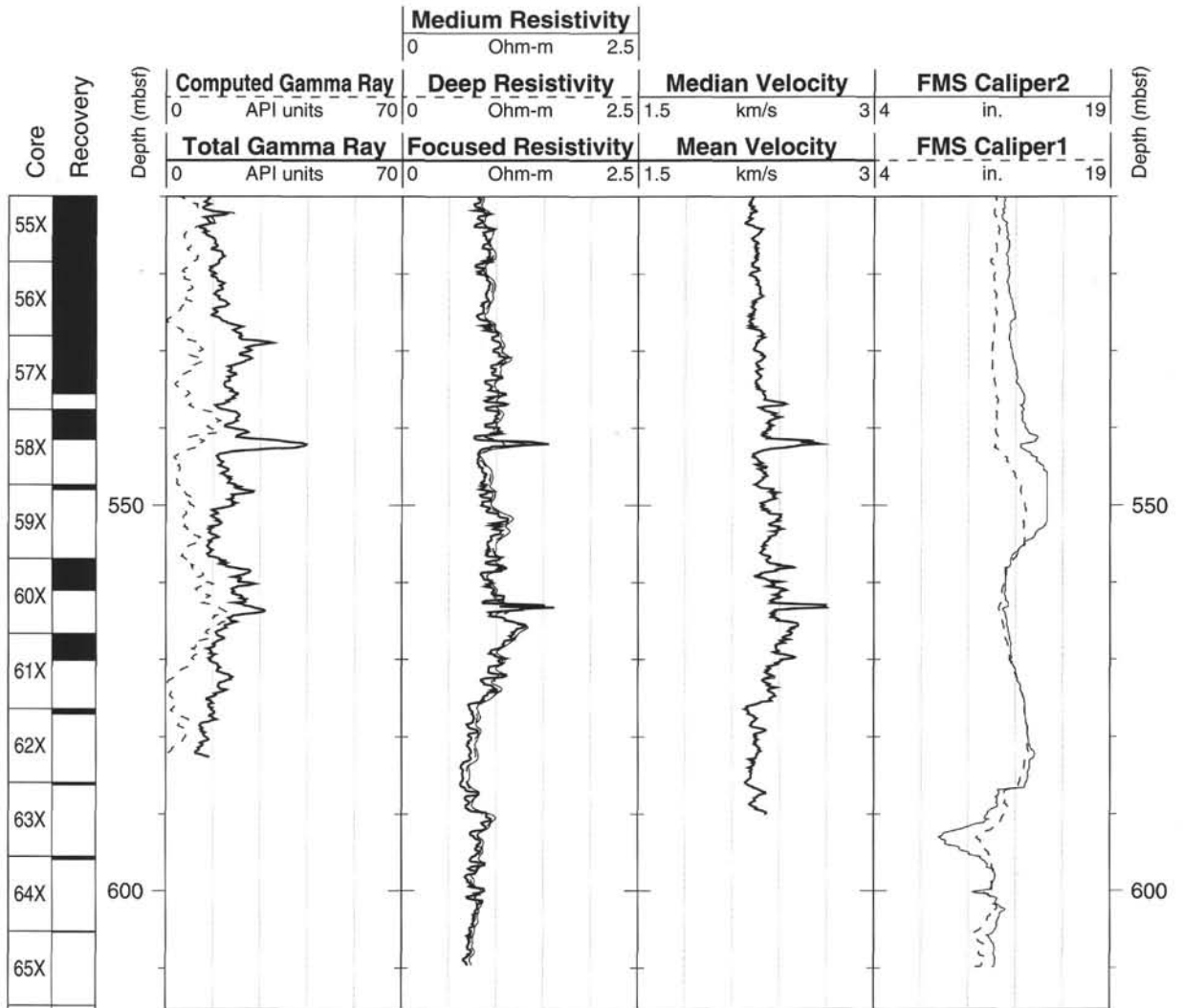
Hole 982B: Natural Gamma Ray-Resistivity-Sonic Logging Data (cont.)



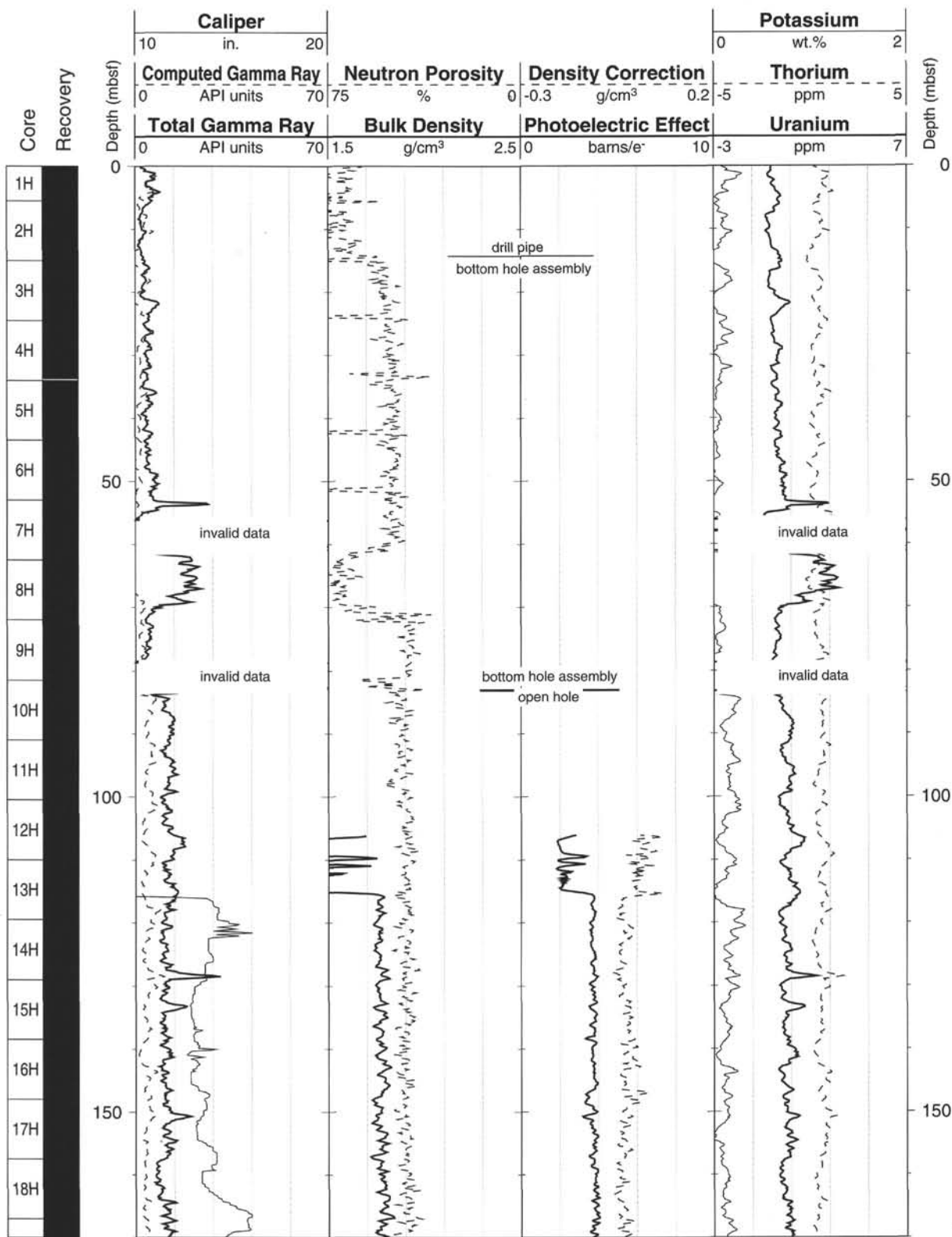
Hole 982B: Natural Gamma Ray-Resistivity-Sonic Logging Data (cont.)



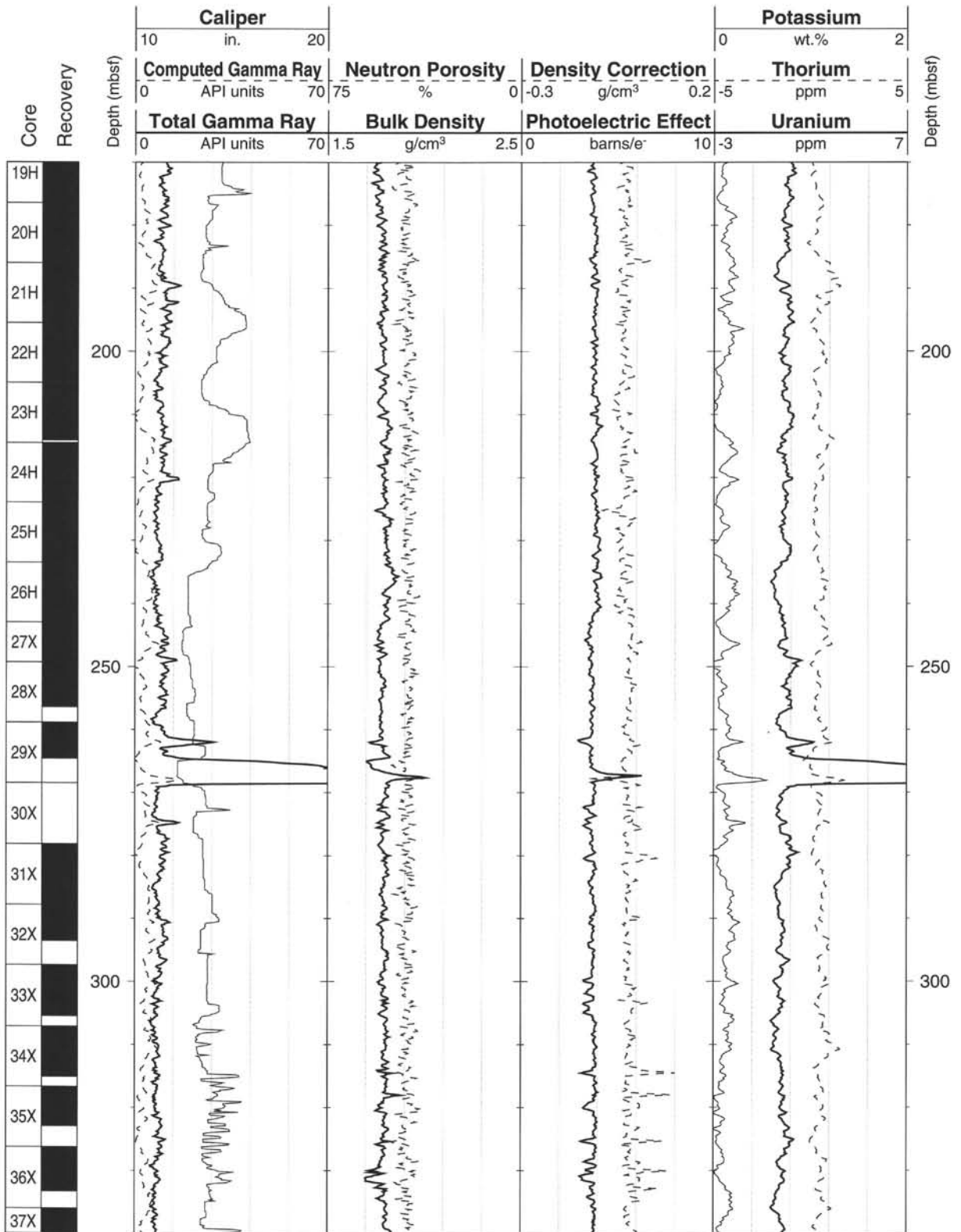
Hole 982B: Natural Gamma Ray-Resistivity-Sonic Logging Data (cont.)



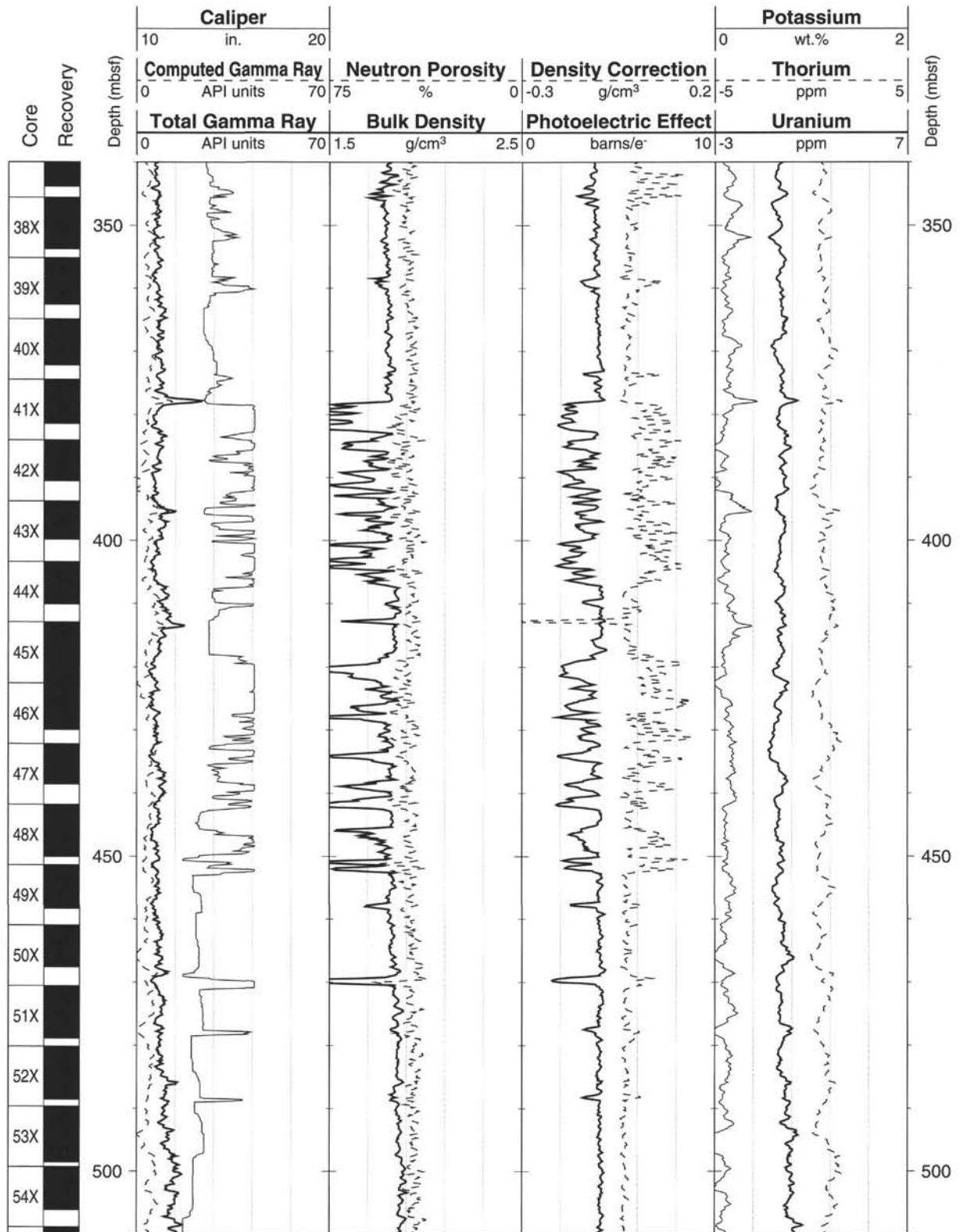
Hole 982B: Natural Gamma Ray-Density-Porosity Logging Data



Hole 982B: Natural Gamma Ray-Density-Porosity Logging Data (cont.)



Hole 982B: Natural Gamma Ray-Density-Porosity Logging Data (cont.)



Hole 982B: Natural Gamma Ray-Density-Porosity Logging Data (cont.)

